

TOOL-CHIP INTERFACE TEMPERATURE IN MACHINING:
MODELING AND EVALUATING THE EFFECTS OF
VARIABLE FLOW RATE CUTTING
FLUID APPLICATION

by

Edward John Dorrian

A thesis submitted to the faculty of
The University of Utah
in partial fulfillment of the requirements for the degree of

Master of Science

Department of Mechanical Engineering

The University of Utah

May 2018

Copyright © Edward John Dorrian 2018

All Rights Reserved

The University of Utah Graduate School

STATEMENT OF THESIS APPROVAL

The thesis of Edward John Dorrian

has been approved by the following supervisory committee members:

Alagar Krishnan Balaji, Chair 12/12/2017
Date Approved

Ashley Spear, Member 12/12/2017
Date Approved

Wenda Tan, Member 12/12/2017
Date Approved

and by Tim Ameel, Chair/Dean of

the Department/College/School of Mechanical Engineering

and by David B. Kieda, Dean of The Graduate School.

ABSTRACT

Cutting fluids, typically an emulsion containing a lubricant within a larger cooling medium, are expected to reduce the cutting temperature at the interface between the chip and tool in machining, which improves both part quality and tool life. Traditionally, cutting fluids are applied as a flood, completely wetting the tool for maximum heat removal. However, flood coolant has adverse effects on both the environment and workplace safety, leading industry towards developing alternative solutions, such as dry and minimum quantity cutting fluid (MQCF) application. The capability of MQCF to access and cool the tool-chip interface is not completely understood or modeled with no ability to deliver a desired fluid volume to achieve a desired temperature or friction reduction.

This research attempted to model and study dry, flood, and various levels of MQCF cooling targeted onto the rake face of the tool. Experiments were conducted to determine the effectiveness of each level of fluid condition, which could then be parameterized as an effective heat transfer coefficient, h_{eff} . The model created here is based off of an established dry analytical model and now expands its capabilities to model machining operations under varying levels of coolant application.

The model presented in this thesis was validated with Oxley's model, which is widely accepted as the most comprehensive and accurate machining model for plain carbon steels. All machining parameters input into Oxley's model were held constant, but feed rate was increased from 0.05 mm/rev to 0.2 mm/rev. The model closely predicted the

increase in average tool-chip interface temperature, but did not agree with the predicted average tool-chip interface temperatures.

To determine h_{eff} , a near-orthogonal facing experiment on 1045 steel was conducted to measure the change in temperature under six cutting fluid conditions, including dry, MQCF (0, 150, 300, and 500 ml/hr of water mist supplied by compressed air), and flood (6 l/min of synthetic cutting fluid delivered as a water-based emulsion). Using a tool-work thermocouple to measure average tool-chip interface temperature, a decrease in temperature as the flow rate of fluid increased was measured. Cutting forces were largely constant during the experiment, indicating that the MQCF was primarily cooling and that temperature reductions observed were not due to any lubricating action. Increased coolant flow rate likely caused a larger temperature gradient in the chip, resulting in tightly coiled chips. Furthermore, cooling caused a significant reduction in contact length at the tool-chip interface, indicating that there is an indirect friction altering effect due to in-situ thermal changes at the tool-chip interface.

With the aid of experimental measurements, the model calculated the temperature distribution at the interface between the chip and tool as well as discrete points in the chip and tool. The measured temperature decrease with coolant application could be used to solve for h_{eff} . The results from this research give insight into the minimum amount of cutting fluid needed to achieve a measurable temperature difference at the tool-chip interface. Additionally, this model can serve as a predictive machining tool to calculate temperature profiles for dry, flood, as well as minimized cutting fluid conditions.

TABLE OF CONTENTS

ABSTRACT.....	iii
LIST OF TABLES.....	vii
NOMENCLATURE.....	viii
ACKNOWLEDGMENTS.....	x
Chapters	
INTRODUCTION.....	1
1.1 Modeling of Metal Cutting.....	2
1.2 Cutting Fluids in Machining.....	5
1.3 Research Objectives.....	7
1.4 Overview of Thesis.....	7
BACKGROUND.....	12
2.1 Temperature Measurement Methods.....	12
2.2 Thermal Modeling Methods for Machining.....	17
2.2.1 Finite Element Methods.....	17
2.2.2 Analytical Thermal Modeling.....	18
2.2.3 Slip Line Models.....	22
2.2.4 Models for Predicting Tool-Chip Contact Length.....	23
2.2.5 Thermal Models with Coolant Conditions.....	24
MODEL METHODOLOGY AND EXPERIMENT PLAN.....	36
3.1 Model Methodology.....	36
3.1.1 Inputs.....	37
3.1.2 Calculation Heat Source Values.....	37
3.1.3 Temperature Change Caused by Shear Plane Heat Source.....	38
3.1.4 Temperature Change Caused by the Frictional Heat Source.....	40
3.1.5 Temperature Change Cause by the Rake Cooling Heat Source.....	42
3.2 Experiment Plan.....	45
3.2.1 Workpiece.....	45
3.2.2 Tooling.....	45
3.2.3 Cut Conditions.....	46
3.2.4 Fluid Conditions.....	46

3.2.5	Temperature Measurement.....	46
3.2.6	Force Measurement.....	47
3.2.7	Tool-Chip Contact Length.....	47
3.2.8	Chip Measurements.....	48
3.2.9	Hardness Testing.....	48
3.2.10	Experiment Procedure.....	48
RESULTS AND DISCUSSION.....		62
4.1	Experiment Results.....	63
4.1.1	Tool-Chip Interface Temperature.....	63
4.1.2	Cutting Forces.....	63
4.1.3	Effect of Workpiece Diameter.....	64
4.1.4	Chips Forms.....	65
4.1.5	Tool-Chip Contact Length.....	65
4.1.6	Temperature Rise with an Increased Feed Rate.....	66
4.2	Experiment Discussion.....	66
4.3	Model Discussion.....	69
4.3.1	Verification with Komanduri and Hou's Model.....	70
4.3.2	Verification with Oxley's Model.....	70
4.3.3	Numerical Integration Independence Study.....	71
4.3.4	Modeled Dry Conditions with Experimental Measurements.....	72
4.3.5	Determination of Effective Heat Transfer Coefficient.....	73
4.3.6	Modeled Tool Temperature with Cooling.....	74
4.3.7	Model Predictions for Increased Feed Rate.....	74
4.3.8	Summary and Limitations of the Proposed Model.....	75
CONCLUSION.....		97
5.1	Summary and Conclusions.....	97
5.2	Recommendations for Future Work.....	99
APPENDIX: CODE FOR PROPOSED MODEL.....		101
REFERENCES.....		110

LIST OF TABLES

Tables

3.1: List of proposed model inputs, symbols, and units.....	50
3.2: Experiment conditions.	61
4.1: Measured average temperature and comparison to dry conditions.....	78
4.2: Tool-chip contact length images.....	83
4.3: Comparison of measured average tool-chip interface temperature at 0.2 mm/rev and 0.05 mm/rev.....	86
4.4: Comparison of average tool-chip interface temperature.....	87
4.5: Model inputs for Oxley verification.	89
4.6: Verification with Oxley results.....	89
4.7: Model inputs with experimental measurements.	92

NOMENCLATURE

a_{ch}	Thermal diffusivity of the chip, m^2/s
b	Width of cut, mm
L	Tool-chip contact length, mm
L_{ab}	Shear plane length, mm
l_i	Location of differential element on the shear plane relative to X,z coordinate system, mm
F_{cut}	Main cutting force, N
F_{fr}	Friction force, N
F_{thrust}	Thrust force, N
h_{eff}	Effective heat transfer coefficient, W/m^2-K
r	Chip thickness ratio
t_{ch}	Chip thickness, mm
t_{cut}	Depth of cut, mm
q_f	Heat intensity of frictional heat source, W/m^2
q_{ic}	Heat intensity of induced cooling heat source on the chip, W/m^2
q_{isp}	Heat intensity of induced shear plane heat source on the tool, W/m^2
q_{rc}	Heat intensity of rake cooling heat source, W/m^2
q_{sp}	Heat intensity of shear plane heat source, W/m^2
R	Distance from coordinate to heat source, mm

R'	Distance from coordinate to image heat source, mm
S	Heat source distribution coefficient
T_{amb}	Ambient temperature, °C
$\bar{T}_{t,surface}$	Average tool rake surface temperature, °C
V	Cutting speed, m/min
V_{ch}	Chip velocity, m/min
X, y, z	Coordinates of point where temperature rise is to be calculated (mm)
α	Rake angle, deg.
$\Delta T_{ch,f}$	Change in temperature in the chip by the frictional heat source, °C
$\Delta T_{ch,rc}$	Change in temperature in the chip by the rake cooling heat source, °C
$\Delta T_{ch,sp}$	Change in temperature in the chip by the shear plane heat source, °C
$\Delta T_{t,f}$	Change in temperature in the tool by the frictional heat source, °C
$\Delta T_{t,rc}$	Change in temperature in the tool by the rake cooling heat source, °C
$\Delta T_{t,sp}$	Change in temperature in the tool by the frictional heat source, °C
ϕ	Shear plane angle, deg.
λ_{ch}	Thermal conductivity of the chip, W/m ² -K
λ_{tool}	Thermal conductivity of the tool, W/m ² -K

ACKNOWLEDGMENTS

I would first like to thank my advisor, Dr. A.K. Balaji, for his advice, guidance, and support with the research presented in this thesis. I would also like to thank Dr. Ashley Spear and Dr. Wenda Tan for the support as well.

I would like to thank Mohanad Abbood for setting up the MQCF device used in this research as well as his help during the experiments. I would like to thank Jeff Kessler for letting me use the resources in his laboratory. I would like to thank Tom Slowik for his help with the CNC machine and advice. I would also like to thank Moncktons machine tools for providing tooling in a timely manner.

Last but not least, I would like to thank my parents for their constant support and encouragement throughout my graduate studies.

CHAPTER 1

INTRODUCTION

Machining refers to the process of removing material from a workpiece to cut it into the desired shape. Therefore, machining is subtractive, such that unwanted material is removed from the workpiece. Machining improves both surface finish and tolerance, all the while creating shapes that cannot be achieved with many other manufacturing processes, such as casting or forming [1].

The process of machining generally refers to chip-forming operations in metal cutting. As a wedge-shaped tool cuts into the workpiece, the thin layer removed plastically deforms and shears, creating a chip. The speeds at which the tool cuts through the work material often exceeds 100 m/min, generating temperatures in excess of 1000°C, and the work material experiences strain rates of over $10^6/s$ as it is plastically deformed.

The focus of this thesis is the facing process in which a workpiece is rotated while a translating tool removes material. The process takes place on a lathe, or a similar machine tool, and produces parts that are generally round and axisymmetric in shape. Common operations of the turning process include turning, facing, boring, drilling, and parting. A diagram of the facing operation and lathe tool geometry are shown in Figure 1.1 and Figure 1.2, respectively.

In the United States, costs associated with material removal, including machining,

account for about 10% of the gross national product [2]. With such economic significance, it is evident why machining has been a continuous research topic for over 150 years. Early studies are reviewed in detail by Finnie [3], who describes many of the first experiments to investigate chip formation and cutting forces. However, it was Taylor [4] who made the first significant scientific advances, laying the foundation for understanding cutting temperature and tool life, which ultimately led to the Taylor tool-life equation. Taylor's [4] approach was purely experimental by varying only one factor at a time, which took over 26 years to complete and consumed over 800,000 pounds of metal [5], revealing the inefficiency of experimental analysis and empirical models.

1.1 Modeling of Metal Cutting

Models of the machining process can be divided into three categories: empirical, numerical, and analytical. Early studies used empirical models, as in Taylor [5], which fit curves to experimental data, although these models require considerable amounts of data and are restricted to variables that can be measured. Further, experimental data are only accurate for the conditions in which the study was performed and cannot predict beyond experimental conditions without extrapolation, another disadvantage to empirical modeling.

Advancements in computing over the past 30 years have led to an increased use of numerical models. Remeshing methods have greatly improved the accuracy and solution convergence for the extreme element distortions caused by the machining process [6]. However, the accuracy of finite element models is highly dependent on a reliable material model.

The process of machining, however, has historically been explained with the use of analytical models. During the advent of these models, computers were not available and, therefore, numerical solutions were impractical or impossible. Analytical models give insight into the fundamental mechanics of the inherently complex machining process, providing an efficient method to study the effects of cutting parameters. The simplified 2-D model of machining, referred to as orthogonal machining, is the basis for many of the analytical models discussed in this thesis.

Orthogonal machining assumes that the tool edge is straight, normal to the direction of cutting, and normal to the feed direction. Figure 1.3 shows a diagram of the orthogonal machining model. The thickness of the uncut chip is labeled t_{cut} . In the orthogonal model, t_{cut} is the same as the feed, f . The cutting speed, V , is the speed at which the tool moves relative to the workpiece. The rake angle, α , is the angle of tool face relative to perpendicular from the workpiece, which can be positive or negative.

For simplified orthogonal analysis, the work material is assumed to shear at a plane as opposed to a zone. This implies there is no built-up edge and that chip formation is continuous, resulting in a “type 2” continuous chip that is common for machining metals [5]. The angle at which the shear plane forms, relative to the work material, is ϕ . As the material is plastically deformed, the thickness of the chip, t_{ch} , is larger than t_{cut} due to the plastic deformation at the shear plane. The contact length, L , is the length over which the chip is in contact with the tool before it curls away. The chip flows over the tool with a chip velocity, V_{ch} .

Shear plane angle and chip thickness are not constrained by the tool geometry, making them dependent variables of the machining process. The pioneering work of Ernst

and Merchant [7] developed a solution to determine the shear angle assuming that the shear angle takes a value at which cutting force is minimized. With the angle of the shear plane, friction force, F , and normal force, F_N , can be determined. A diagram of Merchant's force circle, which relates the geometry and forces acting on the chip-tool interface and shear plane, can be seen in Figure 1.4. While the assumption that F and N in Figure 1.4 are uniformly distributed over the contact length is oversimplified, the analysis of Ernst and Merchant is still used and gives a straightforward way of describing forces and energy in the machining process [8].

Much of the energy in the machining process is converted to heat. Heat is primarily generated in the shear plane as the work material is plastically deformed at a high strain rate and also generated by friction as the chip rubs against the rake, or top, surface of the tool. Figure 1.5 depicts the location of the two heat sources acting on the tool and chip.

As observed by Taylor [4], heat is directly related to tool life, which has been the motivation for research on temperature distributions in the chip and tool. While experimental measurements of cutting temperatures have remained relatively constant since 1920 [9], advancements in modeling have been slow, even with the advent of numerical modeling techniques. Trigger and Chao [10], Hahn [11], and Loewen and Shaw [12] all made early contributions to modeling temperatures during the machining process, taking a heat-transfer-based, analytical approach. These models are the basis for this research and are described in greater detail in Chapter 2.

1.2 Cutting Fluids in Machining

To help with dissipating the heat generated in the machining process, cutting fluids are applied to the cutting zone. In reference to machining, cutting fluid is often referred to as “coolant.” The cutting fluid serves three main purposes: remove heat from the cutting zone, lubricate the cutting zone, and remove chips from the cutting zone [13].

The primary function of a cutting fluid is dependent on the operation. For high-speed operations, cooling and chip clearing are the primary functions of the cutting fluid. At cutting speeds above 60 m/min, contact pressures at the tool-chip interface are high enough that coolant cannot penetrate the contact area [14], leading to a small, if any, impact on temperature at the tool-chip interface [15]. Low-speed operations, however, rely on cutting fluids with lubricating abilities to reduce friction in the cutting zone. A reduced friction force increases the shear angle, which in turn reduces the thickness of the chip. As a result, both temperature and power consumption decrease [1].

There are several types of cutting fluids, each with unique advantages and disadvantages. A list of common cutting fluids and their characteristics are described below, but are reviewed in greater detail in references [16] and [5]:

1. Straight oils use petroleum- or vegetable-based oil. These are primarily used for severe cutting operations and for machining difficult metals.
2. Soluble oils, or emulsified oils, are the most commonly used fluid in cutting. Small droplets of mineral oil are dispersed in a volume of water at a ratio of 1% to 20%, which combines the lubricating properties of oil and the cooling properties of water. At high cutting speeds, soluble oils are preferred over straight oil.

3. Semi-synthetic fluids are emulsified mineral oils, similar to soluble oils, but with a smaller emulsion particle size. These fluids balance the advantages and disadvantages of soluble oils and synthetic fluids.
4. Synthetic fluids are water-based fluids with no mineral oil. These fluids have a high cooling ability, yet poor lubricity. Additives are emulsified to increase lubricating properties, typically at 1% to 10% concentration.

Traditionally, coolants are applied as a flood, completely wetting the tool for maximum heat removal. However, flood coolant has adverse effects on both the environment and workplace safety, leading industry towards alternative solutions, such as dry and minimum quantity cutting fluid (MQCF) machining [13]. MQCF delivers a mist cutting fluid to the cutting zone with compressed air. There is no clearly defined “minimum” to MQCF, but cutting fluid flow rates are typically on the order of 10 ml/hr, using straight oils, and as high as 300 ml/hr with synthetic coolants [17].

Studies involving MQCF have been primarily focused on minimum quantity lubrication (MQL). In the case of MQL, the cutting fluid applied is typically a straight oil in order to lubricate the cutting zone to reduce forces. The effectiveness is often small, only reducing tool-chip interface temperatures by less than 10% [18]–[20].

Few studies have investigated the use of soluble oils or synthetic cutting fluids applied in minimum quantities. These fluids not only have superior cooling ability compared to straight oil, but also, when applied as a mist, it can increase heat transfer with convective and evaporative cooling [21]. This significant knowledge gap is the motivation for this research.

1.3 Research Objectives

There are two objectives of this research: (1) to develop an analytical model to predict the cooling effects of coolant on the tool-chip interface and (2) to experimentally measure the decrease in tool-chip interface temperature with varying levels of cutting fluid flow rate including: dry, MQCF (0, 150, 300, and 500 ml/hr of water mist supplied by compressed air), and flood (6 l/min of synthetic cutting fluid delivered as a water-based emulsion).

The experiments will be used with the model and to determine the cooling effectiveness, parameterized as the effective heat transfer coefficients, of the various cutting fluid conditions. The work presented in this thesis attempts to establish the minimum quantity of cutting fluid needed to reduce tool-chip interface temperature. This research is a step towards real-time strategically applied coolant based on machine sensory information, further enhancing the capabilities of the targeted MQCF dispensing system developed in the Sustainable Manufacturing Lab [22].

1.4 Overview of Thesis

The first chapter of this thesis gives an introduction to machining and heat generated during the machining process. It also outlines the research objectives. Chapter 2 provides background information and a literature review on temperature-measurement methods. Common modeling and predictive machining methods are also presented. Chapter 3 explains the model created for this research, which is an adaption of the Komanduri and Hou [23] moving heat source model. The experimental plan used to determine convective cooling inputs is then outlined. Chapter 4 discusses the results and

provides conclusions from the experiment as well as the model. Finally, Chapter 5 gives conclusions and further research recommendations.

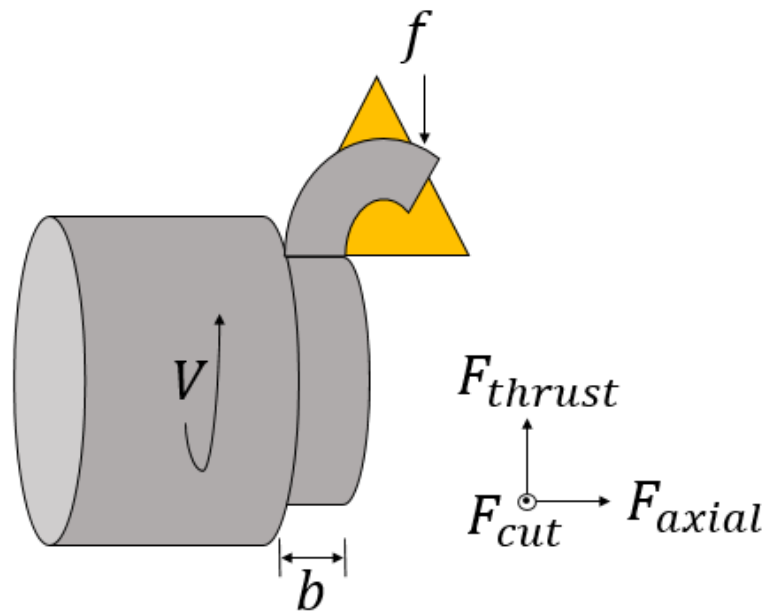


Figure 1.1: Diagram of facing operation.

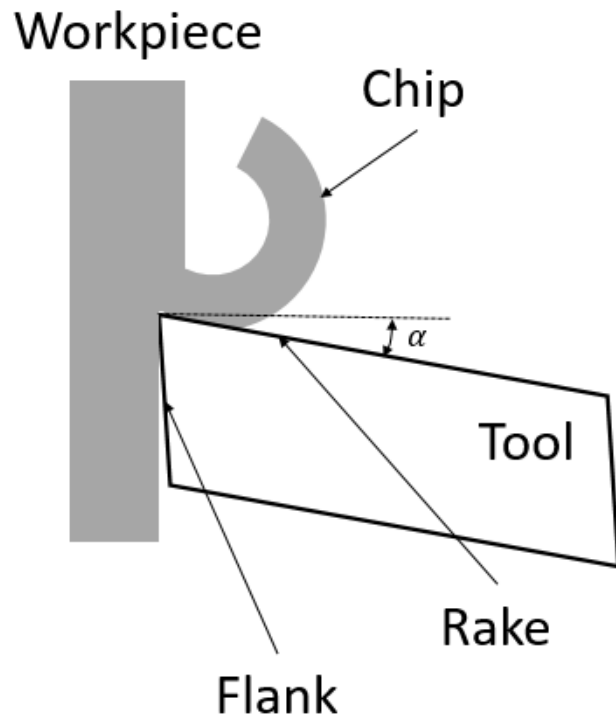


Figure 1.2: Diagram of lathe tool and common nomenclature.

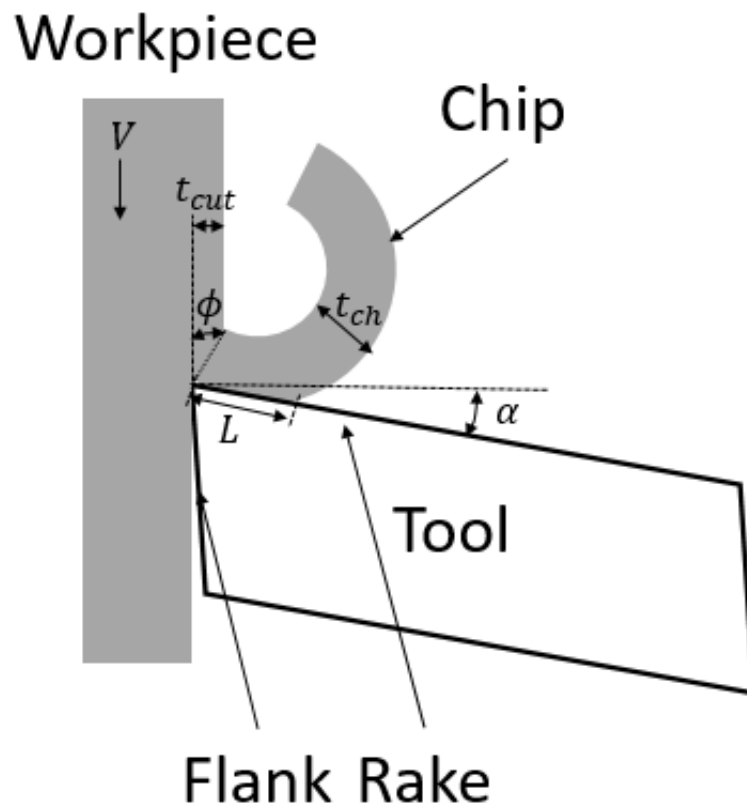


Figure 1.3: Orthogonal model.

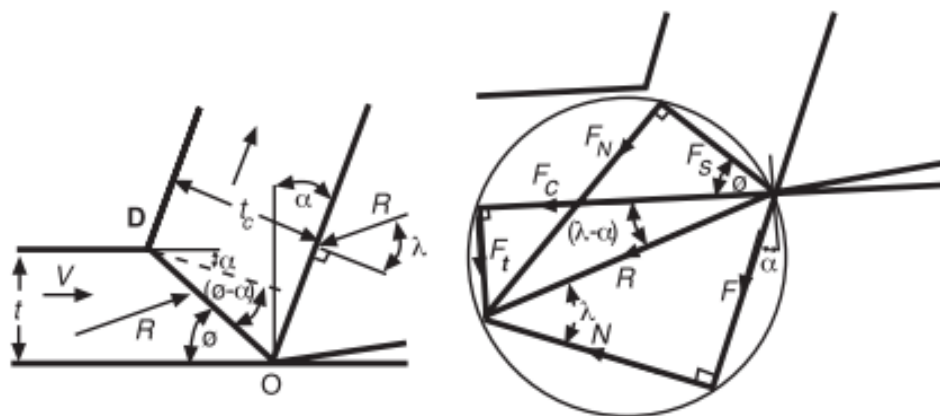


Figure 1.4: Merchant model (adapted from Trent [8]).

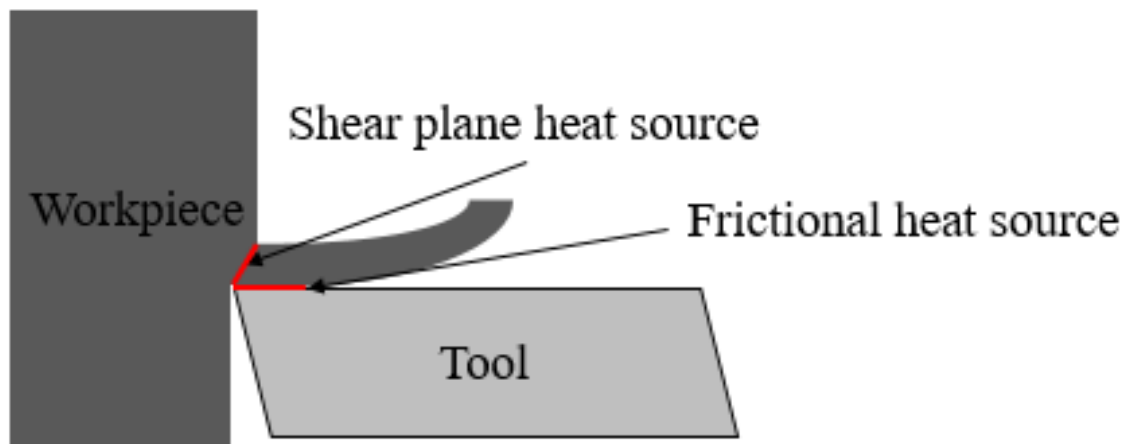


Figure 1.5: Diagram showing the location of the shear plane heat source and the frictional heat source.

CHAPTER 2

BACKGROUND

This chapter provides background information on temperature measurement methods commonly used in machining research in Section 2.1. In addition to explaining each of the methods, findings from each method related to temperature measurements in the presence of a metal working fluid will be discussed. Section 2.2 then focuses on developments for modeling machining. Finite element methods, analytical thermal modeling, slip line models, tool-chip contact length models, and thermal models for coolant application are discussed.

2.1 Temperature Measurement Methods

Temperatures during the machining process can exceed 1000°C [24]. Cutting temperature is directly related to both tool life and wear, rendering any reduction in temperature beneficial for production. While active monitoring of temperature may not be practical during manufacturing processes due to the extensive instrumentation required for such measurements, it is crucial to understand the heat generated during the machining process in a laboratory setting.

Davies et al. [9] comprehensively review temperature-measurement methods used in machining research, and highlight turning studies that use the following temperature-

measurement methods: thermophysical, tool-work thermocouple, embedded thermocouple, spectral band radiance, and ratio radiation (two-color pyrometer). Of the discussed methods, the tool-work thermocouple and two-color pyrometer are the only methods capable of a direct measurement of the tool-chip interface. Many studies have also utilized the remote thermocouple, which measures temperatures remotely, away from the interface. The three aforementioned temperature-measurement methods can all perform in the presence of a cutting fluid—a unique advantage these methods have over many thermal imaging methods, such as an infrared camera.

Both Ueda et al. [25] and Al Huda et al. [18] have measured temperature changes at the tool-chip interface with the two-color pyrometer method, by using both dry and cutting fluid conditions. Both studies found that there was a small decrease in temperature at the tool-chip interface with a cutting fluid, rendering the two-color pyrometer a useful measurement method for detecting the cooling ability of a cutting fluid at the tool-chip interface.

Under nearly identical turning experiments for 1045 steel conducted by Ueda et al. [25] and Al Huda et al. [18], MQL has outperformed flood coolant in reduction of interface temperature. Ueda et al. [25] investigated interface temperatures with MQL targeted on the rake face of the tool. The experiment was conducted with a continuous turning operation and a 60°C decrease in temperature was observed. With a similar setup, Al Huda et al. [18] used a synthetic cutting fluid applied as a flood. The flood coolant conditions reduced interface temperature by only 30°C at all speeds tested (200-300 m/min). These results indicate that MQCF can produce comparable, if not more, temperature reductions compared to flood coolant.

As with most radiation-based methods, measurements require expensive imaging and detection equipment. A ceramic alumina tool, which is transparent to the wavelengths of light used for the measurement, must be used to measure interface temperature. The optical fibers are placed under the rake face of the tool through a hole and measure the temperature above a single point, as seen in Figure 2.1. The measurement can be related to the temperature distribution at the interface, but must be properly located [18]. While ceramic tools are gaining popularity in industry, they are still outnumbered by coated sintered tungsten carbide (WC) tools [5].

The most straightforward way to directly measure average temperature at the tool-chip interface is with a tool-work thermocouple, as seen in Figure 2.2. The resources needed for setting up a tool-work thermocouple are relatively inexpensive, especially compared to radiation-based methods. A number of researchers have used the tool-work thermocouple method for a wide variety of work materials and tools with various coatings. Stephenson [26] notes that calibration and error sources are the main issues with the tool-work thermocouple, listed below. The three sources of error are simple to overcome with proper instrumentation and insulation of the circuit.

1. The tool-work thermocouple measures the electromotive force (EMF) at the interface. This only corresponds to temperature if the temperature and EMF relationship between the tool and workpiece is linear.
2. Isolation of the tool and workpiece can reduce stiffness and create chatter during machining. It is unnecessary to completely isolate the tool and workpiece from the machine.
3. Extraneous EMFs from temperature differences at secondary junctions can

alter the temperature measurement. Lead wires of a material with low thermoelectric power with the tool material, such as alumel, should be used.

Oxley and Hastings [27] show that the tool-work thermocouple method adequately predicts interface temperatures from machining theory. Although the researchers reported a discrepancy between the interface temperature predicted with machining theory and tool-work thermocouple measurements, the two values show the same trends as cutting speed increases. This finding indicates that the tool-work thermocouple method can reliably predict temperature changes.

The tool-work thermocouple is also capable of measuring interface temperature with flood coolant application. Kurimoto and Barrow [28], as well as Shaw et al. [15], utilized the tool-work thermocouple for experiments with flood coolant to measure interface temperature. Both researchers concluded that flood coolant did not penetrate the tool-chip contact region and, therefore, did not cause any short-circuiting.

From measurements taken with a tool-work thermocouple, the effect of cutting fluids on tool-chip interface temperature is uncertain. Under flood-coolant conditions, Shaw [2] found that the effectiveness of coolant decreased as feed and speed increased. It was suggested that at higher feed rates, the increased cutting pressure made it difficult for coolant to penetrate the contact region. Kurimoto and Barrow [28] reported similar results, with coolant effectiveness diminishing above feeds of 0.1 mm/rev for cutting plain carbon steel.

Under MQL and flood conditions, while using a tool-work thermocouple, Dhar et al. [19] reported a reduction in temperature under MQCF during turning of 1040 steel at a feed rate of 0.2 mm/rev. Straight oil was delivered to the rake face of the tool at a rate of

200 ml/hr, which decreased the interface temperature by roughly 75°C, or 10%. The effectiveness of MQL was improved at low speeds and feeds, similar to Shaw's observations, as previously mentioned. MQL generally outperformed flood coolant in reducing interface temperature, but as cutting speed increased, the temperature difference between flood and MQL was reduced.

With flood coolant shown to have a small impact on the tool-chip interface temperature, remote methods provide an alternative approach to measuring temperatures away from the tool-chip interface. At all cutting speeds, temperatures away from the interface can be reduced by cooling of the tool [8]. A remote thermocouple is usually placed between the tool and shim, as seen in Figure 2.3. Despite the fast response time of the thermocouple itself, conduction of heat through the tool is slow, requiring up to 20 seconds to reach steady state, as reported by Li and Liang [20] and Ren [29], who both used remote thermocouples placed between the tool and shim.

To improve the response time, thermocouples can be inserted into the bulk of the tool via a small hole in the tool. Ay et al. [30] used nine thermocouples inserted at different locations inside of the tool, improving response time to less than 1 second. The strategic placement of thermocouples allowed for an understanding of the temperature gradients in the tool, which cannot be achieved by the other methods mentioned in this section.

With the advancement of computing power and finite element models, remote thermocouples have been paired with finite element solvers to determine the heat flux through the chip-tool interface by using the remote temperature measurement as a boundary condition. Jayal [31] used remote thermocouple temperature measurements to calculate temperatures at the tool-chip interface, accounting for change in thermal

conductivity in the tool. It was found that MQL conditions did not have a significant effect on the tool-chip interface heat flux, but flood coolant greatly reduced both heat flux and temperature. MQL conditions, however, are targeted cooling solutions—applying coolant and/or lubricant, where necessary, in areas of concentrated, high temperatures. Remote measurement methods, especially at large distances away, may not be capable of measuring the targeted cooling that would not have as large of an effect on the bulk temperature of the tool.

2.2 Thermal Modeling Methods for Machining

Thermal models of the machining process can be divided into three categories: empirical, numerical, and analytical. Many of the first attempts at modeling the machining process used empirical models, which fit curves to experimental data. These studies are outlined in detail by Finnie [3], who describes many of the first experimental methods to understand the machining process. As shown by Taylor's [5] extensive research in the early 1900s, empirical models require considerable amounts of data and are restricted to variables that can be measured. Further, experimental data are only accurate for the conditions in which the study was performed and cannot predict without extrapolation. It is an inefficient way to understand machining given the infinite combinations of tools, work materials, and processes.

2.2.1 Finite Element Methods

Advancements in computing over the past 30 years have led to an increase in numerical finite element models. However, there is not a single model that can simulate

the wide range of cut conditions, materials, and geometries in machining [32]. Finite element models rely on accurate material data (elastic constants, flow stress, friction, density, thermal conductivity, specific heat, etc.) at the extreme conditions of machining. For many common materials, these data do exist, but significant uncertainties need to be addressed. In addition to a reliable material model, a realistic friction model must be developed for the tool-chip interface. High strains in the machining process result in highly distorted elements, but advancements in remeshing methods have greatly improved the accuracy and solution convergence for the extreme element distortions caused by the machining process [6]. While these methods have improved, finite element models are also computationally expensive with CPU times in excess of four hours [33]. Despite the challenges, finite element models have been proven to be reliable for dry machining [32].

Despite the success with dry machining, finite element models lack the ability to incorporate coolant conditions. With established knowledge of the shear plane and frictional heat source, simplified finite element models only investigate the heat transfer in machining and disregard the deformation process. Much like the analytical models discussed in the next section, the finite element heat transfer models assume heat is generated at the shear plane and tool-chip interface. These models provide an understanding of thermal profiles and effectiveness of coolant in the chip and tool, as described in [34], [35], [14], and [36], and as discussed in greater detail in Section 2.2.5.

2.2.2 Analytical Thermal Modeling

Analytical models give insight into the fundamental mechanics of the inherently complex machining process, providing an efficient method to study the effects of cutting

parameters. Analytical thermal modeling solutions for heat generation in the machining process provide a solution that is less computationally expensive than that from thermal finite element models. Most models [11], [37], [38] assume 2-D orthogonal turning with a continuous chip and are based off of the moving heat source approach, originally proposed by Jaeger [39]. Jaeger's solution can be used to model the shear plane as a moving heat source through an infinite solid, i.e., the chip. At the tool-chip interface, the frictional heat source can be modeled using Carslaw and Jaeger's [40] solution for a rectangular, stationary heat source conduction into a solid.

The analytical solutions developed and discussed in this section can be quickly solved, are not iterative, and do not have grid-dependence. The moving heat source model is a heat-transfer-based approach that does not take the material's flow stress characteristics into consideration. The moving heat source models are, however, highly dependent on the thermal properties of the workpiece and the tool, which are functions of temperature.

Early studies on chip temperature focused primarily on the shear plane heat source. The shear plane heat source analytical model is developed from Jaeger's [39] moving heat source solutions for heat conduction in solids. Hahn [11] applied the classical moving heat source solution to orthogonal metal cutting theory to model the shear plane heat source as an oblique moving band through an infinite solid. This model was adequate for predicting shear plane temperature, but did not account for the frictional heat source and did not evaluate temperatures at the tool-chip interface.

Chao and Trigger later [37] modified Hahn's model to consider the chip as a semi-infinite medium and analyzed temperatures at the interface between the chip and tool. Their analysis included both the shear plane and the frictional heat sources. To model

temperature rise in the chip, the shear plane was considered a moving heat source and the frictional heat source was considered stationary. Their method eliminated the need to partition heat between the workpiece and chip at the shear plane, as this is an exact analytical solution [41].

The aforementioned models only looked at the temperatures in the chip, but it is well known that tool temperatures are directly linked to tool life [4]. Heat from both the shear plane and frictional heat sources conduct into the tool through the tool-chip interface. Using the classical solution by Jaeger [40], conduction of the frictional heat generated at the interface can be modeled as a rectangular, stationary heat source.

The model used in this research is based on Komanduri and Hou's [23], [41], [42] modification, and combination of Chao and Trigger's [41] chip side solution with Jaeger's [40] tool side solution. Komanduri and Hou implemented a new common coordinate system that could be used to solve the temperature rise in the shear plane and frictional heat source in both the chip and in the tool.

Komanduri and Hou superimpose temperature fields generated by the two heat sources. It is assumed that, since the tool and the chip are in intimate contact, the temperatures calculated at the interface must be equal. To equate the temperatures on the tool side of the interface to the chip side of the interface, the flow of heat generated at the interface must be partitioned. The model assumes that the uniformly heated source is non-uniformly partitioned between the chip and the tool. In other words, a varying percentage of the heat flows into the tool *or* into the chip. This partitioning is used to equate the temperatures on either side of the interface and to describe where the heat flows.

To solve for the partition of heat taken between the chip and tool at the interface,

Komanduri and Hou [42] used Chao and Trigger's [10] functional analysis approach. The functional analysis approach solves for a nonuniform partition function of the heat generated at the interface to equate temperatures on both sides of the interface. This method iterates on different coefficients to "direct" the flow either into the tool or into the chip. The iterative procedure is slow, especially with high-resolution calculations.

Stephenson [43] experimentally investigated analytical steady-state temperature models and their accuracy using tool-work thermocouple measurements and infrared measurements. He compared measurements to Boothroyd [24], Loewen and Shaw [12], Wright [44], and Venuvinod and Lau [45] for cutting 1018 steel, CA360 brass, 2024 aluminum, and gray cast iron. These models generally overestimated measured temperatures, but gave reasonable approximations of mean interface temperature. Loewen and Shaw's model and Venuvinod and Lau's model were most accurate and are based on the moving heat source method.

While the moving heat source models predict average tool-chip interface temperatures well, the assumption of a uniform frictional heat source with a nonuniform distribution along the tool-chip interface does affect the validity of the modeled distribution. Komanduri and Hou's [23] model concentrates high temperatures near the end of the contact length, which does not agree with experimental measurements that generally show the areas of highest temperatures near the middle of the contact length [8]. Huang and Liang [46] first addressed this discrepancy, adding a nonuniform heat intensity based on sticking and sliding friction zones at the tool-chip interface. M'Saoubi and Chandrasekaran [47] applied variable tool-chip contact friction conditions on the rake surface that produced a distribution much closer to experimental measurements, as seen in

Figure 2.4.

The moving heat source thermal models discussed here have proven to be accurate for calculating temperature distributions in the machining process, but they are far from comprehensive, predictive machining models. Often in the literature, the moving heat source model is used to visualize and explain rather than to predict the distribution of temperatures because the model inputs are outputs of the machining process.

The moving heat source models require *a priori* knowledge of machining outputs including: cutting forces, contact length, chip thickness, and even shear plane temperature. Shear plane temperature is used to evaluate thermal properties, as suggested by Chao and Trigger [10]. However, unless the shear plane temperature is directly measured, there is not a way to calculate it without the use of another model.

Karpat and Özel [48] incorporated Oxley's [49] model, discussed in the next section, to create a more comprehensive temperature distribution analytical model. Oxley's model was used to calculate the cutting forces, contact length, chip thickness, and thermal properties used as inputs for the thermal model. Their study showed good agreement with prediction of cutting forces for both aluminum and steel, but lacked experimental validation of interface temperature or remote tool temperature.

2.2.3 Slip Line Models

Understanding the shear zone is vital to understanding the physics of the machining process. Merchant's [7] shear plane theory explains the relationship with shear plane angle and cutting force. The Merchant equation explains that increasing the shear plane angle decreases cutting forces, reducing the energy required to perform the cut, which in turn

reduces temperature [50].

Lee and Shaffer [51], expanding upon the work of Merchant, applied plasticity theory to the shear plane. They assumed that the shear plane represents a direction of maximum shear stress. Their work laid the foundation for Oxley [52] to develop the most comprehensive analytical model to date, creating a machining theory model that relates workpiece material properties, cutting conditions, and cutting geometry.

Oxley's model, discussed in full in his book [49], is predictive for plain carbon steels based on extensive research and the development of a material model of flow stress at high strain rates and temperatures. With a given set of machining inputs, the model can predict cutting forces, chip geometry, tool-chip contact length, shear plane temperature, and interface temperature for dry machining. The temperatures reported are average temperatures for the interface and shear plane. Oxley does not account for the distribution of temperatures, heat flow into the tool, or the tool material properties.

2.2.4 Models for Predicting Tool-Chip Contact Length

Tool-chip contact length is the distance that the chip is in contact with the tool, starting from the cutting edge, as shown by L in Figure 2.5. Heat generated by the shear plane is conducted through the chip and into the tool through the tool-chip contact length. Additionally, frictional heat is generated at the tool-chip interface by sticking and sliding as the chip flows over the tool.

Understanding tool-chip contact length is essential to understanding temperatures in the machining process. Thermal analysis of cutting tools is highly dependent on contact length, which is an input to all thermal models [53]. Sadik and Lindstrom [54] pointed out that contact length is an important parameter in tool life and, therefore, temperature.

Shorter contact lengths resulted in higher temperatures near the cutting edge, which in turn reduced tool life.

Gad et al. [53] reviewed several existing models that predict tool-chip contact length, with many based on the shear zone theory. Many of the models required fitting of extensive experimental data and generally fall in the range of +/-20% of experimental measurements. The most reliable measurement of tool-chip contact length for predictive temperature models is to use empirical equations by conducting experiments and curve-fitting experimental data.

2.2.5 Thermal Models with Coolant Conditions

The analytical models discussed in this section are only able to calculate the temperature of the tool-chip interface under dry conditions. There is limited literature of work towards an expansion of an analytical model to predict the decrease in tool-chip interface temperature with coolant application. Additionally, thermal analytical models are highly dependent on contact length and thermal conductivity, both of which are outputs of the machining process.

In order to develop a model to estimate the cooling ability of cutting fluids, the heat transfer characteristics must be well understood. The primary mode of heat transfer for coolant is convection. Estimating the heat transfer coefficient of the cutting fluid is crucial to understanding the effect that cooling can have on the interface temperature. Previously, studies have used experimental measurements to calculate the convection coefficient based on the measured temperature decrease at the interface. These models all assume forced convection over a defined area.

Many studies have measured the interface temperature decrease due to coolant application, but few have attempted to quantify and predict the heat removed with modeling. Childs [14] approximated the heat transfer coefficient in the range of 10^3 – 10^4 W/m²-K using experimental measurements combined with a finite element model. The boundary conditions of the model imposed convective heat transfer on all of the free surfaces of the tool, labeled S_h in Figure 2.6. The free surfaces of the workpiece and chip are modeled as adiabatic in order to reduce computational time. Childs argued that the adiabatic surfaces have little effect on the tool temperature, which was the primary focus of the study. For the heat generation from the shear plane and frictional heat source, it is assumed that the distribution is uniform, though it is known that the distribution of heat along the interface is dependent on location along the tool-chip interface.

In the analysis of convection coefficients by Li et al. [34], [55], it was assumed that forced convection occurred on all free surfaces of the chip and tool, as seen in Figure 2.7. Their model also incorporated a nonuniform distribution of heat along the tool-chip interface, calculated using Oxley's [52] machining theory. The complex model resulted in similar convection coefficients to Childs, with a reported convection coefficient of 7600 W/m²-K on the rake face behind the chip. Greater convection coefficients were observed in other regions of the model, such as cooling on the top surface of the chip, which resulted in a convection coefficient up to 23,000 W/m²-K. However, the additional cooling on the free surfaces only resulted in a maximum temperature decrease of $\sim 50^\circ\text{C}$.

Both of the studies discussed in this section reported small changes in tool-chip interface temperature, indicating that the magnitude of heat generated during a machining process is significantly greater than the heat that can be removed from forced convection.

The simplified model by Childs [14] and complex model by Li et al. [35] both resulted in maximum tool-chip interface reductions of $\sim 50^{\circ}\text{C}$, which is less than 10% in both cases.

The adiabatic boundary conditions used by Childs are the same as the boundary conditions assumed in the moving heat source model. The moving heat source model could be further expanded by adding convective cooling boundaries to the free surfaces of the tool, which would provide a less computationally-expensive alternative to the finite element method. Lowewen and Shaw [38] recognized that bulk cooling of the tool with liquid carbon dioxide or a liquid-vapor mist was an effective way to reduce tool-chip interface temperatures without decreasing cutting speed or depth of cut, but never expanded their moving heat source-based model to account for cooling.

Their suggestion is the basis for this research, as little work has been done in the way of expanding the moving heat source model to accommodate bulk cooling of the tool. Li and Liang [20] expanded the model by adding another rectangular stationary heat source to the flank face of the tool to model rake face cooling. The magnitude of the cooling heat rate was estimated from the convection coefficient, which was calculated by Nusselt and Reynolds numbers of the dry-air flow. The magnitude of the cooling heat rate was two to three orders of magnitude smaller than the heat generation of the primary shear zone, resulting in a small drop in interface temperature (8.1% decrease from dry).

Li and Liang [20] did not investigate cooling of the rake face of the tool, which is where the highest temperatures are concentrated. However, the chip-tool interface is difficult and often inaccessible due to blockage by the chip. With proper targeting and a more effective cooling fluid, however, the rake face of the tool could work as a better heat sink to remove heat from the tool and, thus, the tool-chip interface.

Li and Liang's [20] assumption of dry air may be valid if evaporative cooling does not take place, which is the case with using oil, but cooling could be improved with a cutting fluid that has evaporative cooling properties, such as water. As suggested by Loewen and Shaw [38], liquid-water evaporative cooling has the potential to provide a significant cooling effect, but convection coefficients for mist cooling are largely unexplored in machining literature.

To estimate the heat transfer coefficient, the evaporative cooling process of the tool can be modeled as an impinging jet of an air-water mixture onto a hot plate. At the temperatures observed in machining near the tool-chip interface, which are often over 500°C, film boiling is likely to occur since the water impinges on a surface above the Leidenfrost temperature [56]. Film boiling creates a vapor layer that insulates the heated surface and results in a decrease in heat flux [56], as seen in Figure 2.8.

Sozbir et al. [57] performed a mist impinging jet experiment with water droplet flow rates ranging from 0–575 ml/hr sprayed with compressed air onto a heated plate at 500°C. Their results concluded that heat transfer coefficients can be estimated in the range of 500 W/m²-K with dry air to 2000 W/m²-K with 575 ml/hr of water. Their results show that mist cooling is beyond the 1000 W/m²-K threshold determined by Childs [14] for an observable reduction in interface temperature. It was also observed that the Leidenfrost temperature decreased as nozzle exit velocity increased, which resulted in better heat transfer.

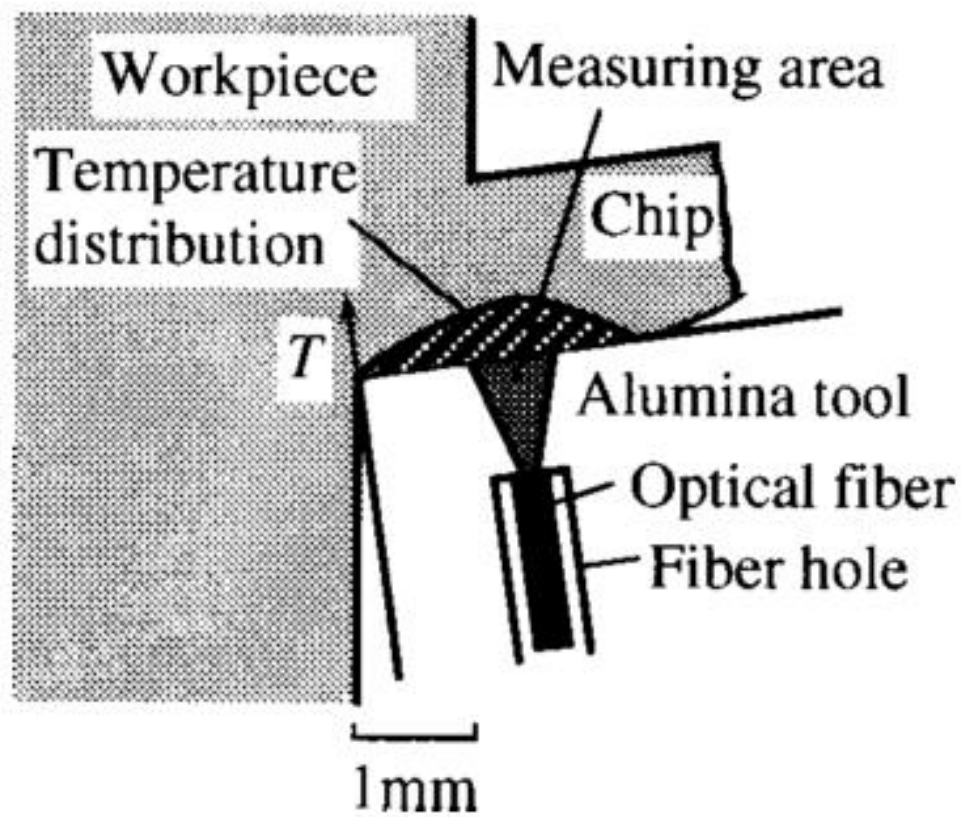


Figure 2.1: Two color pyrometer (adapted from [18]).

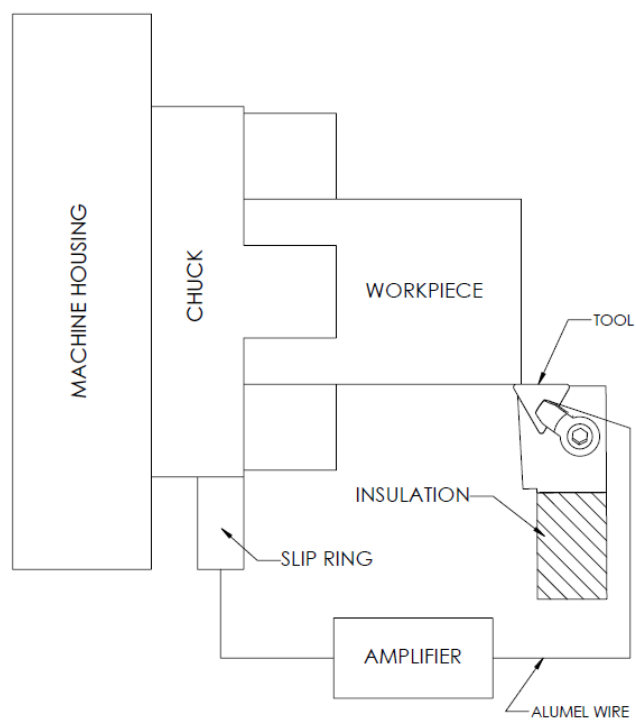


Figure 2.2: Tool-work thermocouple diagram.

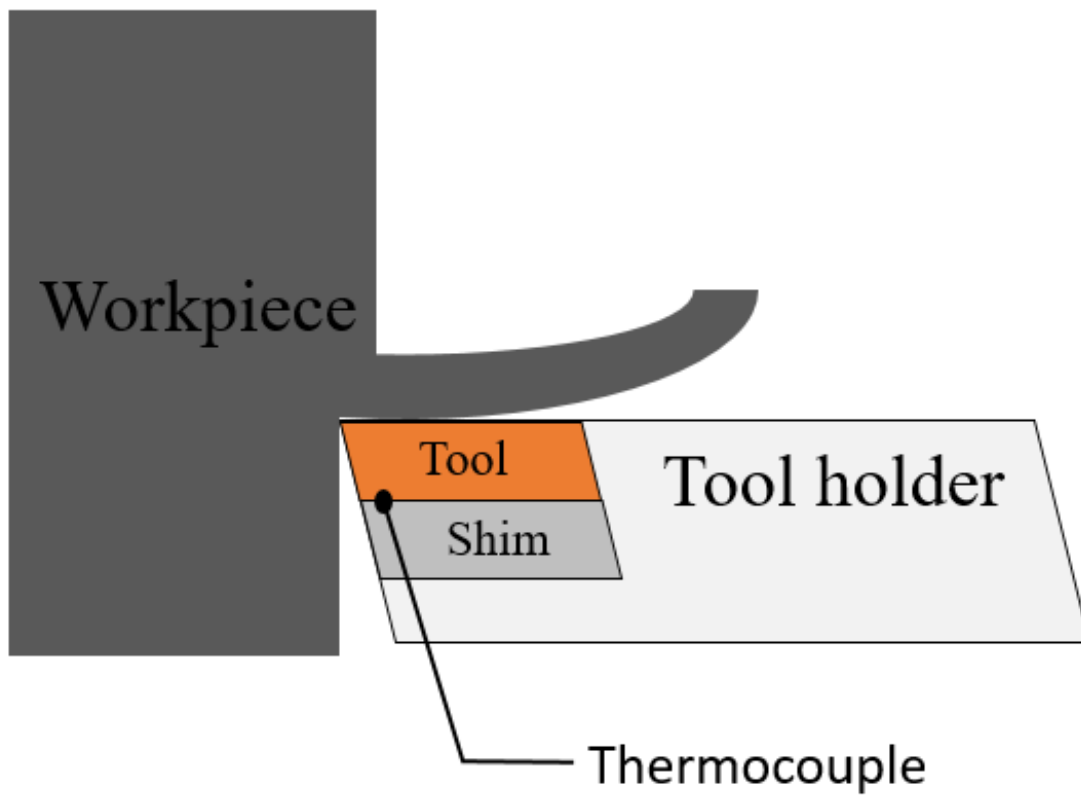


Figure 2.3: Remote thermocouple diagram.

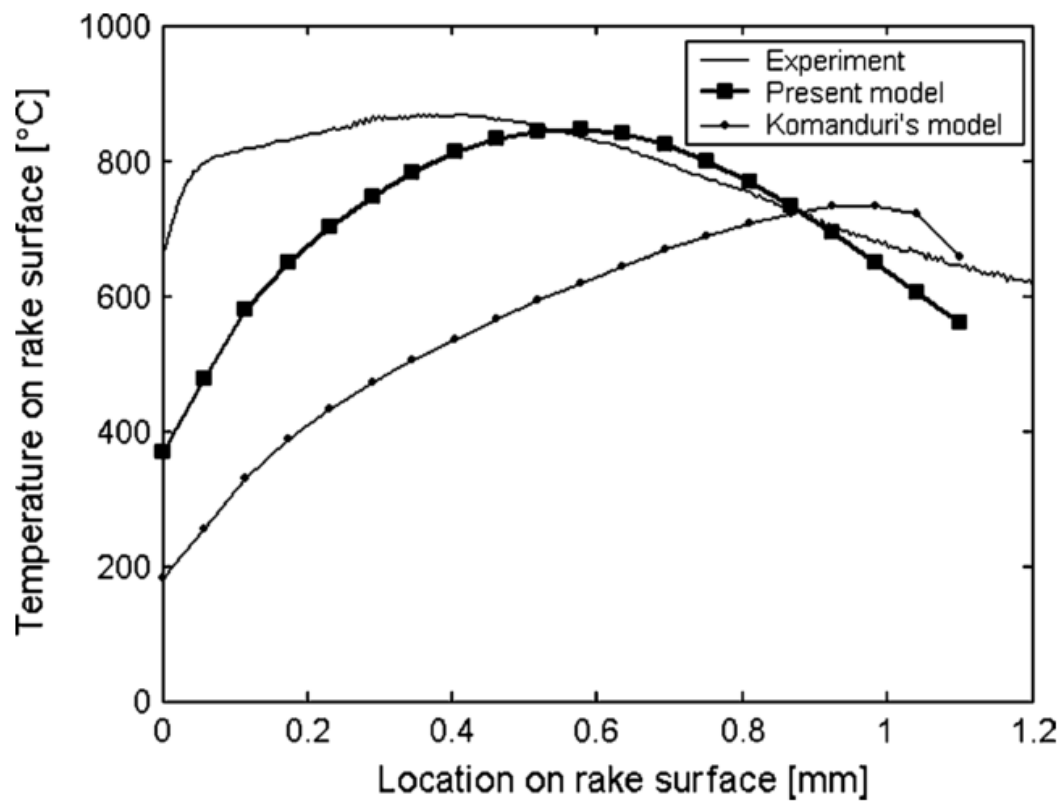


Figure 2.4: M'Saoubi and Chandrasekaran's updated Komanduri and Hou model with nonuniform frictional heat source (adapted from [47]).

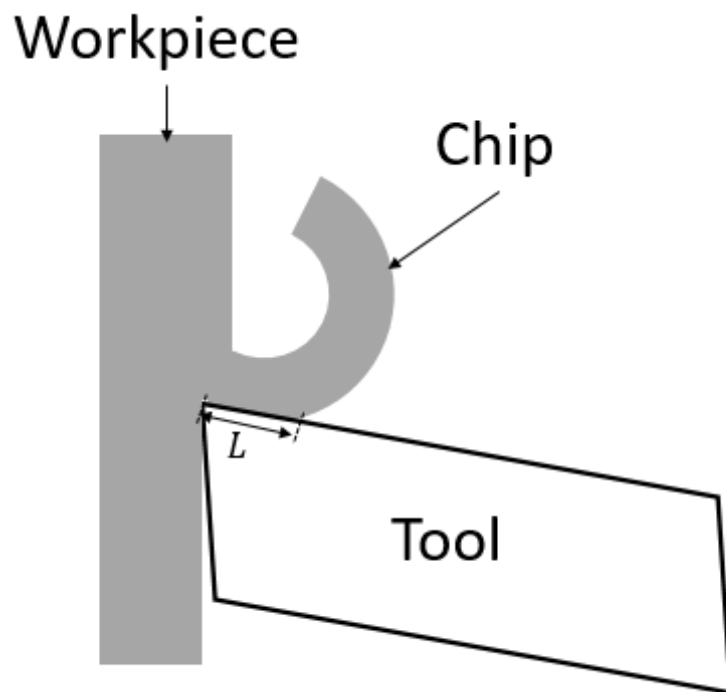


Figure 2.5: Diagram of tool-chip contact length.

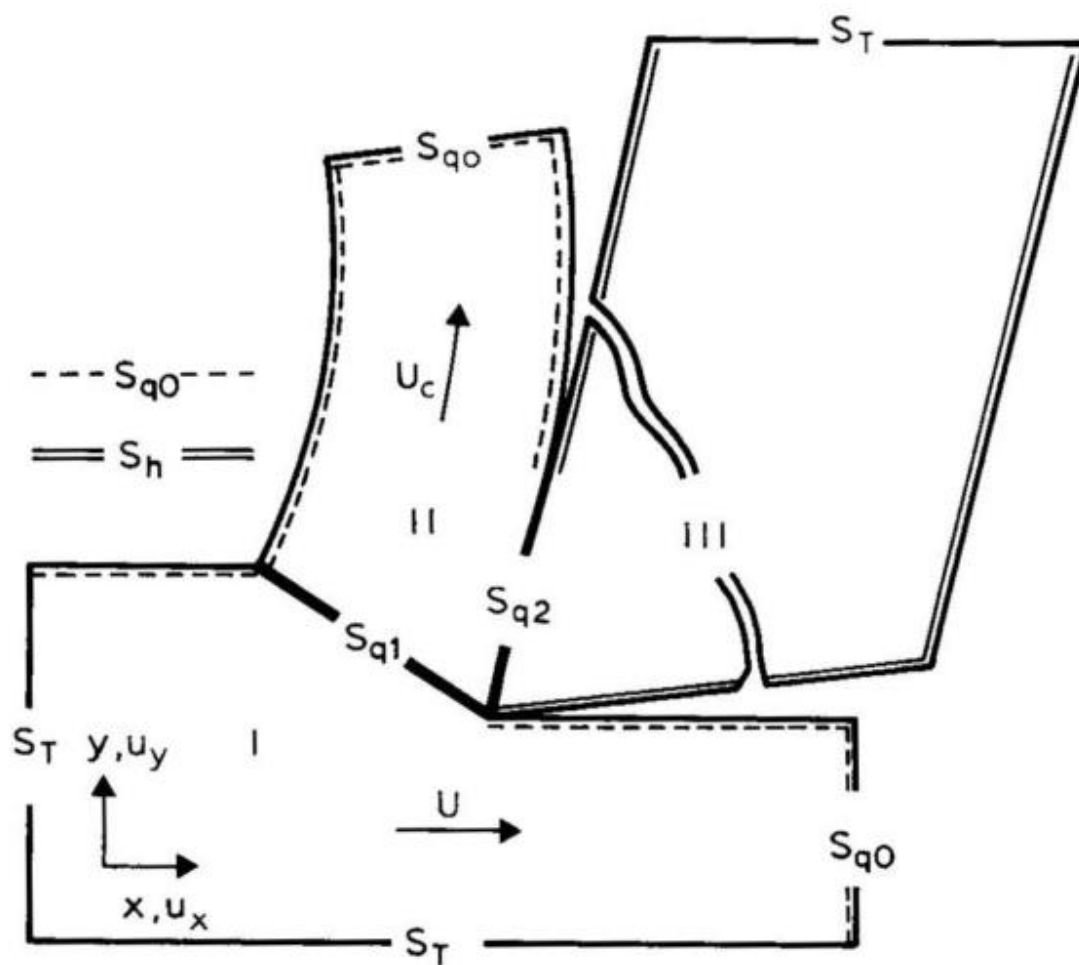


Figure 2.6: Diagram of boundary conditions used by Childs (adapted from [14]).

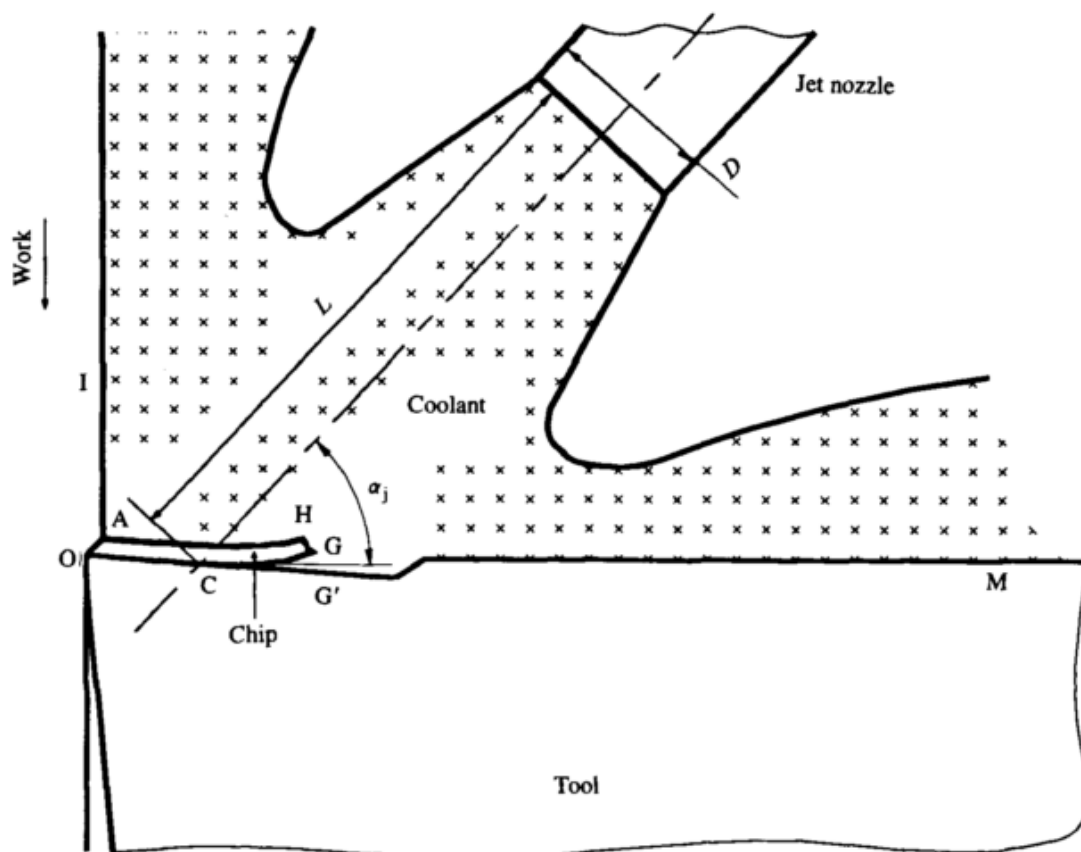


Figure 2.7: Diagram of Li and Oxley coolant model (adapted from [34]).

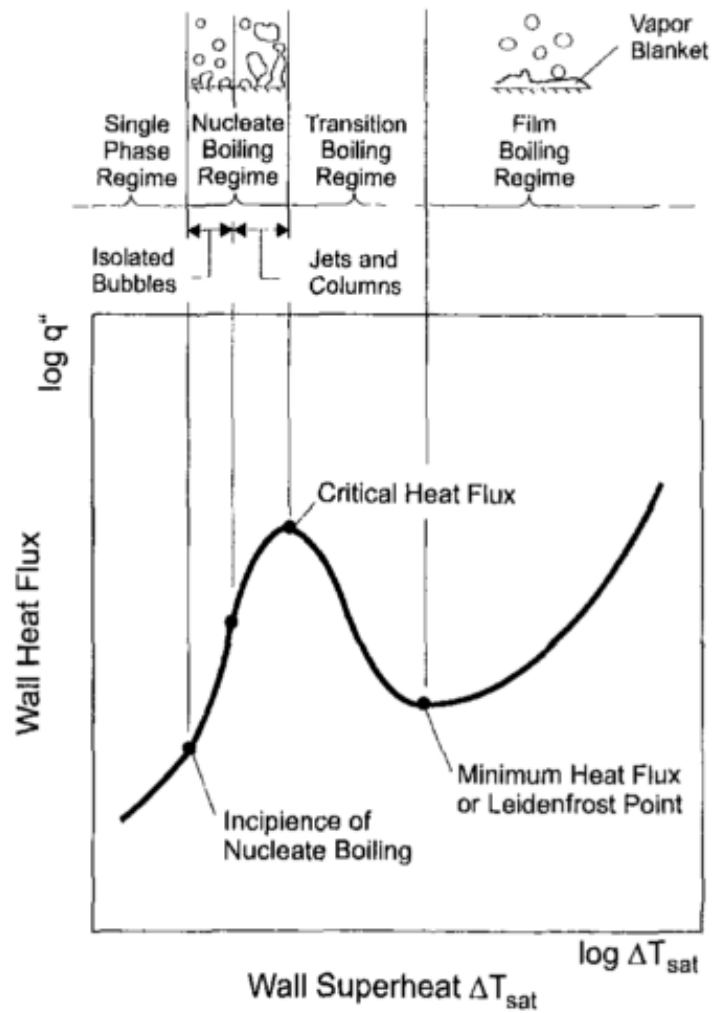


Figure 2.8: Heat flux as a function of wall temperature for film boiling (adapted from [58]).

CHAPTER 3

MODEL METHODOLOGY AND EXPERIMENT PLAN

This chapter discusses the methodology of the proposed analytical model for calculating temperature in the tool and chip. Section 3.1 discusses the model methodology, giving an overview of the equations used, new solving method developed, and new convective cooling additions. In order to determine the magnitude of the heat removed by convective cooling, parameterized by the effective heat transfer coefficient, an experiment plan is discussed in Section 3.2

3.1 Model Methodology

The proposed model for this research is based on Komanduri and Hou's dry machining model. The model discussed in this section adds convective cooling to the rake and flank surfaces of the tool to model coolant application. A new solving method is discussed that eliminates an iterative procedure for equating the interface temperature at the tool-chip interface. The new solving method produces comparable results significantly faster than the iterative functional analysis method used by Komanduri and Hou [42]. The computational time reported by Komanduri and Hou is 5-10 seconds per point, whereas the proposed solver is approximately 0.001 second per point because of the direct solving method used. The code for the model can be seen in Appendix A.

3.1.1 Inputs

The model proposed uses a combinations of cut parameters, such as speed and feed rate, along with experimental measurements to predict the steady-state temperature rise at any point in the chip or the tool. A complete list of model inputs, symbols, and units can be seen in Table 3.1 and a flowchart of the model can be seen in Figure 3.1.

3.1.2 Calculation Heat Source Values

The model first calculates the intensity of the shear plane and frictional heat source. Machine and tooling parameters for cutting speed (V), depth of cut (t_{cut}), width of cut (b), and rake angle (α) are used as inputs to the model. Cut force (F_{cut}), thrust force (F_{thrust}), tool-chip contact length (L), and chip thickness (t_{ch}) are also model inputs that must be measured experimentally or calculated using some other means, such as Oxley's model. Machining theory equations, outlined by Shaw [2] and Boothroyd [24], are used to calculate the heat generated during the metal cutting process. Chip thickness ratio (r), chip velocity (V_{ch}), shear angle (ϕ), friction force (F_{fr}), length of the shear plane (L_{AB}), heat generation by the frictional heat source (q_f), and heat generation by the shear plane heat source (q_{sp}) are calculated in equations (1)-(7).

$$r = \frac{t_{cut}}{t_{ch}} \quad (1)$$

$$V_{ch} = V * r \quad (2)$$

$$\phi = \text{atan}\left(\frac{r \cos(\alpha)}{1 - r \sin(\alpha)}\right) \quad (3)$$

$$F_{fr} = F_{cut} \sin(\alpha) + F_{thrust} \cos(\alpha) \quad (4)$$

$$L_{AB} = \frac{t_{ch}}{\cos(\phi - \alpha)} \quad (5)$$

$$q_f = \frac{F_{fr} V_{ch}}{Lb} \quad (6)$$

$$q_{sp} = \frac{F_{cut} V}{L_{AB} b} - \frac{F_{fr} V_{ch}}{L_{AB} b} \quad (7)$$

3.1.3 Temperature Change Caused by Shear Plane Heat Source

A diagram of the shear plane heat source in the chip can be seen in Figure 3.2, which is used to calculate the temperature rise at any point in the chip. The shear plane heat source is assumed to be uniform and is divided into differential elements, dw_i , that are distance w_i from the tip of the tool. The subscript i denotes points along the differentially segmented heat sources. The image heat source is imposed on the chip to enforce the adiabatic boundary condition on the top surface of the chip. This is explained in greater detail by Komanduri and Hou [41].

The temperature rise caused by to the shear plane heat source at any point in the chip can be calculated with equation (8). The inside of the integral in represents a non-dimensional temperature, which is a function of the distance away from the heat source.

$$\begin{aligned} \Delta T_{ch,sp}(X, z) &= \frac{q_{sp}}{2\pi\lambda_{ch}} \int_0^{L_{AB}} e^{-(X-X_i)V_{ch}/2a_{ch}} \left\{ K_0 \left[\frac{V_{ch}}{2a_{ch}} \sqrt{(X-X_i)^2 + (z+z_i)^2} \right] \right. \\ &\quad \left. + K_0 \left[\frac{V_{ch}}{2a_{ch}} \sqrt{(X-X_i)^2 + (2t_{ch}-z-z_i)^2} \right] \right\} dl_i \end{aligned} \quad (8)$$

where

$$l_i = 0 \text{ to } L_{AB}$$

$$X_i = L - w_i \sin(\phi - \alpha)$$

$$z_i = w_i \cos(\phi - \alpha)$$

The heat generated at the shear plane conducts through the chip and flows into the tool through the tool-chip interface. From the tool's perspective, this is a stationary heat source. This heat source is referred to as the induced shear plane heat source, q_{spi} . A diagram for heat conduction into the tool through the interface can be seen in Figure 3.3. The induced heat source on the tool-chip interface is divided along the contact length into differential elements, dx_i , that are distance l_i from the end of the contact length. In the width direction, the induced shear plane heat source is divided into differential elements, dy_i , that are distance y_i from the center of the tool. $R_{t,i}$ and $R'_{t,i}$ are the distance that the point of interest is from each of the differential elements of the induced shear plane heat source and its image heat source, respectively. The image heat source is imposed on the tool to enforce the adiabatic boundary condition on the flank face of the tool. This is explained in greater detail by Komanduri and Hou [42].

The interface of the tool ($z = 0$) must first be solved in order to determine how the induced shear plane heat source is distributed into the tool. This allows for the temperatures on the chip side and the tool side of the interface. The temperature rise in the tool at the interface due to the induced shear plane heat source, q_{isp} , is first calculated in equation (9). The magnitude of the induced heat source is unknown and can be solved for by increasing the magnitude incrementally until the average temperature on the tool side matches the average temperature calculated for the chip side.

$$\Delta T_{t,isp}(X, z = 0) = \frac{q_{isp}}{\pi \lambda_t} \int_{-\frac{w}{2}}^{\frac{w}{2}} \int_0^L \left(\frac{1}{R_{t,i}} + \frac{1}{R'_{t,i}} \right) dy_i dx_i \quad (9)$$

where

$$R_{t,i} = \sqrt{(x - x_i)^2 + (y - y_i)^2 + z^2}$$

$$R'_{t,i} = \sqrt{(X - 2L + x_i)^2 + (y - y_i)^2 + z^2}$$

Once the average temperatures at the interface for the tool side and chip side match, temperatures can then be equated on both sides of the interface with the induced heat source distribution coefficient, S_{isp} , as seen in equation (10). Equations (9) and (10) can be multiplied together to find the shear plane's temperature rise contribution to any point in the tool with equation (11).

$$S_{isp}(x_i) = \frac{\Delta T_{ch,sp}(x_i, z = 0)}{\Delta T_{t,sp}(x_i, z = 0)} \quad (10)$$

$$\Delta T_{t,sp}(X, z) = S_{isp} \frac{q_{isp}}{\pi \lambda_t} \int_{-b}^b \int_0^L \left(\frac{1}{R_{t,i}} + \frac{1}{R'_{t,i}} \right) dy_i dx_i \quad (11)$$

3.1.4 Temperature Change Caused by the Frictional Heat Source

A diagram of the frictional heat source for the chip side can be seen in Figure 3.4, which is used to calculate the temperature rise at any point in the chip. It is assumed that the distribution of the frictional heat source is uniform. The frictional heat source is divided into differential elements, dx_i , that are distance l_i from the end of the contact length. $R_{ch,i}$ and $R'_{ch,i}$ are the distance that the point of interest is from each of the differential elements of the frictional heat source and its image heat source, respectively.

A diagram for the frictional heat source on the tool side can be seen in Figure 3.5. The frictional heat source is divided along the contact length into differential elements, dx_i , that are distance l_i from the end of the contact length. In the width direction, the frictional heat source is divided into differential elements, dy_i , that are distance y_i from

the center of the tool. $R_{t,i}$ and $R'_{t,i}$ are the distance that the point of interest is from each of the differential elements of the frictional heat source and its image heat source, respectively.

The interface ($z = 0$) must first be solved to determine the partitioning of the frictional heat source between the chip in the tool. The chip side can be solved with equation (12) and the tool side can be solved with equation (13).

$$\begin{aligned} \Delta T_{ch,f}(X, z = 0) &= \frac{q_f}{\pi \lambda_{ch}} \int_0^L e^{-(X-l_i)V_{ch}/2a_{ch}} \left[K_0 \left(\frac{R_{ch,i}V_{ch}}{2a_{ch}} \right) \right. \\ &\quad \left. + K_0 \left(\frac{R'_{ch,i}V_{ch}}{2a_{ch}} \right) \right] dx_i \end{aligned} \quad (12)$$

where

$$\begin{aligned} R_{ch,i} &= \sqrt{(X - x_i)^2 + z^2} \\ R'_{ch,i} &= \sqrt{(X - x_i)^2 + (2t_{ch} - z)^2} \\ \Delta T_{t,f}(X, z = 0) &= \frac{q_f}{\pi \lambda_t} \int_{-\frac{w}{2}}^{\frac{w}{2}} \int_0^L \left(\frac{1}{R_{t,i}} + \frac{1}{R'_{t,i}} \right) dy_i dx_i \end{aligned} \quad (13)$$

where

$$\begin{aligned} R_{t,i} &= \sqrt{(x - x_i)^2 + (y - y_i)^2 + z^2} \\ R'_{t,i} &= \sqrt{(X - 2L + x_i)^2 + (y - y_i)^2 + z^2} \\ x_i &= 0 \text{ to } L \end{aligned}$$

With both sides solved at the tool-chip interface, the distribution coefficients can be determined. The distribution coefficient determines what percentage of the heat flows into the tool and what percentage flows into the chip. The temperature rise calculated for

the chip side must match the tool side. The two temperatures can be equated with a tool side distribution coefficient, $S_{t,f}$, and a chip side distribution coefficient, $S_{ch,f}$, as seen in equation (14).

$$\Delta T_{t,f} S_{t,f} = \Delta T_{ch,f} S_{ch,f} \quad (14)$$

Substituting $S_{t,f} = 1 - S_{ch,f}$ into equation (14) and rearranging, $S_{ch,f}$ can be solved for in equation (15).

$$S_{ch,f}(x_i) = \left(\frac{\Delta T_{ch,f}(x_i, z = 0)}{\Delta T_{t,f}(x_i, z = 0)} + 1 \right)^{-1} \quad (15)$$

With the frictional heat source distribution coefficient determined, the temperature rise due to the frictional heat source can be solved at any point in the chip with equation (16) and at any point in the tool with equation (17).

$$\begin{aligned} \Delta T_{ch,f}(X, z) = S_{ch,f} \frac{q_f}{\pi \lambda_{ch}} \int_0^L e^{-(X-l_i)V_{ch}/2a_{ch}} \left[K_0 \left(\frac{R_{ch,i} V_{ch}}{2a_{ch}} \right) \right. \\ \left. + K_0 \left(\frac{R'_{ch,i} V_{ch}}{2a_{ch}} \right) \right] dx_i \end{aligned} \quad (16)$$

$$\Delta T_{t,f}(X, z) = S_{t,f} \frac{q_f}{\pi \lambda_t} \int_{-\frac{w}{2}}^{\frac{w}{2}} \int_0^L \left(\frac{1}{R_{t,i}} + \frac{1}{R'_{t,i}} \right) dy_i dx_i \quad (17)$$

3.1.5 Temperature Change Cause by the Rake Cooling Heat Source

A diagram for the rake cooling source, q_{rc} , on the tool side can be seen in Figure 3.6. The cooling heat source is divided along the tool-chip contact length into differential elements, dx_i , that are distance $L_c + x_{i,r}$ beyond the end of the contact length. In the width direction, the frictional heat source is divided into differential elements, dy_i , that are distance y_i from the center of the tool. $R_{t,i}$ and $R'_{t,i}$ are the distance that the point of interest

is from each of the differential elements of the frictional heat source and its image heat source, respectively.

$$\Delta T_{t,fc}(X, z) = \frac{q_{rc}}{\pi \lambda_t} \int_{-b}^b \int_0^L \left(\frac{1}{R_{t,i}} + \frac{1}{R'_{t,i}} \right) dy_i dx_i \quad (18)$$

where

$$R_{t,i} = \sqrt{(X + x_i)^2 + (y - y_i)^2 + z^2}$$

$$R'_{t,i} = \sqrt{(X - 2L + x_i)^2 + (y - y_i)^2 + z^2}$$

$$x_i = 0 \text{ to } -L_r$$

The magnitudes for the rake cooling heat source are unknown, but can be estimated with the effective heat transfer coefficient, h_{eff} , as seen in equation (19) for the rake cooling heat source. Average tool face temperatures beyond the contact length, $\bar{T}_{t,surface}$, ambient temperature, T_{amb} , and h_{eff} can be used to approximate the amount of cooling power on the rake face of the tool. The value for h_{eff} can be approximated from literature on forced convection or determined experimentally, which is discussed in the following section.

$$q_{rc} = h_{eff} * (\bar{T}_{t,surface} - T_{amb}) \quad (19)$$

The heat removed from the interface also affects the chip temperature by conduction through the interface, similar to the shear plane heat source's effect on tool temperature, as seen in Figure 3.7. The interface temperatures ($z = 0$) must match to determine how much of the cooling effect is felt by the chip. From the chip's perspective, the induced cooling heat source, q_{irc} , is modeled as a stationary heat source, similar to the frictional heat source, in equation (20). The magnitude of the induced heat source is unknown and can be solved for by increasing the magnitude until the average temperature on the chip side matches the average temperature on the tool side, which was calculated

previously in equation (18).

$$\begin{aligned} \Delta T_{ch,c}(X, z = 0) &= \frac{q_{irc}}{\pi \lambda_{ch}} \int_0^L e^{-(X-l_i)V_{ch}/2a_{ch}} \left[K_0 \left(\frac{R_{ch,i}V_{ch}}{2a_{ch}} \right) \right. \\ &\quad \left. + K_0 \left(\frac{R'_{ch,i}V_{ch}}{2a_{ch}} \right) \right] dx_i \end{aligned} \quad (20)$$

where

$$\begin{aligned} R_{ch,i} &= \sqrt{(X - x_i)^2 + z^2} \\ R'_{ch,i} &= \sqrt{(X - x_i)^2 + (2t_{ch} - z)^2} \end{aligned}$$

Once the average interface temperature changes match on the tool side and chip side, temperatures can then be equated with the induced cooling heat source distribution coefficient, S_c , with equation (21). Equations (20) and (21) can be multiplied to find the cooling temperature change contribution to any point in the tool with equation (22).

$$S_{c,i}(x_i) = \frac{\Delta T_{t,c}(x_i, z = 0)}{\Delta T_{ch,c}(x_i, z = 0)} \quad (21)$$

$$\begin{aligned} \Delta T_{ch,c}(X, z) &= S_{c,i} \frac{q_{ci}}{\pi \lambda_{ch}} \int_0^L e^{-\frac{(X-l_i)V_{ch}}{2a_{ch}}} \left[K_0 \left(\frac{R_{ch,i}V_{ch}}{2a_{ch}} \right) \right. \\ &\quad \left. + K_0 \left(\frac{R'_{ch,i}V_{ch}}{2a_{ch}} \right) \right] dx_i \end{aligned} \quad (22)$$

With temperatures calculated at every point in the chip and the tool and distribution coefficients determined, the contributions from the four heat sources can be superimposed to calculate the overall change in temperature for the chip in equation (23) and for the tool in equation (24).

$$\Delta T_{ch,total} = \Delta T_{ch,sp} + \Delta T_{ch,f} + \Delta T_{ch,c} \quad (23)$$

$$\Delta T_{t,total} = \Delta T_{t,sp} + \Delta T_{t,f} + \Delta T_{t,fc} + \Delta T_{t,rc} \quad (24)$$

3.2 Experiment Plan

Experiments were conducted to determine the effectiveness of coolant as an input for q_{rc} in the model. The measured temperature change can be used to determine what value of q_{rc} and h_{eff} result in the same temperature change in the model

3.2.1 Workpiece

The experiment used discs of AISI 1045 hot rolled steel. The steel was used in its as-manufactured condition and was not annealed. A single workpiece was used to ensure proper tool-work thermocouple calibration. The workpiece was 127 mm (5 in) in diameter and approximately 101 mm (4 in) in length.

3.2.2 Tooling

All experiments used a flat faced Kennametal TPGN 322 insert (Figure 3.8) with a single layer TiN (KC730) coating applied by physical vapor deposition (PVD). The tool was held by a Kennametal CTFPR-123B facing tool holder with a $+5^\circ$ rake angle and an 11 degree clearance angle (Figure 3.9). The tool is fed into the workpiece at a 90° angle, resulting in near orthogonal conditions. The small nose radius, R , results in a third, axial component of force. However, this force is very small relative to the cut and thrust force.

3.2.3 Cut Conditions

The experiment used a facing operation with near-orthogonal cut conditions. A 2 mm width of cut was made at a cutting speed of 200 m/min. Feed rate was originally 0.2 mm/rev, but was reduced to 0.05 mm/rev based on results published by Shaw [2], who found that coolant was ineffective at reducing tool-chip interface temperature at high feed rates.

3.2.4 Fluid Conditions

For MQCF, water was applied as a mist at flow rates of 150, 300, and 500 ml/hr using the MQCF delivery device developed in the Sustainable Manufacturing Lab [22]. Water was chosen to specifically study the cooling effectiveness and not the lubricating effect. Water was pumped through tubing to a co-axial nozzle aimed at the rake face of the tool. Air supplied at 345 kPa (50 psi) flowed around the outside of the tubing and combined with the water to form a mist at the outlet of the nozzle. The nozzle, as seen in Figure 3.10, was approximately 2 inches away to ensure proper wetting of the rake face. For flood conditions, a 1:20 mixture of Cimcool Cimtech 310 synthetic coolant was aimed at approximately the same location on the rake face.

3.2.5 Temperature Measurement

Figure 3.11 shows a diagram of the experimental setup and the placement of the tool-work thermocouple circuitry. The tool-work thermocouple wire was held in contact with the tool by the tool holder's clamp. The other wire was connected to the chuck via a slip ring. The slip ring allowed for constant contact to complete the tool-work

thermocouple circuit. An Omega Super MCJ thermocouple amplifier was used for temperature measurements. The experimental setup is shown in Figure 3.12.

The tool-work thermocouple was calibrated in the lathe, similar to the method used by Leshock and Shin [59]. The workpiece was heated in a furnace to 250°C and then placed in the jaws of the lathe. A standard type-K thermocouple was used to measure the temperature of the workpiece in the lathe. The tool was then moved in contact with the workpiece to complete the tool-work thermocouple circuit and the amplified voltage was recorded. The voltage-temperature relationship of the tool-work thermocouple can be seen in Figure 3.13. During postprocessing, the voltage recorded during the experiment could then be converted to a temperature using a linear fit. A moving average of 20 points was used to smooth experimental data.

3.2.6 Force Measurement

A Kistler 9121 dynamometer measured force components in the cut, radial, and axial directions. The directions of the force vectors for the facing experiment are shown in Figure 3.14. Temperature and force measurements were recorded by a LabView data acquisition program at 1000 samples per second.

3.2.7 Tool-Chip Contact Length

Tools used for contact length measurements only performed one cut of equal length. When viewed under the digital microscope, it was revealed that contact length did vary slightly along the width of the cut. Contact traces at 5 different locations along the width of the cut were measured with a digital microscope and the average was taken to account

for variation.

3.2.8 Chip Measurements

Chips were collected during the experiment by placing a tray under the workpiece. Chip thickness was measured with a digital caliper. Representative chips were photographed to document chip shape, color, and curl characteristics.

3.2.9 Hardness Testing

Since the hot rolled steel was not annealed, hardness testing was conducted on the workpiece to consistent properties throughout the diameter. Before hardness testing, the workpiece was lightly machined to remove scaling and band saw markings from the surface. Rockwell B measurements were recorded at various diameters and plotted.

3.2.10 Experiment Procedure

Facing experiments were conducted using near-orthogonal cutting conditions. Due to the continuous chip formation caused by flat faced tools, relatively short cuts were made to avoid chips nesting around the tool. Even when coiled, long chips would inevitably get tangled and create a nest around the tool or the workpiece. All experiments had a cut time of over 8 seconds to ensure that cutting temperatures and forces reached steady state.

Cutting fluid flow rate was varied at six different levels for the single factor experiment design. For each condition, there were three replicate measurements of temperature and force. Speed, feed, and width of cut remained constant during the experiment. Cutting fluid was applied onto the rake face of the tool from an overhead jet

at 345 kPa to ensure that the cutting fluid reached the tool surface. A set of experiments were also conducted at a higher feed rate, 0.2 mm/rev, but with no replicates. Table 3.2 outlines the cut conditions and cutting fluid conditions used in the experiment. Before each test, the starting diameter of the cut was recorded. During each experiment, data were collected at 1000 samples per second for each of the three force directions and temperature. Chips were collected, measured, and photographed. Tools were labeled and then contact length measurements were taken.

Table 3.1: List of proposed model inputs, symbols, and units.

Input	Symbol	Units
Rake Angle	α	Degrees
Depth of cut (feed)	t_{cut}	mm
Width of cut	b	mm
Cut velocity	V	m/min
Main cutting force	F_c	N
Thrust force	F_t	N
Chip thickness ratio	r	-
Tool-chip contact Length	L	mm
Chip thermal conductivity	λ_{ch}	W/m-°C
Tool thermal conductivity	λ_{tool}	W/m-°C
Chip thermal diffusivity	a	m ² /s
Tool thickness	h	cm
Clearance angle	θ	Degrees
Length of area cooled on rake face	L_{flank}	mm
Cooling power on rake face	q_{rake}	W/m ²
Cooling power on flank face	q_{flank}	W/m ²

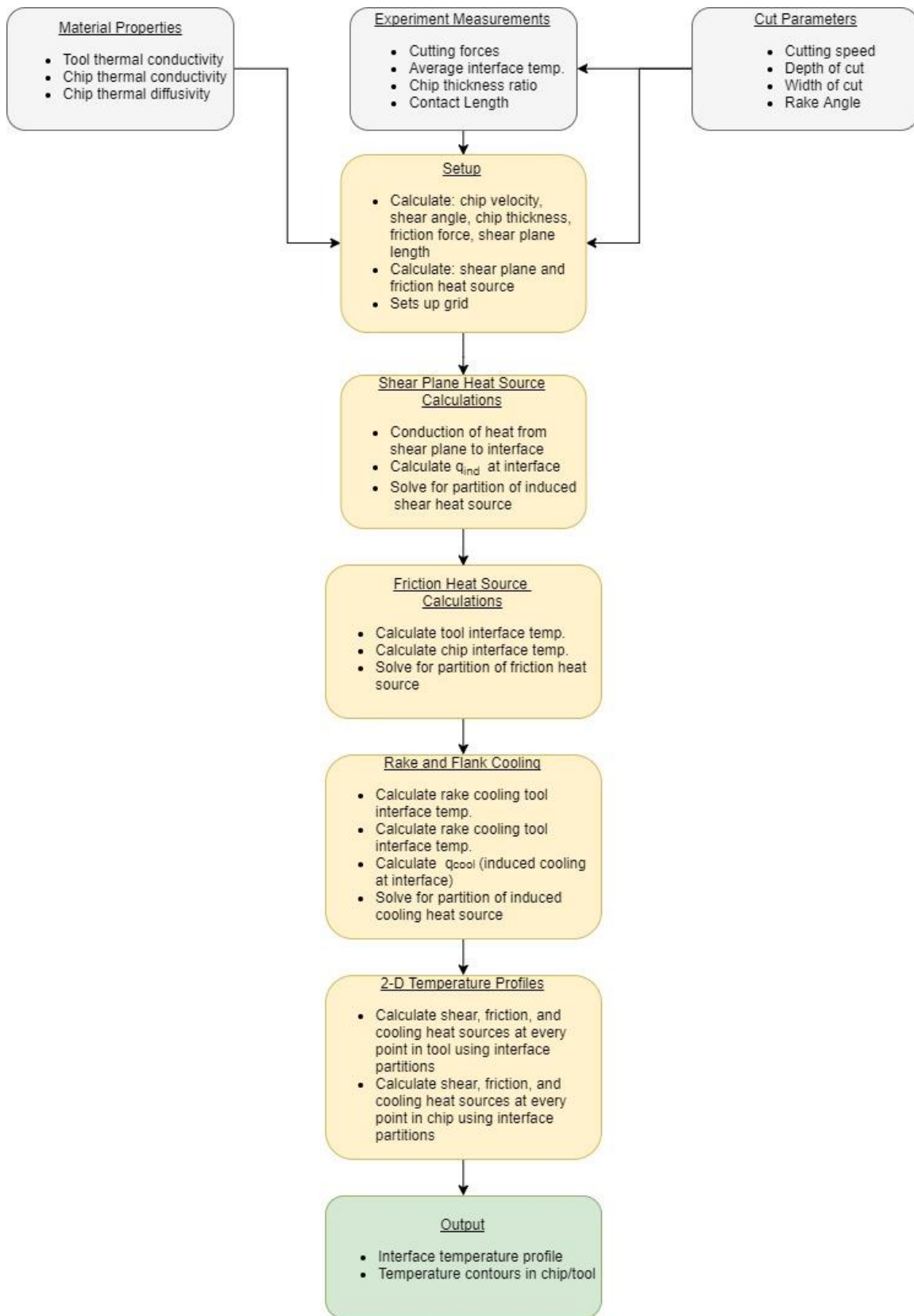


Figure 3.1: Model flow chart.

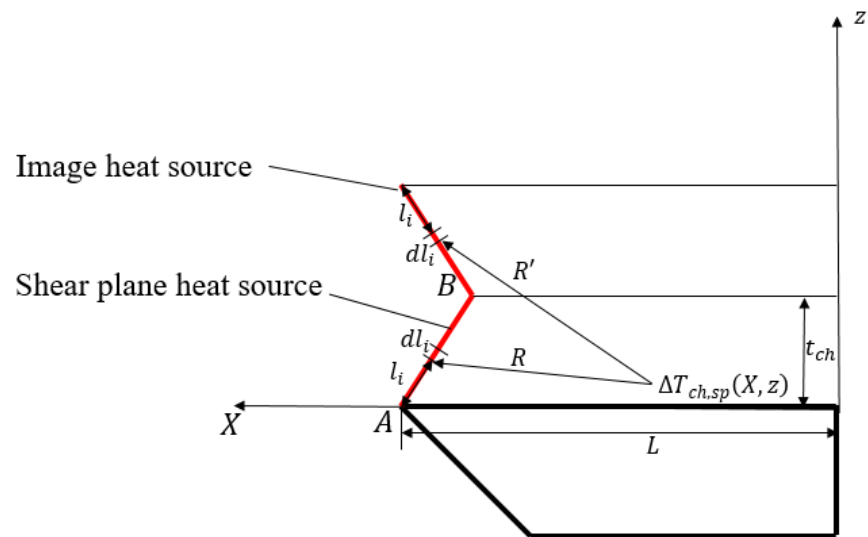


Figure 3.2: Diagram for calculating temperature change in the chip caused by the shear plane heat source.

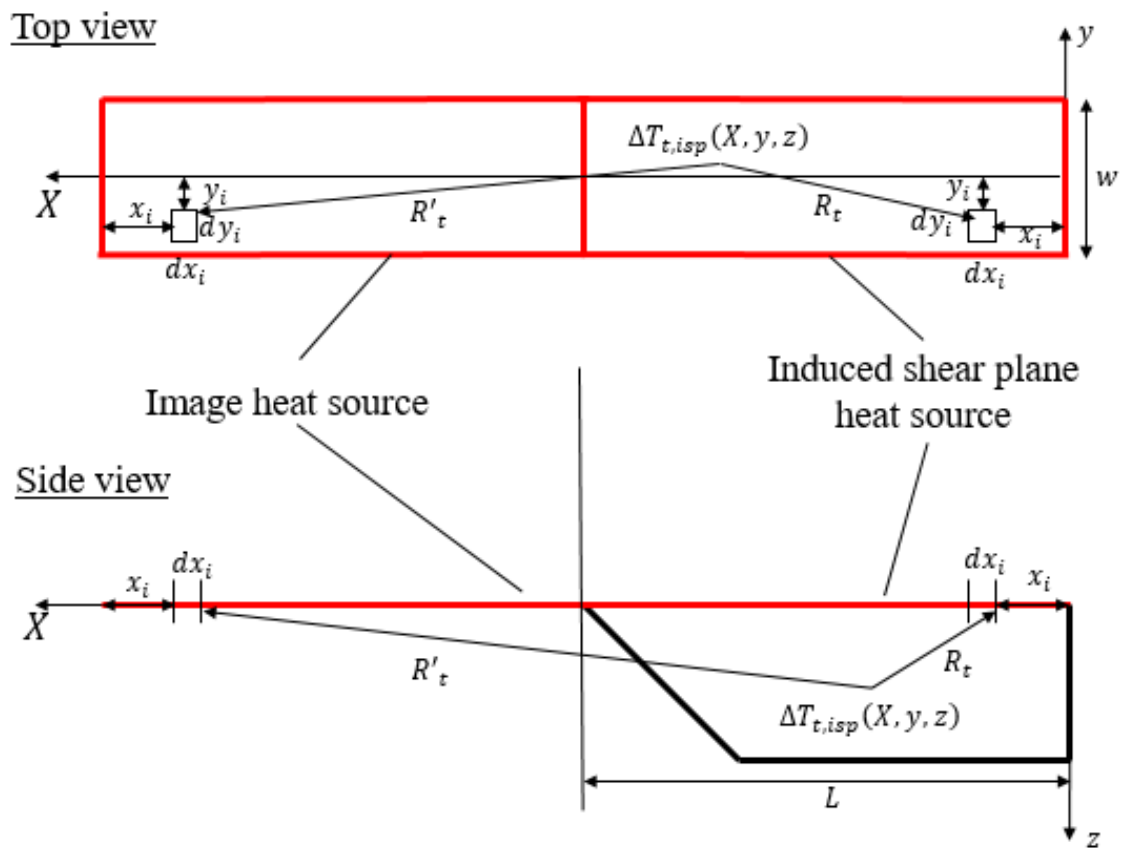


Figure 3.3: Diagram for calculating temperature change in the tool caused by the induced shear plane heat source on the tool.

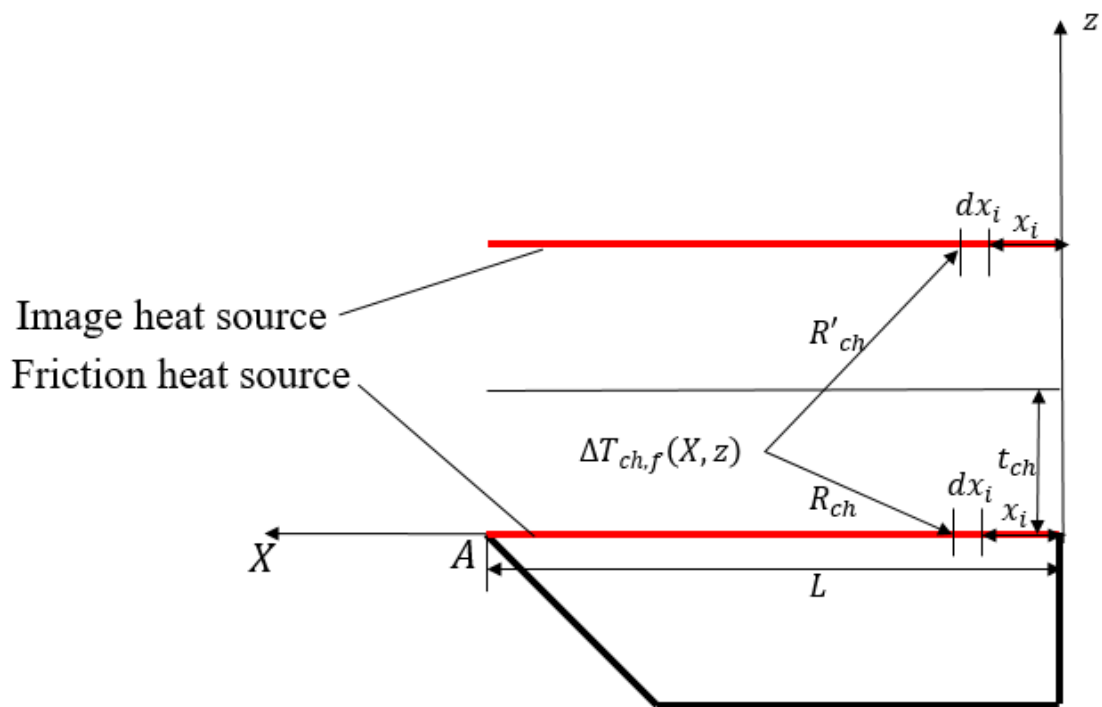


Figure 3.4: Diagram for calculating temperature change in the chip caused by the frictional heat source.

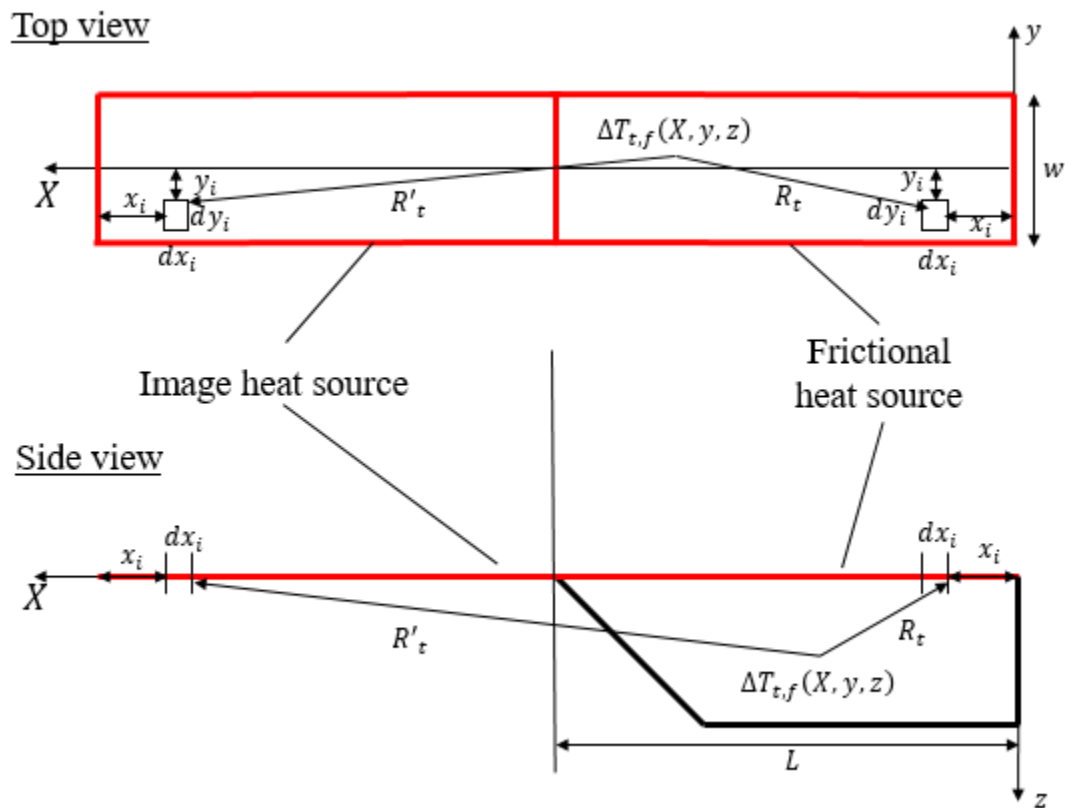


Figure 3.5: Diagram for calculating temperature change in the tool caused by the frictional heat source.

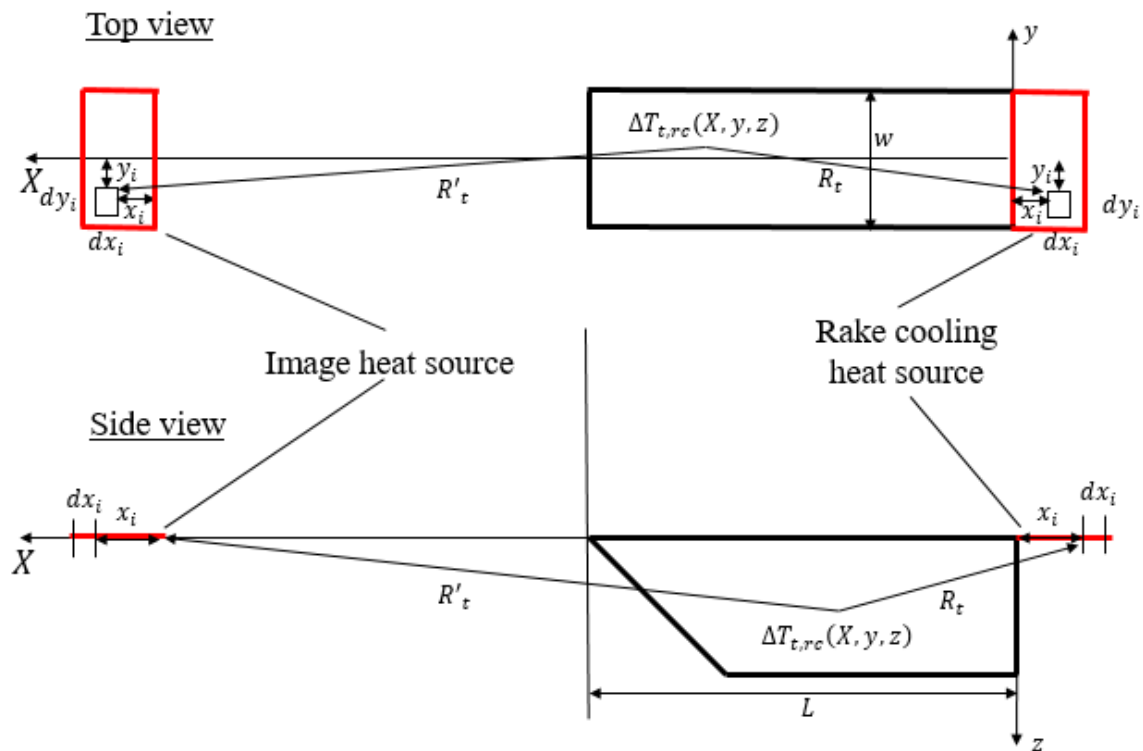


Figure 3.6: Diagram for calculating temperature change in the tool caused by the rake cooling heat source.

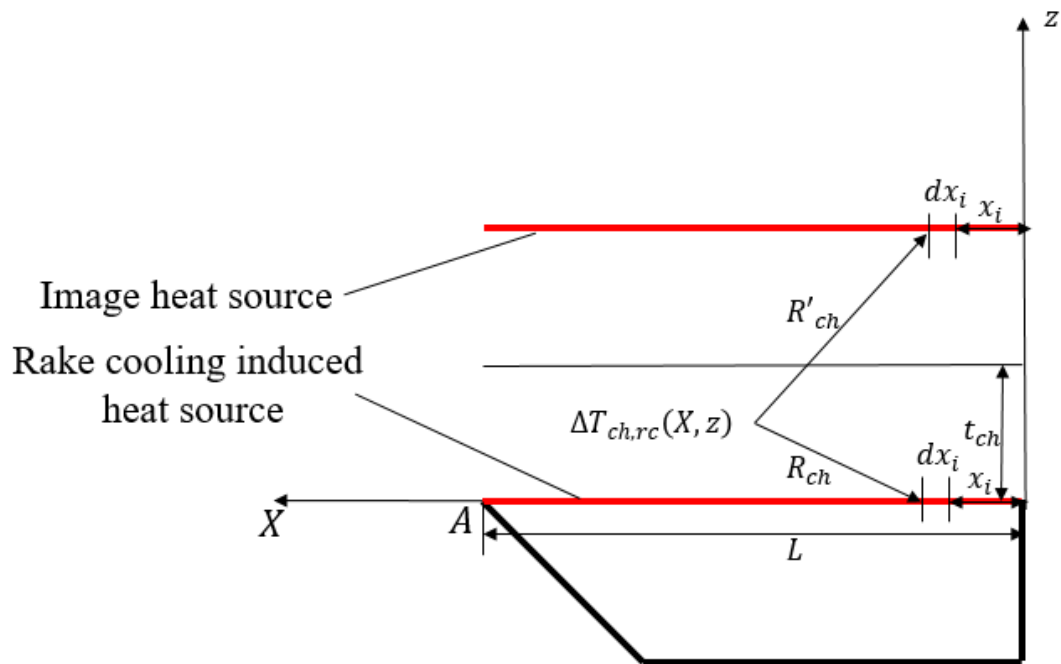


Figure 3.7: Diagram for calculating temperature change in the chip caused by the induced rake cooling heat source.

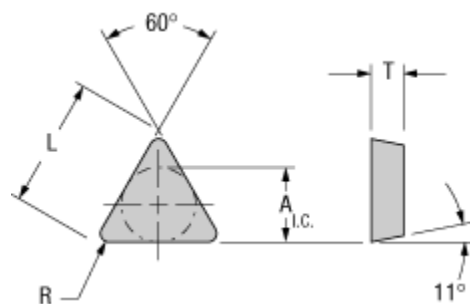


Figure 3.8: Tool geometry. A : 0.375 in., L : 0.650 in., T : 0.125 in., R : 0.031 in. (adapted from [60]).

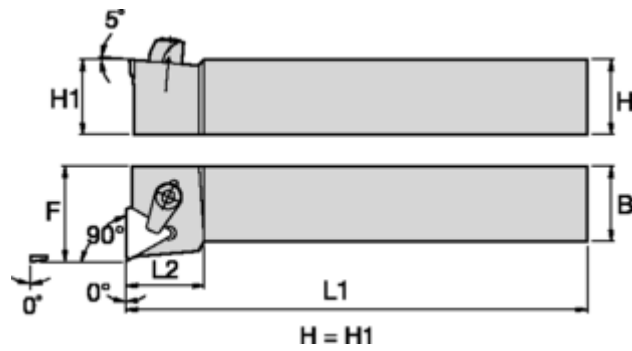


Figure 3.9: Tool holder geometry (adapted from [61]).



Figure 3.10: Nozzle orientation.

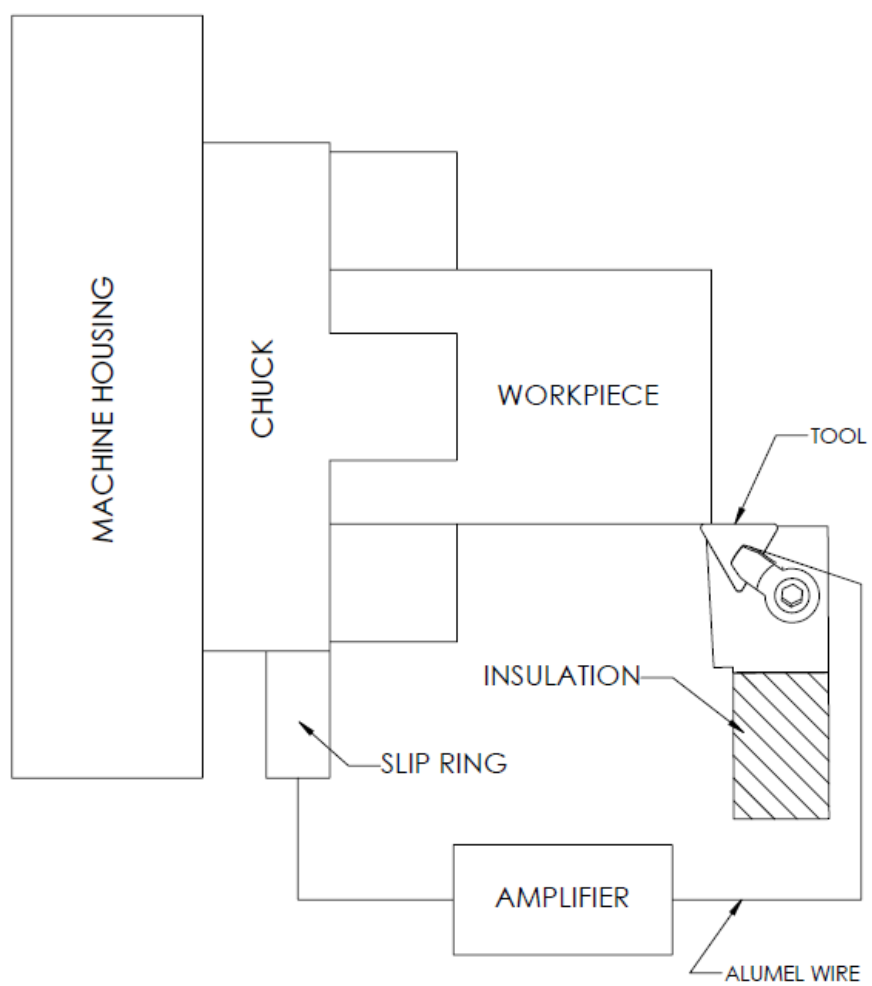


Figure 3.11: Experimental setup diagram.

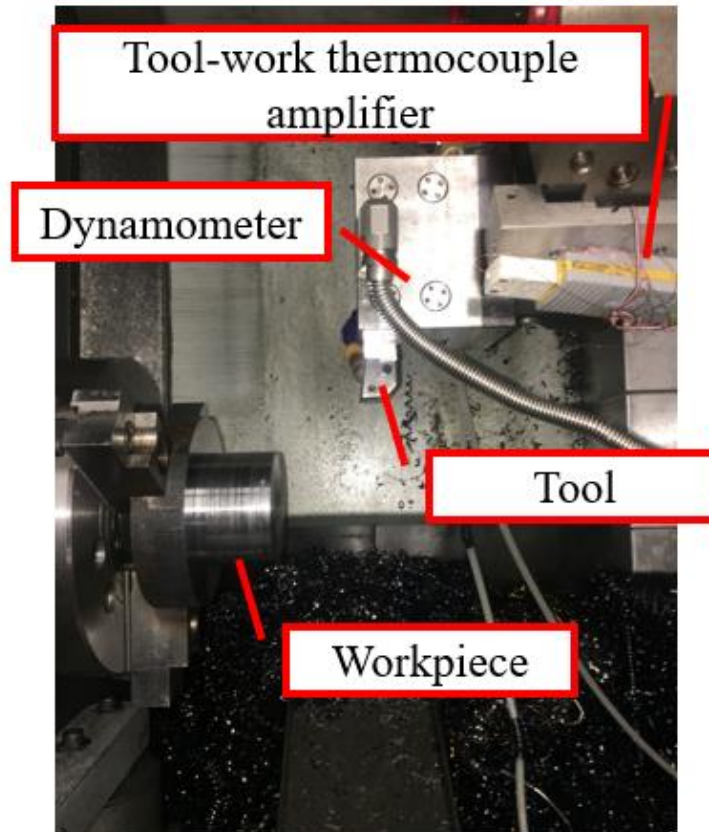


Figure 3.12: Experiment setup (slip ring not pictured).

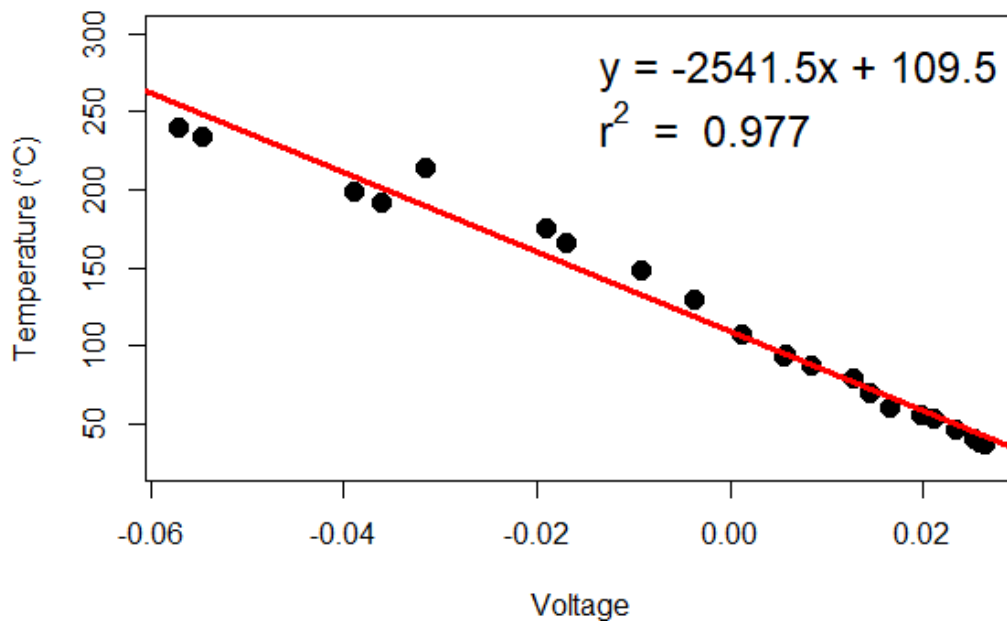


Figure 3.13: Tool-work thermocouple calibration.

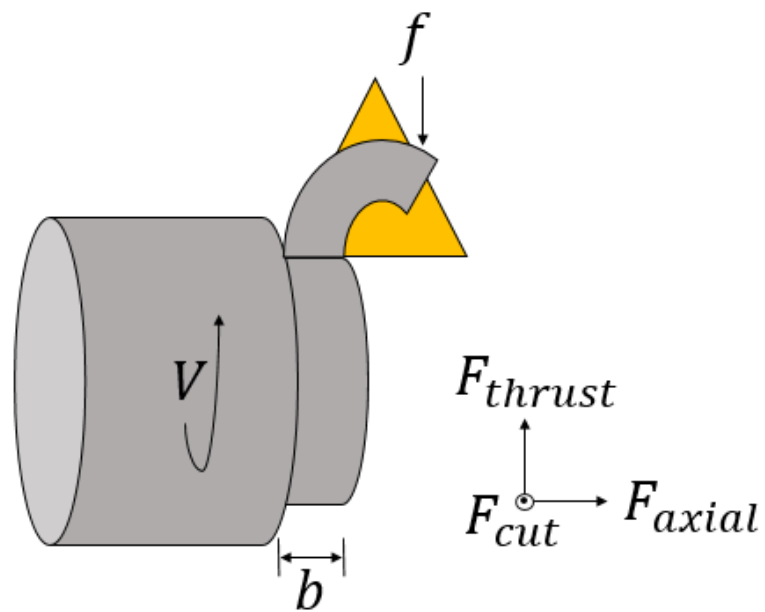


Figure 3.14: Diagram of cutting forces acting on the tool.

Table 3.2: Experiment conditions.

Variable	Level
Speed	200 m/min
Feed	0.05 mm/rev 0.2 mm/rev
Width of cut	2 mm
Rake angle	5°
Nozzle Pressure	345 kPa
cutting fluid flow rate	Dry Compressed air only (referred to as “air”) 150 ml/hr (water mist) 300 ml/hr (water mist) 500 ml/hr (water mist) 6 l/min (flood coolant)

CHAPTER 4

RESULTS AND DISCUSSION

Chapter 3 discussed the methodology of the analytical model and the experiment plan that will be used to determine the magnitude of the convective cooling power and the effective heat transfer coefficient. In this chapter, Section 4.1 presents the experiment results for cutting temperature, cutting forces, workpiece hardness, chip forms, and contact length at a feed rate of 0.05 mm/rev. Additionally, a single experiment is presented to compare the coolant effectiveness at an increased feed rate of 0.2 mm/rev. Section 4.2 discusses the results in detail, with an effort to explain the effects that cutting fluid application had on the machining process.

Section 4.3 discusses the proposed model, with two methods of validation and an analysis on the numerical integration grid dependence. With experimental measurements, the dry conditions are modeled using the proposed model. Furthermore, the magnitude of the convective cooling heat source applied to the rake face of the tool is determined from experimental measurements. The effective heat transfer coefficient is then determined based on the experimental temperature decrease and discussed. Finally, experimental measurements are used to compare the modeled temperature difference between low feed (0.05 mm/rev) and high feed (0.2 mm/rev) to the measured temperature difference in an attempt to validate the model.

4.1 Experiment Results

4.1.1 Tool-Chip Interface Temperature

An example of the tool-work thermocouple measurements during experiments can be seen in Figure 4.1. Temperature measurements quickly reach steady state and remain constant throughout the 8-second cut. Flood coolant did not reach a steady state until 3.5 seconds after the test began. The noise between 1 second and 3.5 seconds could be due to a discontinuous chip. Once a continuous chip formed, interface temperature stabilized.

Figure 4.2 and Table 4.1 show the average tool-chip interface temperature measured with the tool-chip thermocouple. Dry cutting conditions resulted in an average interface temperature of 978°C. The average interface temperature decreases with increased cutting fluid flow rate, but due to the scattered data and low sample size, the reduction in interface temperature is statistically insignificant at fluid flow rates below 500 ml/hr. Statistically significant reductions in interface temperature, calculated with a t-test, were observed at 500 ml/hr and flood flow rates with temperature reductions of 56°C (5.8%) and 158°C (16.2%) relative to dry, respectively.

4.1.2 Cutting Forces

Cut, thrust, and axial forces were comparable at all minimum quantity cutting fluid measurements. These results indicate that the water mist acted primarily as a coolant and did not lubricate the tool-chip interface. Since water could not be used for the flood application, a synthetic coolant was used that is designed for metal cutting operations to both cool and lubricate, which reduced all components of force. Reduced forces decrease interface temperature, indicating that some of the cooling ability of flood may be attributed

to the lubricating properties.

Increased cutting forces resulted in higher temperature measurements, as seen in Figure 4.4. The relationship between force and temperature has statistical significance, indicating that a reduction in force may be a driving factor in reduction of temperature. However, large variations in cut force are not causing large variations in temperature. For example, under dry conditions, the measured cut force varied from 196 N to 314 N, a -30% to 13% change from average. Over the wide range of forces, however, the temperature only varied from 937°C to 1003°C, a -4% to 3% change from average.

4.1.3 Effect of Workpiece Diameter

Figure 4.5 shows that at inner diameters, the cut force is reduced. In particular, dry cut force is reduced from 314 N to 196 N at the outermost diameter to the innermost diameter. It was suspected that this was caused by microstructure and hardness changes during the cooling process of hot rolled steel, but hardness testing proved that there is no change in hardness throughout the diameter range used during the experiment. The work material had consistent properties throughout and annealing was not necessary.

Figure 4.6 shows that at all start diameters, a common trend of decreased temperature with increased flow rate can be seen. Dry, air, and 150 ml/hr performed similarly. 300 ml/hr, 500 ml/hr, and flood all had distinct measurements below dry conditions at the same diameter.

4.1.4 Chips Forms

Cutting fluid application had no measurable effect on chip thickness. Continuous chips were formed that did not automatically break by curling. Dry cuts resulted in chips that formed nests around the cutting tool, compressed air and 150 ml/hr produced a variable chip that would either coil or nest, and 500 ml/hr and flood resulted in a tightly coiled chip. Images of representative chips can be seen in Figure 4.7.

Temperature can also be estimated from chip color based on the tempering colors of steel [62]. Increase in coolant resulted in lower tempering temperatures of the chip. Dry chips had a light blue tint, followed by shades of blue and brown for air, 150, and 300 ml/hr. Flood and 500 ml/hr had metallic color. Although this is not a quantitative measurement, it gives a qualitative understanding that coolant application is changing the temperature in the chip.

4.1.5 Tool-chip Contact Length

Tool-chip contact length decreased with increased cutting fluid flow rate, with dry having the longest tool-chip contact length and 500 ml/hr and flood having the shortest, 0.23 mm and 0.12 mm, respectively. Cooling caused a significant reduction in tool-chip contact length, indicating that there is an indirect friction altering effect at the tool-chip interface. Contact length measurements can be seen in Figure 4.8 and images of measurements at each flow rate can be seen in Table 4.2.

Contact length is likely also related to chip nesting. Conditions prone to nesting (dry, air, 150 ml/hr) all had longer contact lengths than conditions with better cooling. Instead of tightly coiling, the chip produced flows over more area of the tool, which

ultimately hits the clamp and results in a nest.

4.1.6 Temperature Rise with an Increased Feed Rate

One set of experiments were conducted at a feed rate of 0.2 mm/rev as seen in Figure 4.9 and Table 4.3. With an increase in feed, forces tended to increase and therefore caused a temperatures increase. The measured temperature difference caused by coolant application was small and likely caused by noise in the temperature measurement signal. Contact length and forces were relatively unchanged by the application of cutting fluid. No replicates were conducted as these experiments served primarily to determine if a measurable temperature drop could be observed.

4.2 Experiment Discussion

Although statistically significant, the drop in interface temperature caused by minimum quantity cutting fluid delivery is practically insignificant at just 56°C (5.8%) relative to dry. Under MQCF conditions, other researchers have also reported small changes in interface temperature. With a remote thermocouple measurement and moving heat source-based model to inversely calculate interface temperature, Li and Liang [20] predicted an 8.1% drop in interface temperature under MQL conditions compared to dry. It was assumed that forced convection was removing heat from the flank face of the tool, but as previously shown in this research, forced convection of dry air alone does not produce a measurable decrease in interface temperature. This was also confirmed by Ueda et al. [25], who found that air had little effect on reducing the temperature of the interface under intermittent turning conditions. Even with direct access to the contact area, forced

convection of dry air alone does not produce a measurable decrease in interface temperature. Since the temperature was measured with a remote thermocouple between the tool and shim, Li and Liang's [20] measured 10% temperature drop may be due to bulk cooling of the tool. Cutting forces also decreased due to the lubricating effects of the vegetable oil, which could account for some of the measured temperature decrease.

All minimum quantity cutting fluid conditions had comparable average force measurements relative to dry. This result reassures us that the reduction in interface temperatures observed can be attributed to the cooling ability of the evaporative water mist and not to a reduction in forces due to lubrication. The experiment shows that targeted evaporative cooling of the tool is an effective way to reduce interface temperature at low feed rates.

Cutting force has a relationship with temperature and diameter. However, comparing tests performed at the same diameters still shows a cooling effect. As cuts were made deeper into the workpiece, forces were reduced, which in turn reduced interface temperature. Although hardness was unchanged, there may have been microstructural changes throughout the diameter of the workpiece that caused forces to decrease. Although lower forces contributed to lower temperatures, Figure 4.6 showed that temperature could be further reduced with cutting fluid application at all diameters. In other words, the decrease in forces alone would not produce the drop in temperature observed during coolant application.

Cooling caused a significant reduction in contact length at the tool-chip interface, indicating that there is an indirect friction altering effect due to in-situ thermal changes at the tool-chip interface. A possible explanation for the change in contact length is due to

the curl characteristics of the chip changing as fluid is applied. Cutting fluid is targeted at the rake face of the tool, but fluid also comes in contact with the top surface of the chip. Increased cooling on the top surface of the chip creates a larger thermal gradient in the chip. The chip behaves like a bi-metallic spring, curling away from the higher temperatures at the tool-chip interface [63]. This results in a tightly coiled chip, which was observed in high flow rate MQCF experiments.

The tightly coiled chip changes the friction characteristics of the machining process by reducing the sliding contact region. The sticking region of contact may be the same under all conditions, but the sliding region of contact is likely changing due to the changing curl of the chip. As the chip is coiled more tightly, the sliding region of contact decreases. This results in a smaller contribution of the frictional heat source, which in turn results in lower temperatures in the tool.

The application of cutting fluid reduces the temperature of the tool's surface, effectively changing the thermal conductivity. Thermal conductivity of the TiN coating as well as the tungsten carbide tool decreases with temperature [64]. Balaji et al. [65] found that reduced thermal conductivity results in a shorter tool-chip contact length, but increases interface temperature with dry conditions. In the presence of a coolant, however, contact length and interface temperature both decrease in the presence of cutting fluid. This indicates that cooling of the tool could effectively reduce contact length and remove heat.

The shortest contact lengths, which were measured at 500 ml/hr and flood, are closely predicted by Oxley's machining theory [52], which predicts a contact length of 0.1 mm. During these experiments, nesting did not occur at any point during the experiment. The chips produced under the two highest flow rates are an ideal continuously coiled shape,

consistent with the type 2 chip assumption in Oxley's model.

At an increased feed rate (0.2 mm/rev), MQCF had a negligible measured effect on interface temperature. Both processes created continuous chips, but the diameter of the chip curl was larger for tests conducted at 0.2 mm/rev. The larger chip curl makes the cutting zone more difficult to reach, but at the low feed rate, the chip coils tightly and opens up the cutting zone for fluid to access (Figure 4.10). Chip nesting also has a similar effect of blocking the cutting zone.

Shaw [15] reported similar results with flood coolant, noticing that the effectiveness of coolant on the tool-chip interface decreased with an increase in cutting speed or feed rate. At a high feed rate (0.254 mm/rev), the coolant was almost ineffective at cooling the interface, while at a low feed (0.06 mm/rev), it reduced the interface temperature by approximately 150°C at all cutting speeds tested. Shaw suggested that the increased heat generation, caused by the increase in speed and feed rate, does not have enough time to flow into the chip or conduct into the tool and therefore cannot be effectively removed by coolant.

The characteristics of the chip curl have a significant effect on tool-chip interface temperature. With a thicker chip generated at a high feed rate of 0.2 mm/rev, the coolant may not be as effective at creating a large temperature gradient within the chip to promote a tighter curl.

4.3 Model Discussion

Many of the inputs to the model used in this research must either be measured experimentally or determined by other predictive means, such as Oxley's model. For this

discussion, both experimental and predictive inputs are used and tested. The model is first verified with Komanduri and Hou's model to test the solving method discussed previously. The proposed model is then verified using inputs determined by Oxley's model. Experimental forces, chip thickness, and contact length were used in conjunction with Oxley's prediction of shear plane temperature to compare modeled temperatures to experimental measurements. Additionally, the effective heat transfer coefficient was determined for each of the experimental flow rates.

4.3.1 Verification with Komanduri and Hou's Model

To validate the distribution coefficient method proposed in this research, results were compared to Komanduri and Hou's [23] calculations of interface temperatures for experiments conducted by Chao and Trigger [10] and Ueda et al. [66]. Komanduri and Hou reported on average interface temperature and temperatures at 11 equally spaced points on the tool-chip interface. A comparison of average interface temperatures can be seen in Table 4.4 and comparison of points on the interface can be seen in Figure 4.11 and Figure 4.12.

4.3.2 Verification with Oxley's Model

Oxley's model is widely accepted as the most comprehensive and accurate machining model for plain carbon steels. Using Oxley's model to predict main cutting force, thrust force, chip thickness ratio, contact length, and chip thermal conductivity, the average interface temperature determined by the proposed model can be compared to the results from Oxley's model. A table of Oxley inputs/outputs that were then fed into the

model developed in this thesis can be seen in Table 4.5.

The model presented in this research predicts a lower average interface temperature than Oxley's model (Table 4.6). However, both models predict similar differences in average interface temperature as feed is increased. This indicates that there is some uncertainty in the absolute value of temperature, but the model developed as part of this research predicts the expected Oxley calculated change in temperature as feed rate is increased.

Figure 4.13 shows the modeled distribution for tool-chip interface temperature. The values at each point along the contact length show a nonintuitive result that a feed of 0.05 mm/rev can produce higher temperatures than 0.2 mm/rev. This is likely due to changing friction dynamics, resulting in difference in the distribution of heat along the tool-chip interface. The model presented assumes a uniform frictional heat flux, which places more heat at the end of the contact length than is physically there. As a result, temperatures at the end of the contact length are higher than expected.

Huang and Liang [46], Karpat and Özel [48], as well as M'Saoubi [47] have overcome this with the use of a nonuniform heat source. For the model presented in this research, a nonuniform heat source was not added due to the added complexity. Experimental validation was concerned with capturing a change in temperature, which the proposed model shows good agreement with Oxley in predicting.

4.3.3 Numerical Integration Independence Study

Although a grid is used to calculate the temperature rise at every point in the chip and tool, the solution does not have grid dependence because it is a closed form analytical

solution. The solution is, however, dependent on the number of integration points that the shear plane and frictional heat sources are divided into. This is because trapezoidal numerical integration is used. This analysis has not been conducted in literature. Using the Trigger and Chao [10] inputs for the analysis, it was found that the model has errors in the frictional heat source when the number of integration points is fewer than the number of grid points, N , in the X direction. When the number of integration points is roughly 25% more than the grid points in the X direction, the average interface temperature is unchanged and the solution is stable, as seen in Figure 4.14.

4.3.4 Modeled Dry Conditions with Experimental Measurements

A list of model inputs can be seen in Table 4.7, which uses experimental measurements for forces, chip thickness ratio, and contact length. Chao and Trigger [10] suggested that thermal properties be evaluated at the temperature of the chip once it leaves the shear zone. Since the experiment did not have a way to predict shear zone temperature, it needs to be approximated by other means, such as Oxley's machining theory [52], which calculated a shear zone temperature of 233°C . Material properties were evaluated for steel based off of data provided by the ASM handbook for 1045 steel [67].

The modeled average interface temperature is 634°C with a distribution shown in Figure 4.15. Near the end of the contact length, the maximum temperature is 780°C . Temperature contours in the tool and chip can be seen in Figure 4.16. The modeled temperature is significantly lower than the measured temperature of 977°C . This could be due to three possible explanations:

1. The measured contact length is too long. Due to the uncoiled chip, the

measured wear scar is longer than the actual distance that the tool and chip are in contact. Decreasing the contact length in the model would increase the average tool-chip interface temperature.

2. The value of thermal conductivity of the shear zone is incorrect. The model is highly dependent on thermal conductivity. Small changes in thermal conductivity result in large changes in temperature.
3. The measured temperature is incorrect. This could be due to a calibration error.

4.3.5 Determination of Effective Heat Transfer Coefficient

The proposed model, in its current state, is not capable of modeling temperatures beyond the tool-chip contact length. Therefore, temperatures beyond the length of the tool-chip contact length on the rake face of the tool must be evaluated from literature. Childs [14] reported temperatures ranging from 200°C to 650°C on the free surface of the tool. It is assumed that the surface of the tool behind the contact length is 425°C on average, which is between the ranges of temperature reported by Childs. The decrease in tool-chip interface temperature as a function of the magnitude of the coolant heat source can be seen in Figure 4.17.

With the measured average interface temperature drops, the effectiveness of each tested flow rate can be determined, as seen in Figure 4.18. The predicted effective convection coefficients for MQCF agree for the range of mist cooling by Sozbir's [57] findings of 1000-2000 W/m²-K. The experimental h_{eff} also agrees with Childs' [14] findings for flood of 5000 W/m²-K. Air, 150 ml/hr, and 300 ml/hr all fall below the 1000

W/m²-K threshold for measurable difference, as reported by Childs [14].

The effective heat transfer coefficient can be approximated with equation (25). Using the proposed model, the average interface temperature decrease can be predicted for various convection coefficients (Figure 4.19).

$$h_{eff} = \frac{q_{rc}}{\bar{T}_{t,surface} - T_{amb}} \quad (25)$$

4.3.6 Modeled Tool Temperature with Cooling

The focus of the presented research has primarily been on the chip-tool interface. However, cooling through the depth of the tool reduces the temperature of the bulk of the tool, as seen in Figure 4.20. The gradient is uniform with equal spacing between contour lines. The change in temperature with cooling relative to dry can be seen in Figure 4.21. Each coolant flow rate has a similar shape and slope, indicating that the temperature gradient in the tool is unchanged and that the coolant uniformly reduces the bulk tool temperature.

4.3.7 Model Predictions for Increased Feed Rate

Using measurements collected during the 0.2 mm/rev feed rate experiments, the modeled average interface temperature is 753°C with a distribution shown in Figure 4.22. The model shows a 128°C increase above the modeled average interface temperature for experiments with a feed of 0.05 mm/rev. Experimental measurements predicted, on average, a 39°C temperature difference between the two feed rates with a maximum temperature difference of 86°C.

Figure 4.22 shows that the predicted values for temperature at any point along the

contact length for a low feed are greater in magnitude than those for a high feed rate. This is a nonintuitive result that is likely due to the assumed uniform distribution of the frictional heat source. The uniform friction heat source distributes too much heat to the end of the tool-chip contact length, resulting in temperatures that are higher than expected.

4.3.8 Summary and Limitations of the Proposed Model

The model presented contributes a faster solving method and the ability to approximate cooling on the rake face of the tool, expanding the capabilities of the Komanduri and Hou model. The proposed model was able to correctly predict the same change in temperature caused by an increase in feed rate as the Oxley model, demonstrating that the moving heat source method is adequate for predicting changes in temperature. Although the model is experimentally dependent, it is robust enough to capture changes in temperature.

The underlying assumptions are the current model's main limitations. The assumption of a uniform distribution of the frictional heat source produces temperature distributions that have been experimentally proven to be questionable. Additionally, the proposed model requires a measured or assumed value for $\bar{T}_{t,surface}$ to estimate h_{eff} . However, the results agree with published heat transfer coefficient data, suggesting that the proposed method for estimating h_{eff} is sufficient.

While h_{eff} was an adequate way to model temperature change at a low feed rate (0.05 mm/rev), the model would approximate similar decreases in interface temperature at a high feed rate (0.2 mm/rev), which was not observed in the experiments conducted in this research or by Shaw [15]. As discussed in Section 4.2, there was an experimentally

observed complex relationship between tool-chip contact length and coolant application that is not captured by this model. The tool-chip contact length as well as chip morphology changed drastically as cutting fluid application increased. This suggests that these parameters should also be taken into consideration in developing a model for coolant application.

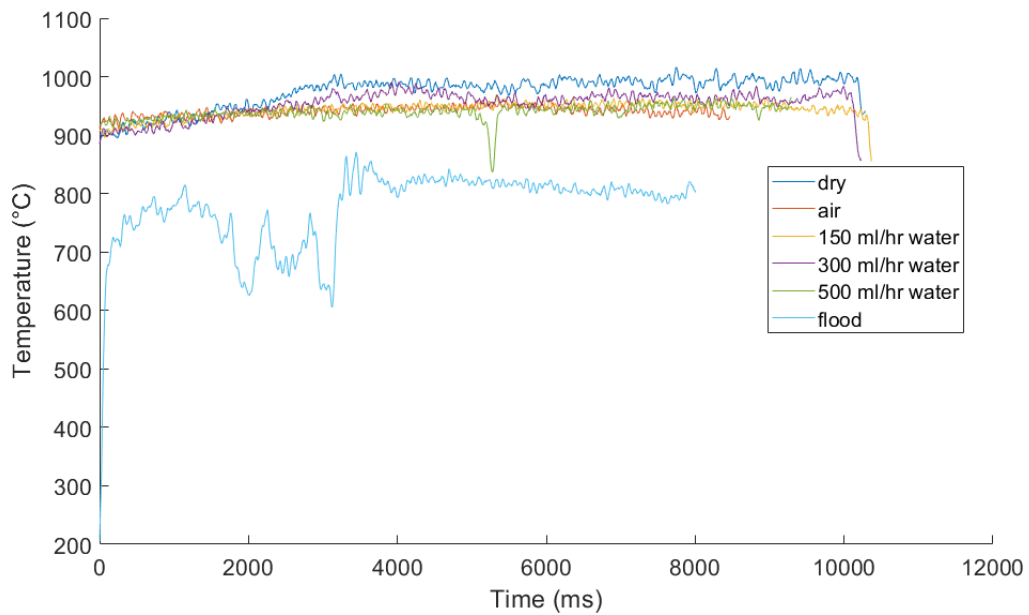


Figure 4.1: Time series temperature measurements.

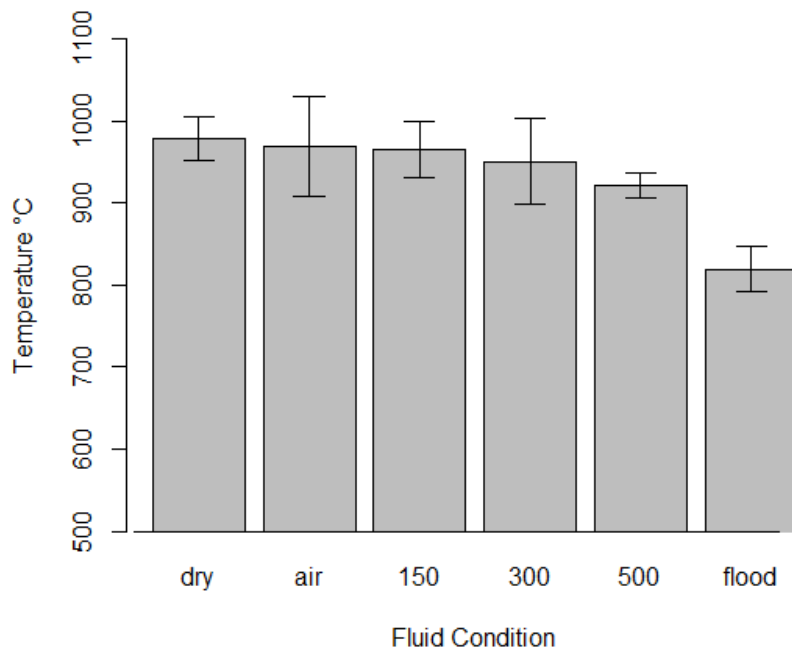


Figure 4.2: Average measured tool-chip interface temperature.

Table 4.1: Measured average temperature and comparison to dry conditions.

Condition	T (°C)	ΔT (°C)	% change
Dry	977	-	-
50 psi air	969	-8	0.8%
150 ml/hr	965	-12	1.2%
300 ml/hr	950	-27	2.8%
500 ml/hr	921	-56	5.8%
flood	819	-158	16.2%

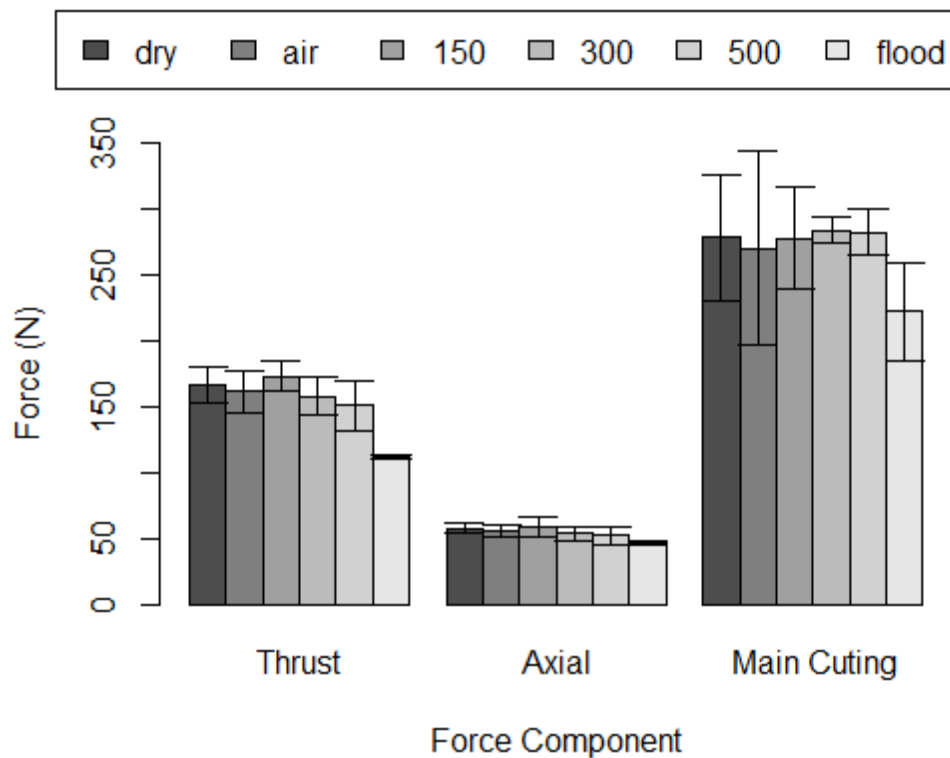


Figure 4.3: Variation in force components for each fluid condition.

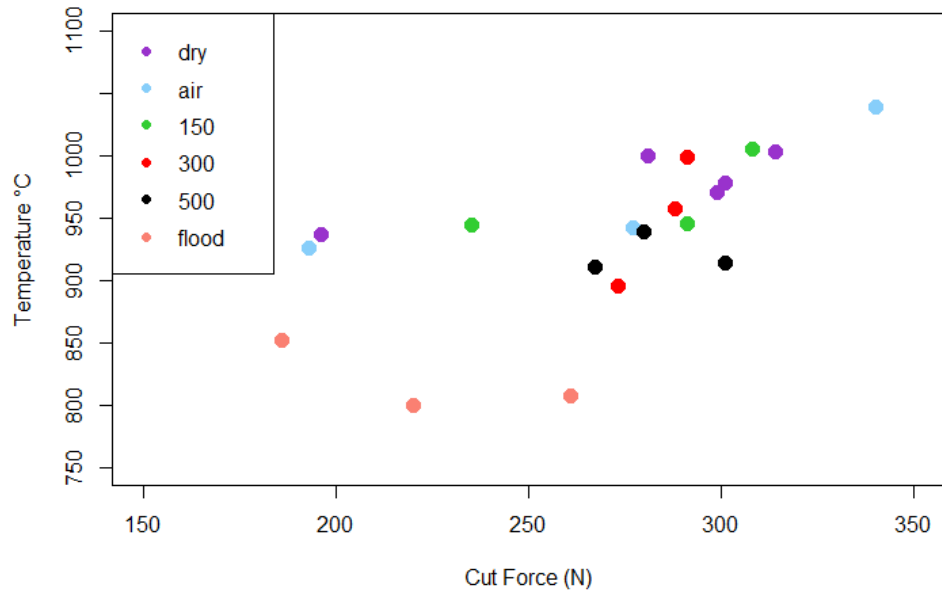


Figure 4.4: Variation of temperature with respect to main cutting force for each fluid condition.

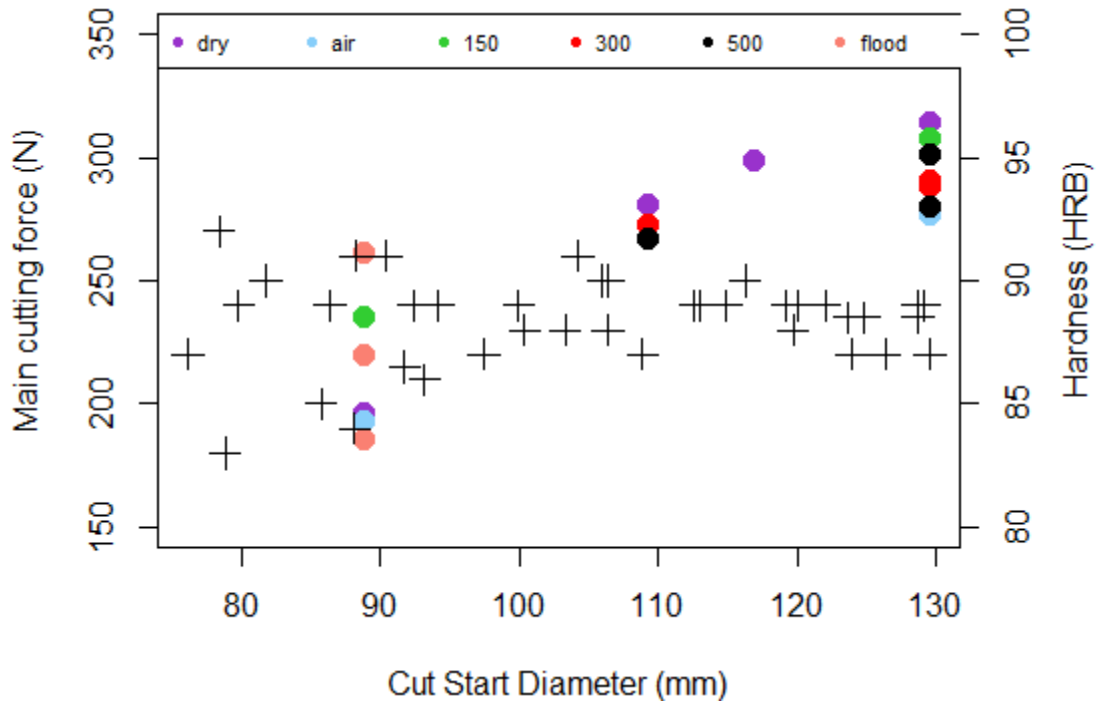


Figure 4.5: Relationship between experiment start diameter on the workpiece and main cutting force. Hardness is shown as a “+” symbol.

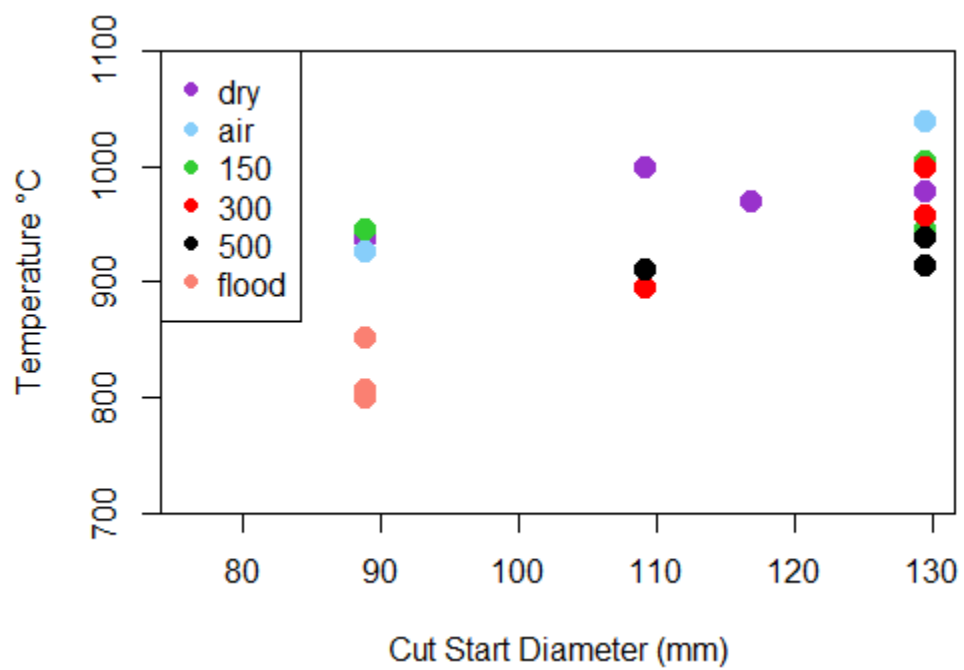


Figure 4.6: Relationship between start diameter and temperature.



Figure 4.7: Chip curl images for dry (A), air (B), 150 ml/hr (C), 300 ml/hr (D), 500 ml/hr (E), and flood (F).

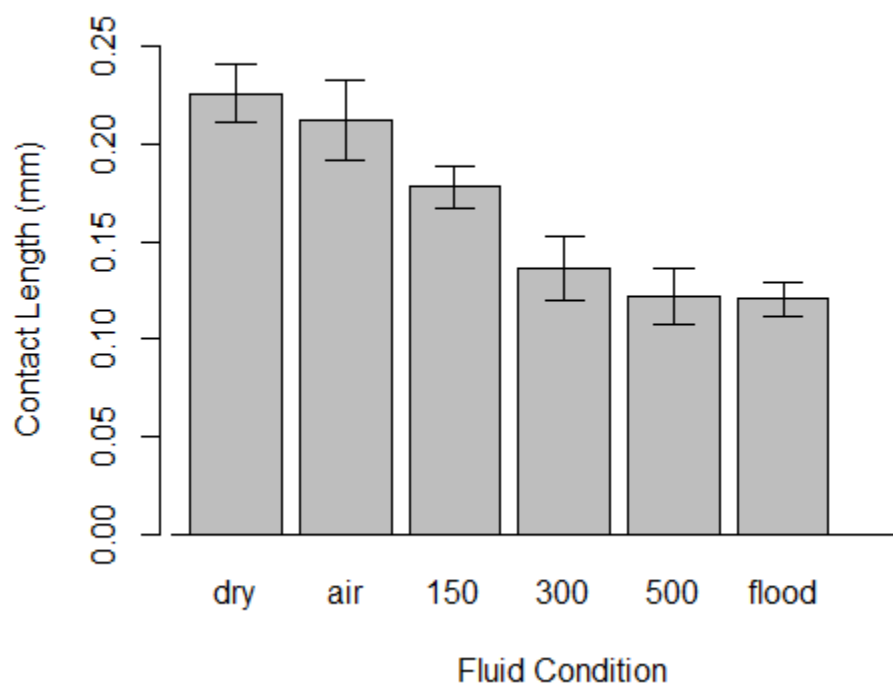


Figure 4.8: Tool-chip contact length.

Table 4.2: Tool-chip contact length images.

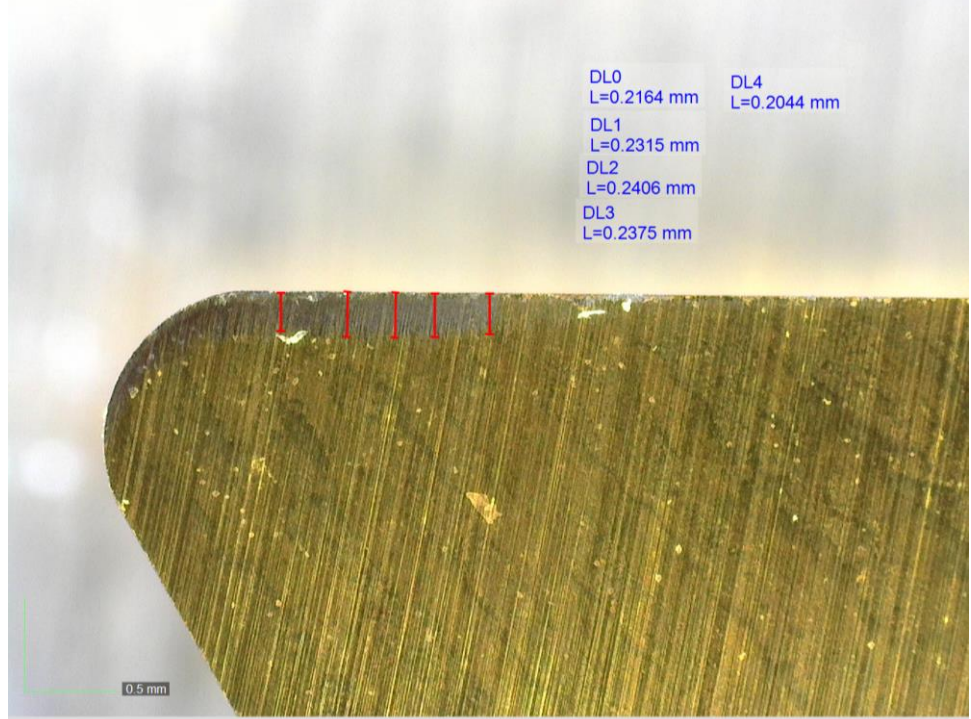
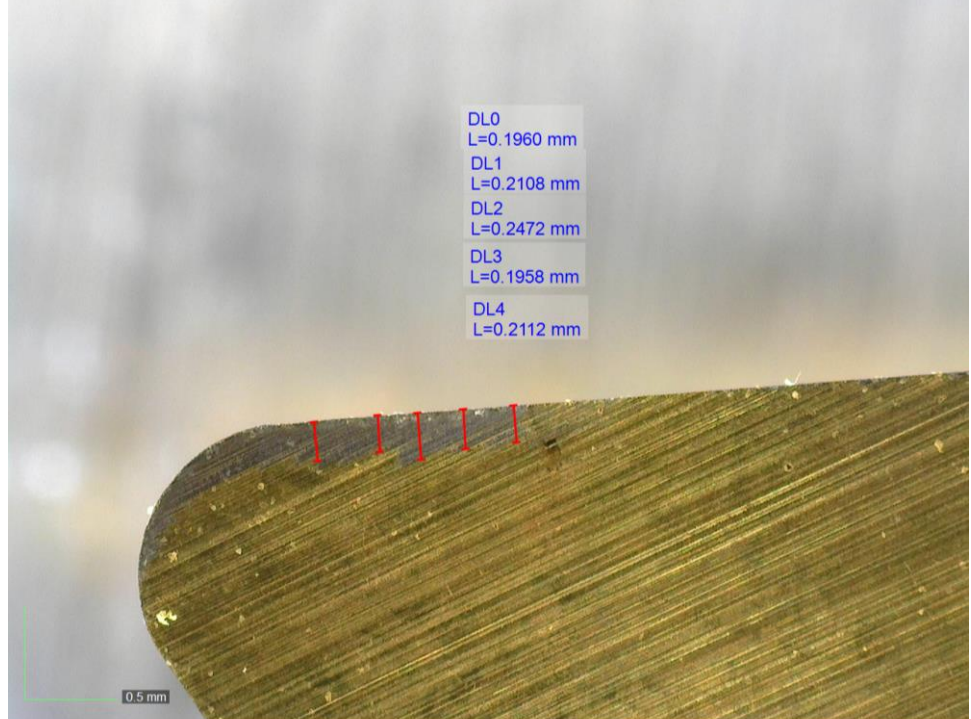
Fluid Condition	Image
Dry	 <p data-bbox="982 415 1242 590">DL0 L=0.2164 mm DL4 L=0.2044 mm DL1 L=0.2315 mm DL2 L=0.2406 mm DL3 L=0.2375 mm</p> <p data-bbox="527 1024 576 1045">0.5 mm</p>
Air	 <p data-bbox="868 1192 982 1423">DL0 L=0.1960 mm DL1 L=0.2108 mm DL2 L=0.2472 mm DL3 L=0.1958 mm DL4 L=0.2112 mm</p> <p data-bbox="527 1766 576 1787">0.5 mm</p>

Table 4.2 continued.

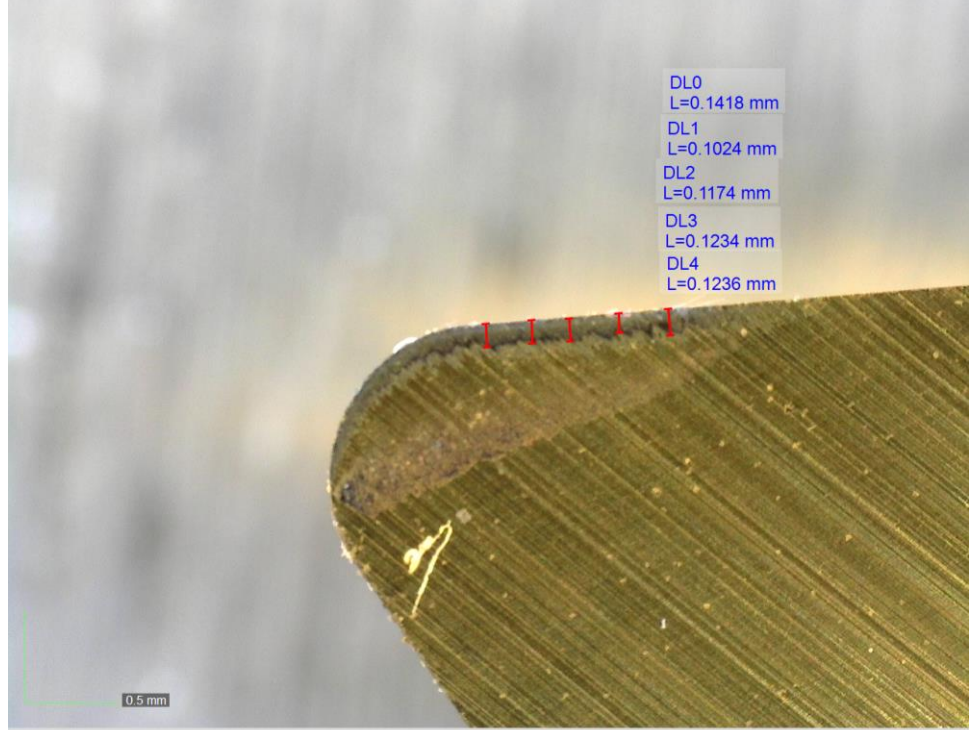
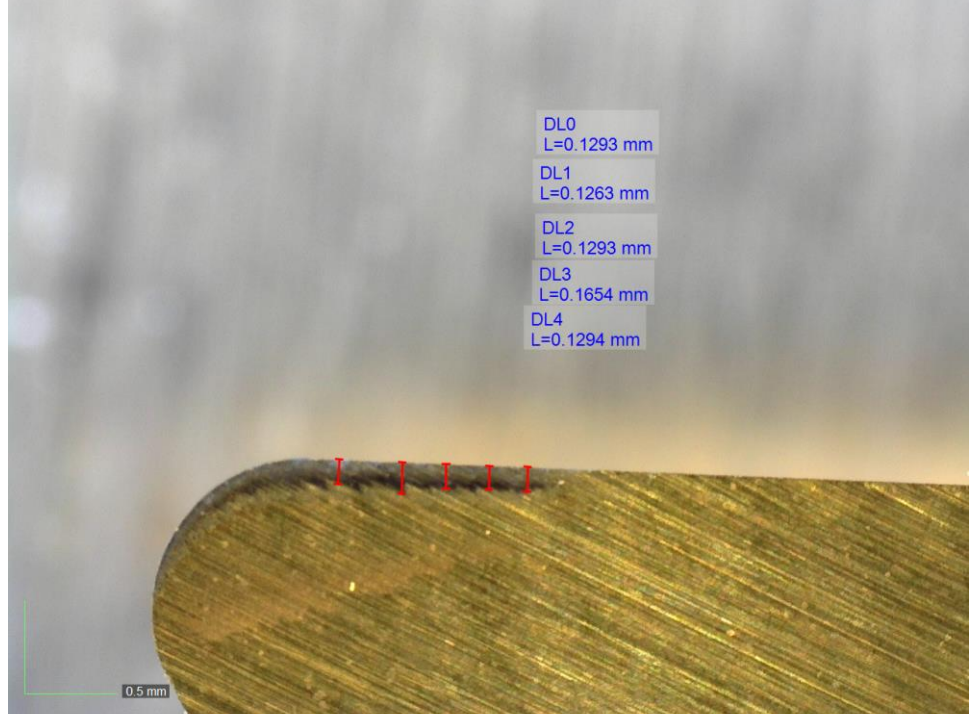
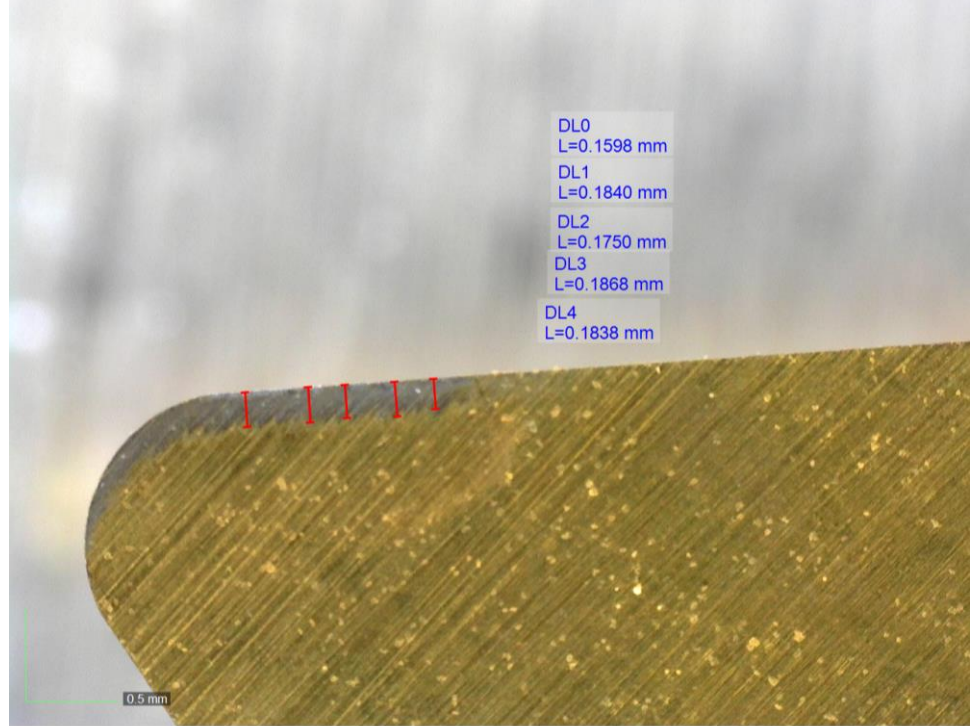
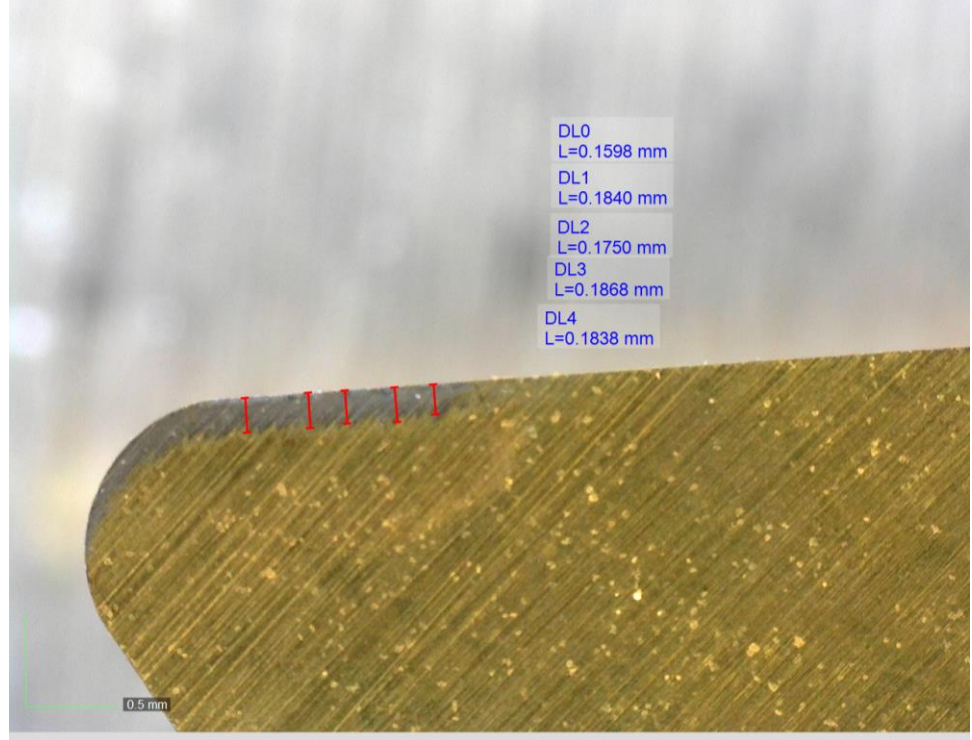
Fluid Condition	Image
150 ml/hr	 <p data-bbox="1062 422 1187 642">DL0 L=0.1418 mm DL1 L=0.1024 mm DL2 L=0.1174 mm DL3 L=0.1234 mm DL4 L=0.1236 mm</p> <p data-bbox="526 1037 574 1058">0.5 mm</p>
300 ml/hr	 <p data-bbox="932 1209 1057 1440">DL0 L=0.1293 mm DL1 L=0.1263 mm DL2 L=0.1293 mm DL3 L=0.1654 mm DL4 L=0.1294 mm</p> <p data-bbox="526 1772 574 1793">0.5 mm</p>

Table 4.2 continued.

Fluid Condition	Image
500 ml/hr	 <p data-bbox="941 462 1071 693">DL0 L=0.1598 mm DL1 L=0.1840 mm DL2 L=0.1750 mm DL3 L=0.1868 mm DL4 L=0.1838 mm</p> <p data-bbox="519 1029 576 1060">0.5 mm</p>
Flood	 <p data-bbox="941 1207 1071 1438">DL0 L=0.1598 mm DL1 L=0.1840 mm DL2 L=0.1750 mm DL3 L=0.1868 mm DL4 L=0.1838 mm</p> <p data-bbox="519 1774 576 1806">0.5 mm</p>

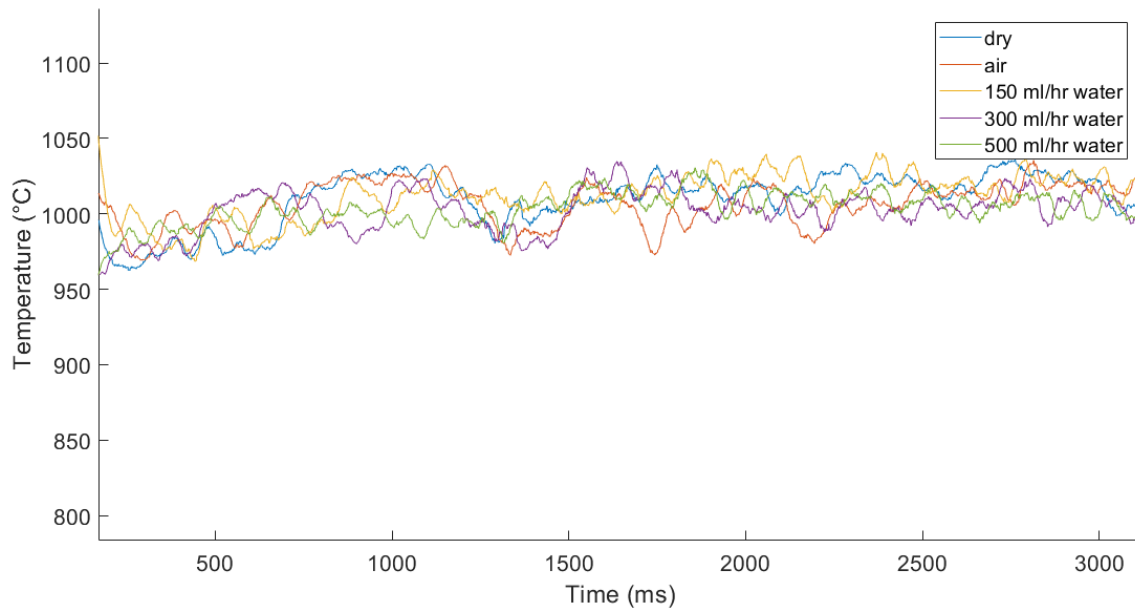


Figure 4.9: Time series of temperature measurements with 0.2 mm/rev feed rate.

Table 4.3: Comparison of measured average tool-chip interface temperature at 0.2 mm/rev and 0.05 mm/rev.

Condition	Feed = 0.2 mm/rev		Feed = 0.05 mm/rev	
	Measured Interface Temperature (°C)	ΔT (°C)	Measured Interface Temperature (°C)	ΔT (°C)
Dry	1016	-	977	-
50 psi air	1007	-9	969	-8
150 ml/hr	1018	2	965	-12
300 ml/hr	1005	-11	950	-27
500 ml/hr	1007	-9	921	-56
flood	-	-	819	158

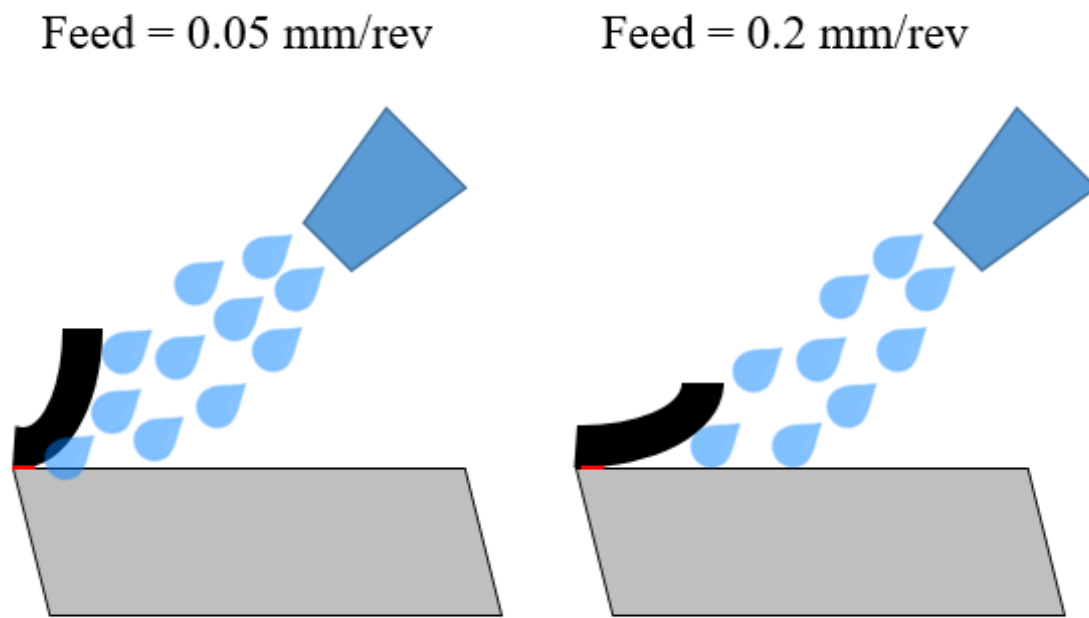


Figure 4.10: Diagram of cutting fluid blockage by larger chip radius.

Table 4.4: Comparison of average tool-chip interface temperature.

Researcher	Measured temperature rise over room temp	Functional Analysis [23]	Thesis Model Result
Chao and Trigger [10]	629°C	633°C	626°C
Ueda et al. [66]	151°C	155°C	161°C

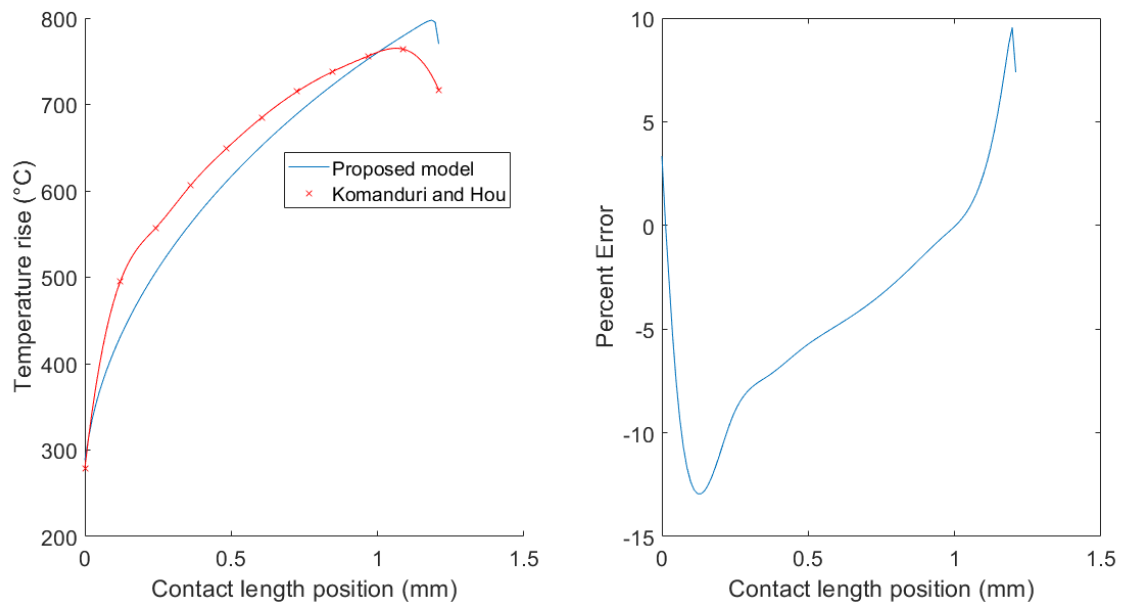


Figure 4.11: Comparison of proposed model compared to Komanduri and Hou's [23] solution using inputs from Chao and Trigger [10].

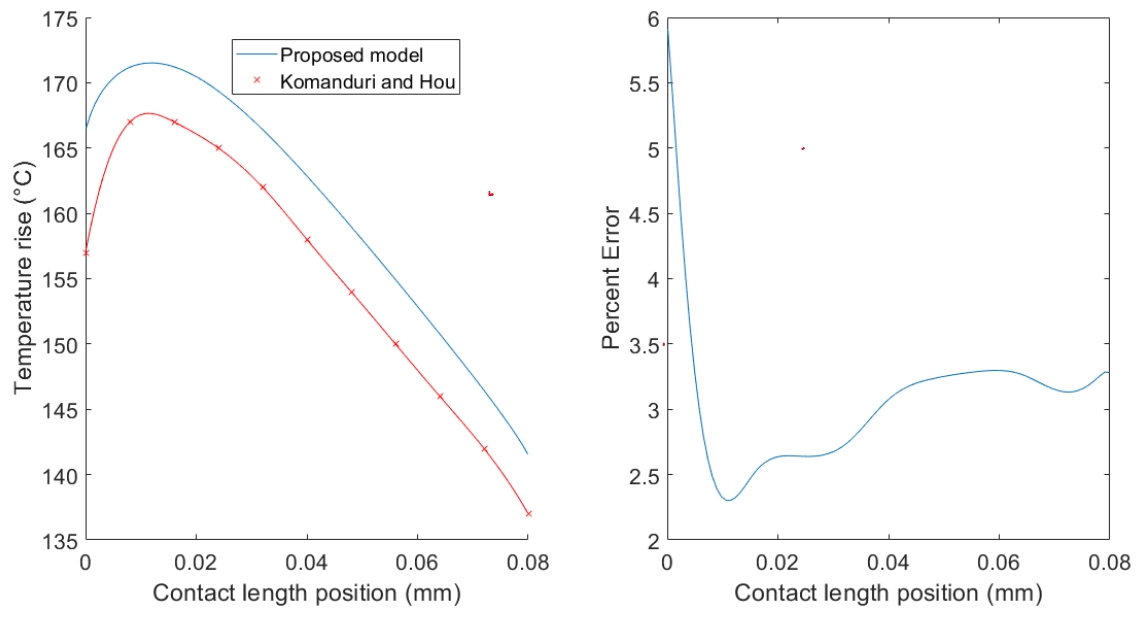


Figure 4.12: Comparison of proposed model compared to Komanduri and Hou's [23] solution using inputs from Ueda et al. [66].

Table 4.5: Model inputs for Oxley verification.

Oxley	Research model input	Oxley $f = 0.05$ mm/rev	Oxley $f = 0.20$ mm/rev	Units
Oxley input	Rake Angle	5	5	Degrees
	Depth of cut	0.05	0.2	mm
	Width of cut	2	2	mm
	Cut Velocity	200	200	m/min
Oxley Output	Cut Force	204	784	N
	Thrust Force	81	312	N
	Chip thickness ratio	0.527	0.512	-
	Contact Length	0.098	0.405	mm
	Chip thermal conductivity	41.5	41.5	W/m-°C
From ASM[67], [68]	Tool thermal conductivity	35	35	W/m-°C
	Chip thermal diffusivity	8.8 E-6	8.8 E-6	m ² /s

Table 4.6: Verification with Oxley results.

Model	Oxley	Proposed Model
Avg. Int. Temp. $f = 0.05$ mm/rev	665°C	519°C
Avg. Int. Temp. $f = 0.20$ mm/rev	945°C	804°C
Difference in temperatures	280°C	285°C

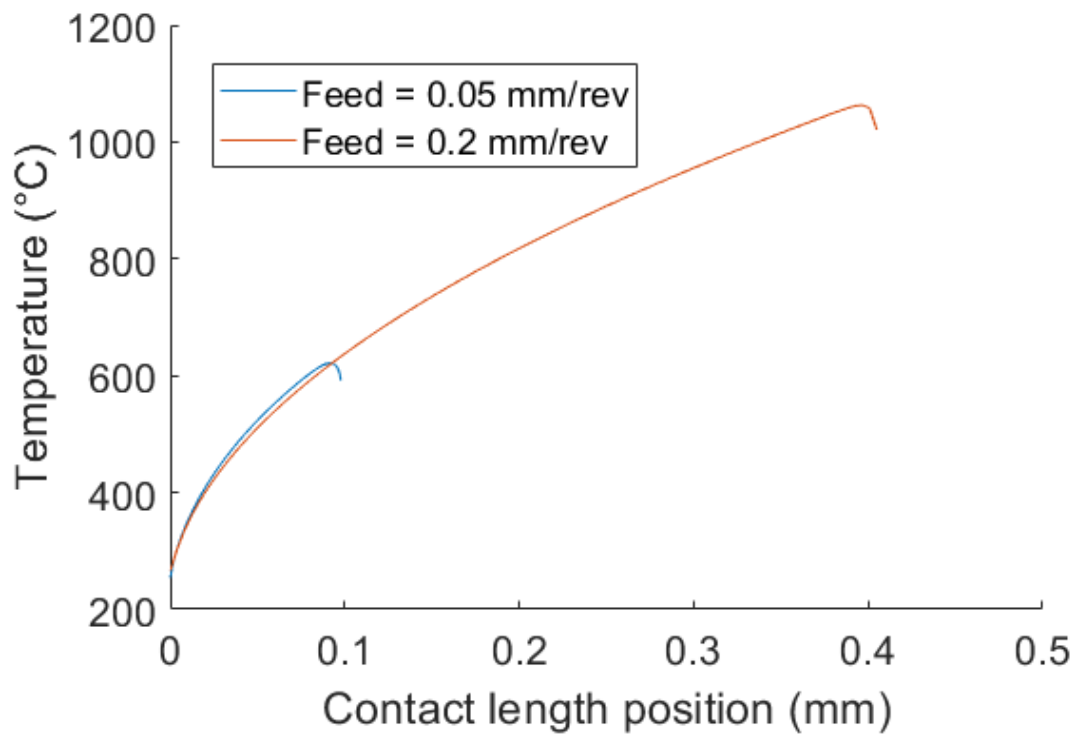


Figure 4.13: Oxley interface temperature distributions calculated with research model.

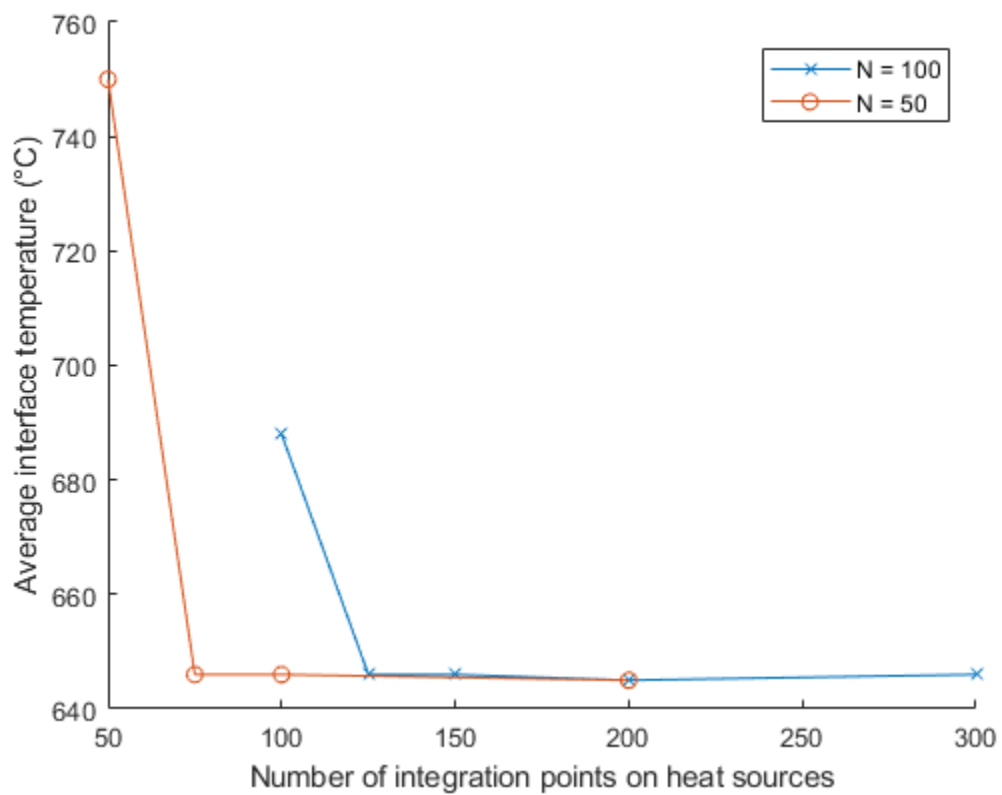
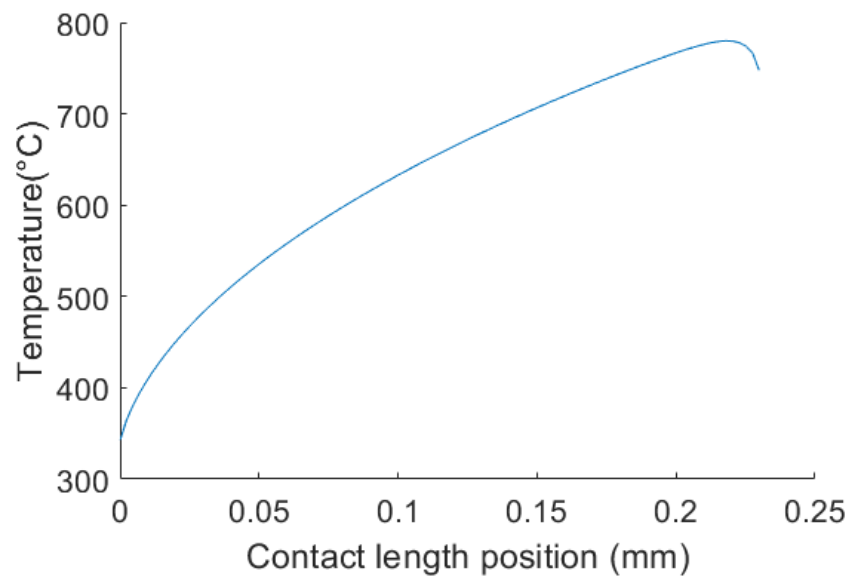


Figure 4.14: Relationship between integration points that heat sources are divided into and their effect on modeled average interface temperature.

Table 4.7: Model inputs with experimental measurements.

Input	Value	Units
Rake angle	+5	Degrees
Depth of cut	0.05	mm
Width of cut	2	mm
Cut velocity	200	m/min
Main cutting force	314	N
Thrust force	161	N
Chip thickness ratio	0.545	-
Contact Length	0.24	mm
Chip thermal conductivity	47	W/m-°C
Tool thermal conductivity	35	W/m-°C
Chip thermal diffusivity	1.2E-5	m ² /s
Tool thickness	3	mm
Clearance angle	11	Degrees
Length of area cooled on rake face	5	mm

Figure 4.15: Modeled interface with contact length of $L = 0.23$ mm.

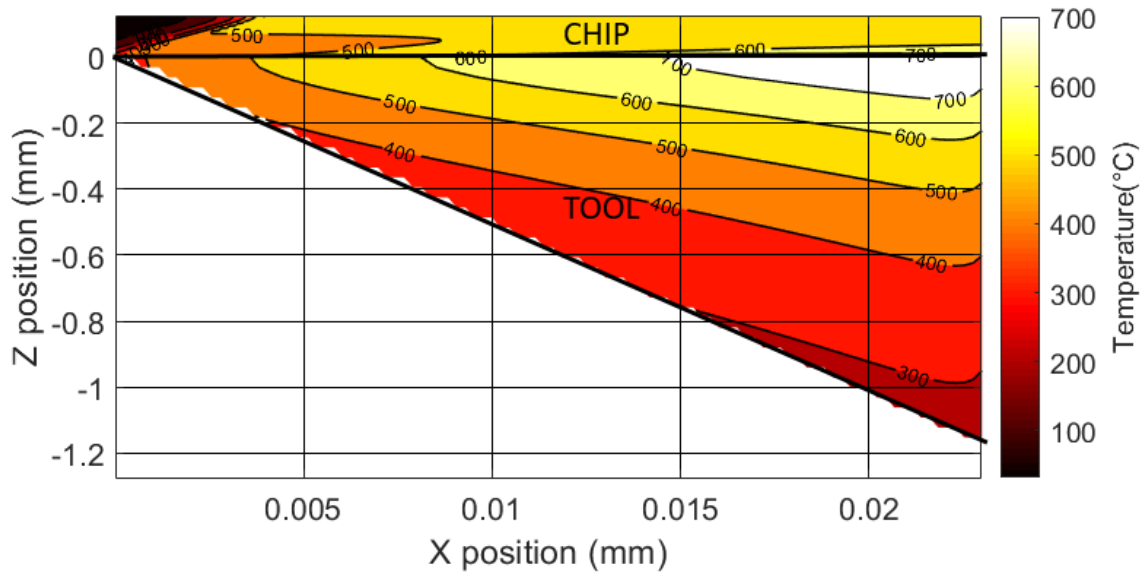


Figure 4.16: Dry modeled temperatures in the tool and chip.

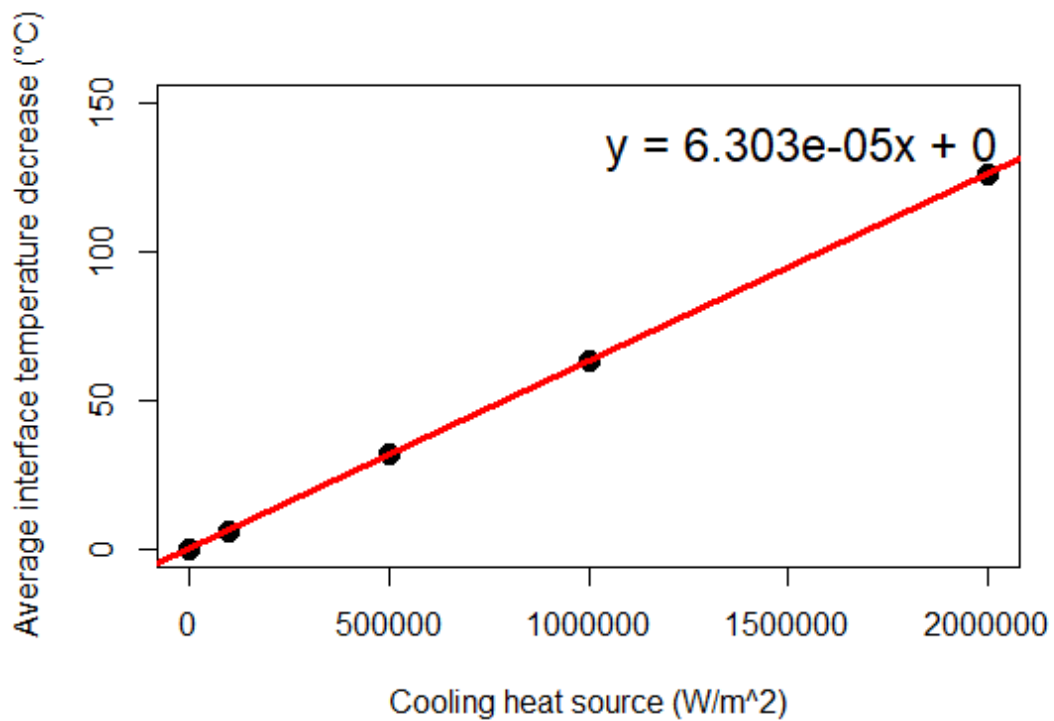


Figure 4.17: Cooling heat source effect on average tool-chip interface temperature.

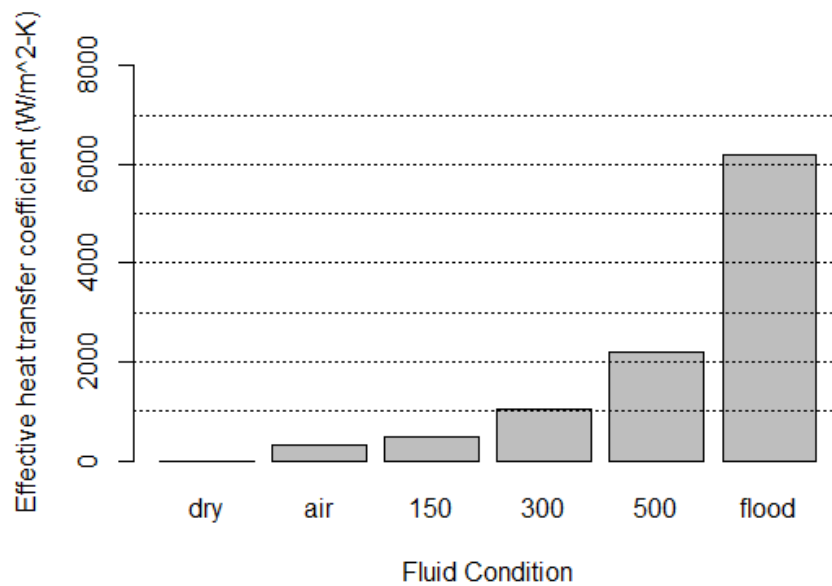


Figure 4.18: Modeled heat transfer coefficients for each experimental condition.

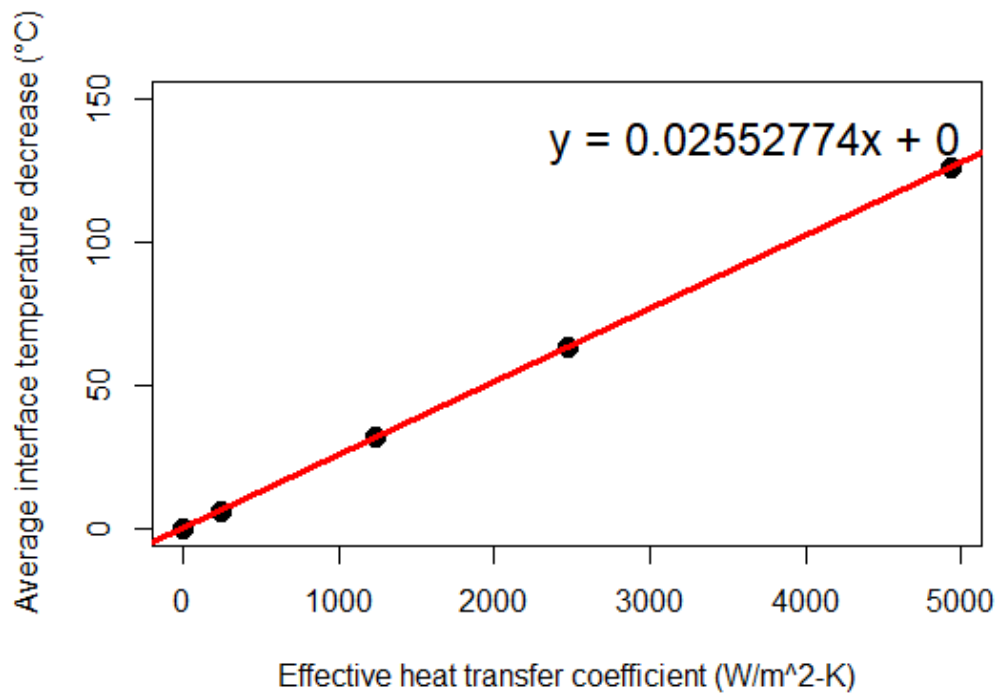


Figure 4.19: Modeled average interface temperature drop as convection coefficient is increased.

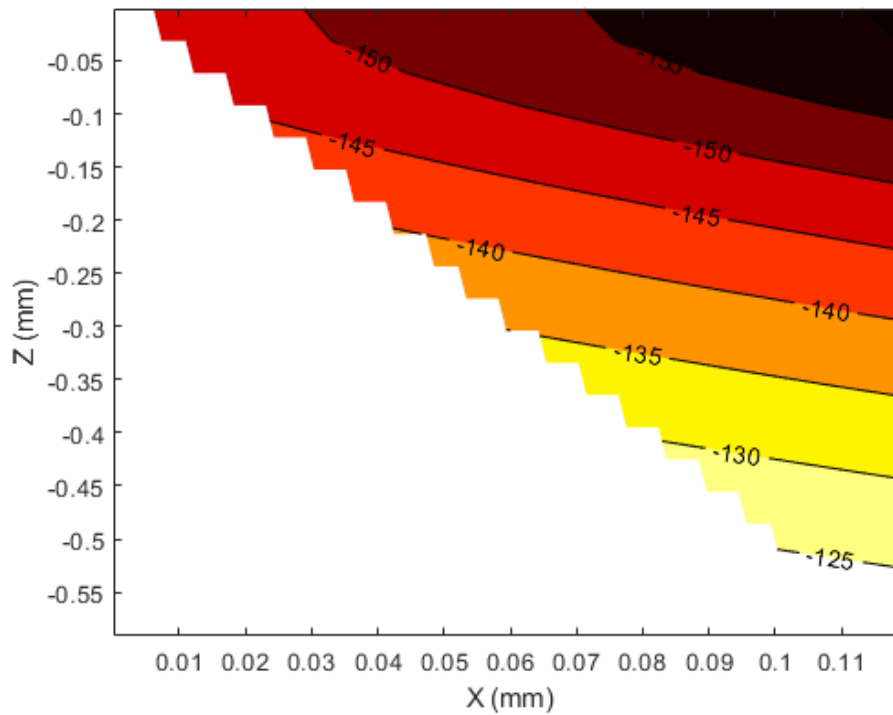


Figure 4.20: Modeled tool temperature reduction profiles under flood cooling conditions

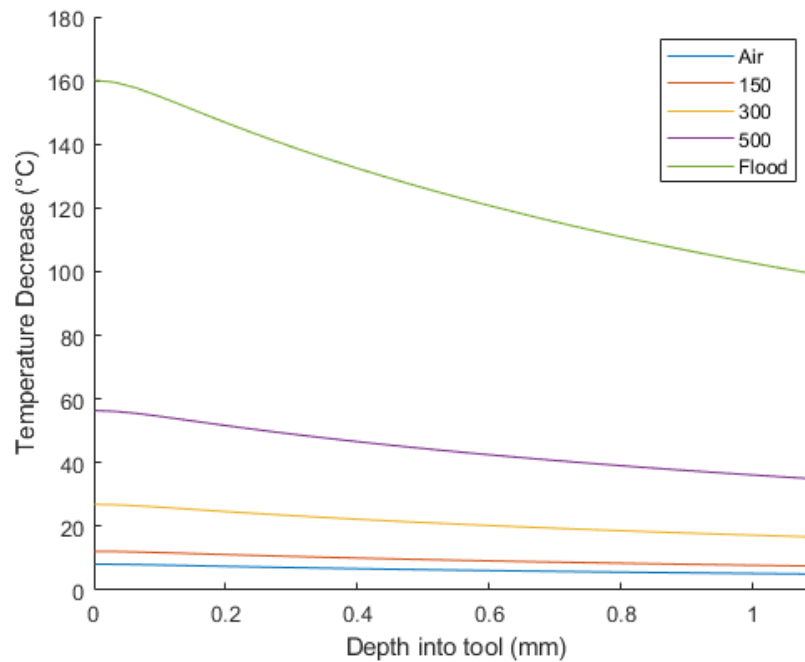


Figure 4.21: Temperature change through depth of tool.

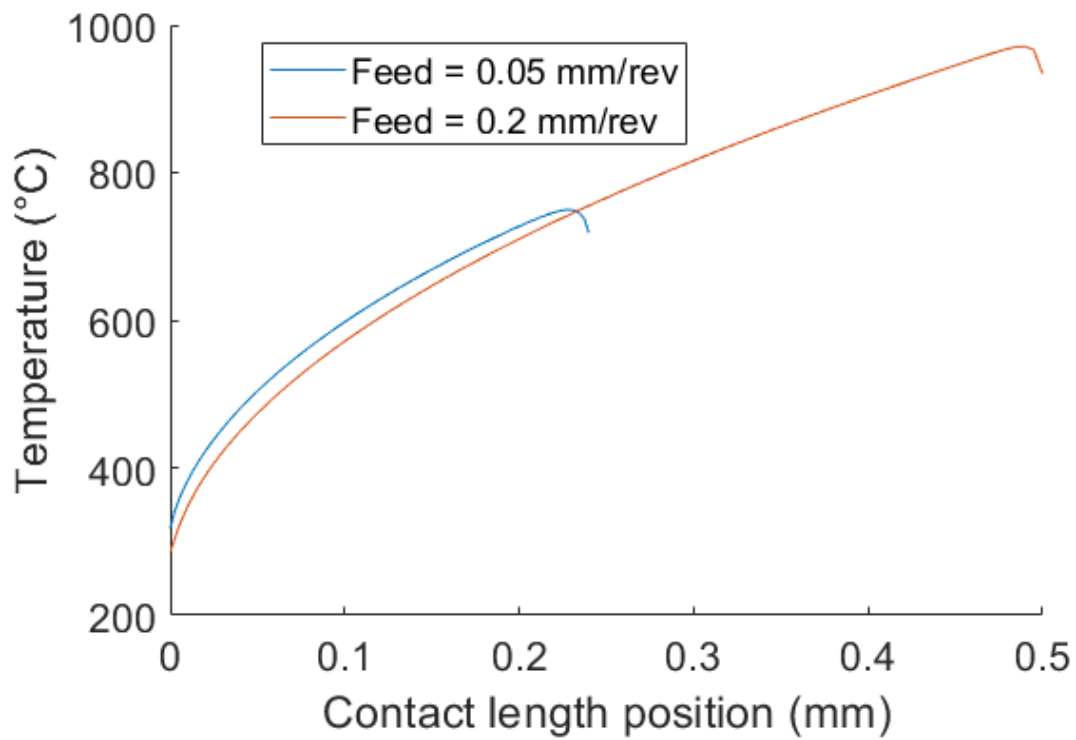


Figure 4.22: Comparison of modeled tool-chip interface temperatures at high feed (0.2 mm/rev) and low feed (0.05 mm/rev).

CHAPTER 5

CONCLUSION

5.1 Summary and Conclusions

This research presented an analytical approach to model the effectiveness of coolant at reducing temperature at the tool-chip interface as well as experiments to measure the effectiveness of coolant at reducing the tool-chip interface temperature. As discussed in Chapter 2, much of the previous work in modeling temperatures in machining focuses on dry machining. In the literature that has studied the effectiveness of coolant, both analytical and numerical approaches have been applied. However, neither are a comprehensive predictive model of machining with coolant. The main limitation to exclusively thermal models is that many of the inputs are outputs of the machining process, rendering them dependent on experiments.

Experimentally measured average tool-chip temperature changes were used to determine the effective heat transfer coefficient, h_{eff} , with the proposed model. As expected, temperature was reduced as cutting fluid flow rate increased. Significant reductions in temperature were observed with 300 ml/hr, 500 ml/hr, and flood, which gives insight into the minimum amount of fluid required for a measurable change in average tool-chip interface temperature. Cutting forces were largely constant during the experiment, indicating that the MQCF was primarily cooling and that temperature reductions observed

were not due to any lubricating action.

Perhaps the most significant observation of this research are the changes in the chip curl and tool-chip contact length. The application of a cutting fluid above flow rates of 150 ml/hr produced tightly coiled chips, as opposed to nested chips formed at lower flow rates and dry machining conditions. Furthermore, cooling caused a significant reduction in contact length at the tool-chip interface, indicating that there is an indirect friction altering effect due to in-situ thermal changes at the tool-chip interface. This was an unexpected result, giving insight into the significant effect that coolant can have on the reduction of contact length and chip morphology.

The model created here is an expansion of an established dry analytical model that expands its capabilities for machining operations under varying levels of coolant application. Verification with Komanduri and Hou determines that the new solving method is adequate and does not lead to large errors. Verification with the Oxley model shows that this model can predict the amount that temperature changes as feed is increased, but it does not agree with the Oxley's model's calculated average tool-chip interface temperature. Experimental forces, chip thickness, and contact length were used in conjunction with Oxley's prediction of shear plane temperature to compare modeled temperatures to experimental measurements. The model did not agree well with experimental measurements, likely due to incorrect thermal properties or tool-chip contact length. However, the model did show the correct trend for increased temperature with increased feed rate based on experimental measurements.

Additionally, the effective heat transfer coefficient was determined for each of the experimental flow rates. The results agreed with published literature that h_{eff} needs to be

greater than $\sim 1000 \text{ W/m}^2\text{-K}$ to have a measurable effect on interface temperature. The model presented is a step towards analytical modeling of tool-chip interface temperature in the presence of coolant, but still needs additional improvements to be more accurate and fully predictive. A better understanding of the effect that MQCF has on chip curl and tool-chip contact length is needed.

The results from this research give insight into the minimum amount of cutting fluid needed to achieve a measurable temperature difference at the tool-chip interface. It also brings to light the effect that MQCF can have on tool-chip contact length and chip morphology. Additionally, this model can serve as a tool to calculate temperature profiles for dry, flood, as well as minimized cutting fluid conditions with experimentally determined changes in temperature to calculate effective heat transfer coefficients.

5.2 Recommendations for Future Work

The following recommendations for future work can be made based on the results of this research:

- Extension of the proposed model to have nonuniform frictional heat flux. This will give a more realistic temperature distribution in the tool and the chip.
- Extension of the proposed model to predict forces and chip geometry. This could be implemented with updates to Oxley's model or coupled with a finite element solver.
- An alternative method to predict cooling with the proposed model that is more robust, perhaps with changing chip thermal conductivity.

- A study on the tool-chip contact length at various coolant flow rates. This could give a better understanding of mechanisms that caused the changes in tool-chip contact length observed in this thesis. Additionally, the chip forms could also be studied to understand the relationship between coolant application and tightly coiled chips observed in this research.

APPENDIX

CODE FOR PROPOSED MODEL

Setup

```
clc
clear all
run('inportexcel.m')
run('setup100.m')
tic
```

Shear plane interface temperature rise

```
%%%%%%%%%%%%%%%%%%%%%%%%%%%%%%%%%%%%%%%%%%%%%%%%%%%%%%%%%%%%%%%%%%%%%%%%
%SHEAR PLANE
%%%%%%%%%%%%%%%%%%%%%%%%%%%%%%%%%%%%%%%%%%%%%%%%%%%%%%%%%%%%%%%%%%%%%%%%
%This section equates the chip and tool interface temperatures due to the
%shear plane heat source. At the interface, the tool gets an "induced" heat
%source. This is essentially a uniform heat source at the surface of the
%tool that accounts for heat coming from the shear plane. Q_pli is the only
%unknown term that does not require fitting parameters. The average
%temperature rise at the chip-tool interface is calculated first from the
%chip side then Q_pli for the tool side is increased until the average
%temperatures match. Then, B (the partition coefficient) is solved for to
%match the two temperatures exactly. B creates the "function" that defines
%how the induced uniform heat source is distributed between the chip and
%tool.

T_cs = chipsurf_shear( V_ch, Xrange, t_ch, L, li, xi,Zi, wi, q_pls, ...
                    lambda_ch, grid,a_ch );

%"cut" off the ends to match the temperature more in the middle. with <100
%data points the ends can be problematic and have large errors.
average_ch = mean(T_cs(3:end-2));

%This assumes that all of the "induced" heat from the shear plane (q_pli)
%travels directly into the tool. This is not the case and it underestimates
%q_pli, but it works out once I solve for Bi_shear.
```



```

%iterates to solve for q_pli by matching the average temperatures.
error = 99;
errorold = 100;
q_pli = 0;
while error > .05
    T_ts = toolsurf_shear(grid, xi, L,lambda_t, yi, Xi_t, Yi_t, q_pli );
    average_t = mean(T_ts(3:end-2));
    error = abs((average_t-average_ch)/average_ch);
    q_pli = q_pli+100;
    if error > errorold
        break
    end
    errorold = error;
end

%Reduced q_pli by the last increments because it increases before the loop
%breaks. Calculates the temperature again with the new q_pli.
q_pli = q_pli - 100;
T_ts = toolsurf_shear(grid, xi, L,lambda_t,yi, Xi_t, Yi_t, q_pli );

%solves for the partition scheme by matching the temperatures on chip and
%tool side
Bi_shear = T_cs./T_ts;
T_ts = Bi_shear.*T_ts;

```

Friction interface temperature rise

```

%%%%%%%%%%%%%%%%%%%%%%%%%%%%%%%%%%%%%%%%%%%%%%%%%%%%%%%%%%%%%%%%%%%%%%%%
%Friction
%%%%%%%%%%%%%%%%%%%%%%%%%%%%%%%%%%%%%%%%%%%%%%%%%%%%%%%%%%%%%%%%%%%%%%%%
%This section partitions the heat along the chip-tool interface due to
%friction. The temperatures from the chip side and the tool side are
%calculated using equations 5' and 6' from part II of K-H. This assumes no
%partitioning scheme. Once the temperatures are calculated, the partition
%coefficient is calculated by equating the two temperature rises and
%solving for the coefficient. This partitions the friction heat source to
%the chip and to the tool.

%Calculates interface temperatures with no partition scheme
T_tf = toolsurf_frict( grid, xi, L,lambda_t, yi, Xi_t, Yi_t, q_pl );
T_cf = chipsurf_frict(V_ch, Xrange, L, li, q_pl, lambda_ch, grid,a_ch);

%Solves for partition. This is what you need to multiply the temperatures
%by in order to get them to match.
Bi_chip = (T_cf./T_tf+1).^-1;
Bi_tool = 1-Bi_chip;

%Multiplies each temperature by it's partition amount
T_tshear = T_tf.*Bi_tool; %tool side
T_cshear = T_cf.*Bi_chip; %chip side

```

Cooling terms temperature rise

```

%%%%%%%%%%%%%%%%%%%%%%%%%%%%%%%%%%%%%%%%%%%%%%%%%%%%%%%%%%%%%%%%%%%%%%%%
%Cooling terms
%%%%%%%%%%%%%%%%%%%%%%%%%%%%%%%%%%%%%%%%%%%%%%%%%%%%%%%%%%%%%%%%%%%%%%%%
%cooling is assumed to be uniform convection applied to the rake and to the
%flank face of the tool. The temperature drop at the interface is
%calculated for both sources then summed. The equivalent heat flux is then
%applied at the chip-tool interface, similar to friction.

if (q_fl < 0 && q_r < 0)
    %flank
    T_tfl = toolsurf_flank( grid, xi, lambda_t, xi_fl, yi_fl, zi_fl, L_fli, Y_fl, q_fl);
    %rake
    T_tr = toolsurf_rake( grid, xi, lambda_t, L, xi_r, yi_r, X_r, Y_r, q_r);
    %combines rake and flank cooling effects
    T_tcool = T_tfl+T_tr;
    %updates tool temperature
    %T_tool = T_tool+T_tcool;
elseif(q_fl > 0 || q_r > 0)
    error('Heat loss terms need to be negative');
else
    %Just gives the cooling term a zero value for easy plotting
    T_tcool = T_tool*0;
end

%Iterates to solve for q_pli by matching the average temperatures. This is
%similar to how q_pli is solved for.
error = 99;
errorold = 100;
q_cool = 0;
average_t = mean(T_tcool(3:end-2));
while error > .05
    T_ccool = chipsurf_cool( v_ch, Xrange, L, li, q_cool, lambda_ch, grid,a_ch );
    average_ch = mean(T_ccool(3:end-2));
    error = abs((average_t-average_ch)/average_t);
    q_cool = q_cool-100;
    if error > errorold
        break
    end
    errorold = error;
end
q_cool = q_cool + 100;

%solve for partition. This just matches the temperature at the interface.
Bi_cool = T_tcool./T_ccool';
toc

```

Save 1-D

```

%Saves the interface temperature rise
save(filename);

```

2-D chip side

```

%This uses the partition schemes determined on the 1-D (interface) solver
%previously calculated. Temperature rise is calculated at every point in
%chip then multiplied by partition.

%shear
T_cshear = chipsurf_shear_2d( v_ch, Xrange, Zrange_ch, t_ch, L, li, xi,Zi, wi, q_pls,
lambda_ch, grid_ch,a_ch );
T_cshear = flip1r(T_cshear);

%friction
T_cfriect = chipsurf_friect_2d( v_ch, Xrange, Zrange_ch, L, li, q_pl, lambda_ch,
grid_ch,a_ch );
T_cfriect = T_cfriect.*Bi_chip';
T_cfriect = flip1r(T_cfriect);

%cooling
T_ccool = chipsurf_cool_2d( v_ch, Xrange, Zrange_ch, L, li, q_cool, lambda_ch,
grid_ch,a_ch );
T_ccool = T_ccool.*Bi_cool';
T_ccool = flip1r(T_ccool);

%superimposes all of the temperatures together
T_chip = T_cshear + T_cfriect + T_ccool;

% figure
% contourf(Xrange, Zrange_ch, T_chip)
% colorbar

```

2-D tool side

```

%This uses the partition schemes determined on the 1-D (interface) solver
%previously calculated. Temperature rise is calculated at every point in
%tool then multiplied by partition.

%shear
T_tshear = toolsurf_shear_2d( grid_t, xi, L,lambda_t,yi,Zrange_t, Xi_t, Yi_t, q_pli );
T_tshear = T_tshear.*Bi_shear';
T_tshear = flip(flip1r(T_tshear));

%friction
T_tfriect = toolsurf_friect_2d( grid_t, xi, L,lambda_t, yi,Zrange_t, Xi_t, Yi_t, q_pl );
T_tfriect = T_tfriect.*Bi_tool';
T_tfriect = flip(flip1r(T_tfriect));

%flank cooling
T_tflank = toolsurf_flank_2d( grid_t, L, theta, xi,Zrange_t,lambda_t, xi_fl, Yi_fl,
Zi_fl,L_fli, X_fl, Y_fl, q_fl);
T_tflank = flip(flip1r(T_tflank));

%rake cooling
T_trake = toolsurf_rake_2d( grid_t, xi,Zrange_t, lambda_t, L, Xi_r, Yi_r, X_r, Y_r, q_r);
T_trake = flip(flip1r(T_trake));

```

```
T_tool = T_tshear + T_tfrict + T_tflank + T_trake;
```

```
%Creates a data file to plot with
```

```
filename = filename(1:end-4);
```

```
filename = strcat(filename, '2d.mat');
```

```
save(filename); plane heat source - chip side
```

```
function [ grid_shear ] = chipsurf_shear_2d( v_ch, Xrange, Zrange_ch, t_ch, L, li, Xi,Zi,
wi, q_pls, lambda_ch, grid_ch,a_ch )
```

```
tau = v_ch/2/a_ch;           %shear plane heat source
```

```
grid_shear = grid_ch;
```

```
for i = 1:length(Xrange)
```

```
    for j = 1:length(Zrange_ch)
```

```
        X = Xrange(i);
```

```
        Z = Zrange_ch(j);
```

```
        Ri = ((X-li).^2+Z^2).^0.5;
```

```
        Rip = ((X-2*L+li).^2+Z^2).^0.5;
```

```
        %shear plane heat source terms
```

```
        B4 = tau*((X-Xi).^2+(Z-Zi).^2).^0.5;
```

```
        T4 = exp(-(X-Xi)*tau) .* bessellk(0,B4);
```

```
        Int4 = trapz(wi,T4);
```

```
        B5 = tau*((X-Xi).^2+(2*t_ch-Z-Zi).^2).^0.5;
```

```
        T5 = exp(-(X-Xi)*tau) .* bessellk(0,B5);
```

```
        Int5 = trapz(wi,T5);
```

```
        Trise_s = q_pls/2/pi/lambda_ch * (Int4+Int5);
```

```
        grid_shear(j,i) = Trise_s;
```

```
    end
```

```
end
```

```
end
```

Frictional heat source – chip side

```
function [ T_cf ] = chipsurf_frict_2d( v_ch, Xrange, Zrange_ch, L, li, q_pl, lambda_ch,
grid_ch,a_ch )
```

```
tau = v_ch/2/a_ch;           %friction heat source
```

```

T_cf = grid_ch;

for i = 1:length(Xrange)
    for j = 1:length(Zrange_ch)
        X = Xrange(i);
        Z = Zrange_ch(j);

        Ri = ((X-li).^2+Z^2).^0.5;
        Rip = ((X-2*L+li).^2+Z^2).^0.5;

        %friction heat source terms
        T1 = exp(-tau * (X-li)) .* ...
            (besselk(0, tau*Ri)+ besselk(0, tau*Rip));
        Int1 = trapz(li,T1);

        %Temperature rise due to friction heat source
        Trise_F = q_p1/pi/lambda_ch *Int1;
        T_cf(j,i) = Trise_F;

    end

end
end

```

Cooling heat source – chip side

```

function [ T_ccool ] = chipsurf_cool_2d( v_ch, Xrange, Zrange_ch, L, li, q_cool,
lambda_ch, grid_ch,a_ch )
tau = v_ch/2/a_ch;

T_ccool = grid_ch;

for i = 1:length(Xrange)
    for j = 1:length(Zrange_ch)

        X = Xrange(i);
        Z = Zrange_ch(j);

        Ri = ((X-li).^2+Z^2).^0.5;
        Rip = ((X-2*L+li).^2+Z^2).^0.5;

        %friction heat source terms
        T1 = exp(-tau * (X-li)) .* ...
            (besselk(0, tau*Ri)+ besselk(0, tau*Rip));
        Int1 = trapz(li,T1);

        %Temperature rise due to friction heat source
        Trise_F = q_cool/pi/lambda_ch *Int1;
        T_ccool(j,i) = Trise_F;

    end

end
end

```

```
end
```

Shear plane heat source – tool side

```
%This calculates the contribution from shear on the tool surface.
```

```
function [ grid_S] = toolsurf_shear_2d( grid_t, xi, L,lambda_t,yi,Zrange_t, Xi_t, Yi_t,
q_pli )
```

```
    Ri = zeros(length(yi), length(xi));
    Rip = zeros(length(yi), length(xi));
```

```
    grid_S = grid_t;
```

```
    for i = 1:size(Xi_t,2)
        for j = 1:length(Zrange_t)
```

```
            X = Xi_t(1,i);
            Z = Zrange_t(j);
            Y = 0;
```

```
            Ri = ((X-Xi_t).^2 + (Y-Yi_t).^2 + Z^2).^-0.5;
            Rip = ((X-2*L+Xi_t).^2 + (Y-Yi_t).^2 + Z^2).^-0.5;
            R_S = (Ri + Rip);
            Int_S = trapz(yi, trapz(xi,R_S,2));
            Trise_S = Int_S*q_pli/2/pi/lambda_t;
            grid_S(j,i) = Trise_S;
```

```
        end
```

```
end
```

Frictional heat source – tool side

```
%This calculates the contribution from friction on the tool surface.
```

```
function [ T_tf] = toolsurf_frict_2d( grid_t, xi, L,lambda_t, yi,Zrange_t, Xi_t, Yi_t,
q_pl )
```

```
    T_tf = grid_t;
```

```
    for i = 1:size(Xi_t,2)
        for j = 1:length(Zrange_t)
```

```
X = Xi_t(1,i);
Z = Zrange_t(j);
Y = 0;

Ri = ((X-Xi_t).^2 + (Y-Yi_t).^2 + Z^2).^-0.5;
Rip = ((X-2*L+Xi_t).^2 + (Y-Yi_t).^2 + Z^2).^-0.5;

R_F = (Ri + Rip);

Int_F = trapz(yi, trapz(xi,R_F,2));
Trise_F = Int_F*q_p1/2/pi/lambda_t;

T_tf(j,i) = Trise_F;
```

end

end

Cooling heat source – tool side

```

%This calculates the contribution from cooling on the rake surface.

function [ T_trk] = toolsurf_rake_2d( grid_t, xi,Zrange_t, lambda_t, L, Xi_r, Yi_r, X_r,
Y_r, q_r)

    T_tf = grid_t;

    for i = 1:length(xi)
        for j = 1:length(Zrange_t)

            X = xi(i);
            Z = Zrange_t(j);
            Y = 0;

            Ri = ((X+Xi_r).^2 + (Y-Yi_r).^2 + (Z).^2).^0.5;
            Rip = ((2*L-X-Xi_r).^2 + (Y-Yi_r).^2 + (Z).^2).^0.5;

            R_F = (Ri + Rip);

            Int_F = trapz(Y_r, trapz(X_r,R_F,2));
            Trise_F = Int_F*q_r/2/pi/lambda_t;

            T_trk(j,i) = Trise_F;

        end
    end

end

```


REFERENCES

- [1] J. A. Schey, *Introduction to Manufacturing Processes and Materials*, 3rd ed. Boston: McGraw-Hill, 2000.
- [2] M. C. Shaw, *Metal Cutting Principles*, 1st ed. New York: Oxford University Press, 1984.
- [3] I. Finnie, "Review of metal-cutting analyses of the past hundred years," *Mech. Eng.*, vol. 78, pp. 715–721, 1956.
- [4] F. W. Taylor, "On the art of cutting metals," *Trans. ASME*, vol. 28, pp. 31–350, 1906.
- [5] D. A. Stephenson and J. S. Agapiou, *Metal Cutting Theory and Practice*, 1st ed. New York: Marcel Dekker, 1997.
- [6] J. P. Davim, *Machining Fundamentals and Recent Advances*. London: Springer, 2008.
- [7] M. E. Merchant, "Mechanics of the metal cutting process i. orthogonal cutting of a type 2 chip," *J. Appl. Phys.*, vol. 16, pp. 267–265, 1945.
- [8] E. M. Trent and P. K. Wright, *Metal Cutting*. Boston: Butterworth-Heinemann, 2000.
- [9] M. A. Davies, T. Ueda, R. M 'saoubi, B. Mullany, and A. L. Cooke, "On the measurement of temperature in material removal processes," *CIRP Ann. - Manuf. Technol.*, vol. 56, no. 2, pp. 581–604, 2007.
- [10] K. Trigger and B. Chao, "An analytical evaluation of metal cutting temperature," *Trans. ASME*, vol. 73, pp. 57–68, 1951.
- [11] Hahn R. S, "On the temperature developed at the shear plane in the metal cutting process," *Proc. first U.S. Natl. Congr. Appl. Mech.*, pp. 661–666, 1951.
- [12] M. C. Loewen, E.G.; Shaw, "On the analysis of cutting tool temperatures," *Trans. ASME*, vol. 76, pp. 217–231, 1954.
- [13] K. Weinert, I. Inasaki, J. W. Sutherland, and T. Wakabayashi, "Dry machining and minimum quantity lubrication," *CIRP Ann. - Manuf. Technol.*, vol. 53, no. 2, pp.

511–537, 2004.

- [14] T. H. Childs, K. Maekawa, and P. Maulik, “Effects of coolant on temperature distribution in metal machining,” *Mater. Sci. Technol.*, vol. 4, no. 11, pp. 1006–1019, 1988.
- [15] M. C. Shaw, J. D. Pigott, and L. P. Richardson, “The effect of the cutting fluid upon chip-tool interface temperature,” *Trans. ASME*, vol. 23, pp. 45–56, 1951.
- [16] J. Byers, Ed., *Metalworking Fluids*, 2nd ed. Boca Raton: CRC Press, 2006.
- [17] N. Rangasamy, “A fundamental multi-scale study on mechanical, microstructural, and topographical characteristics of machining induced surface integrity in Ti-6Al-4V,” University of Utah, 2016.
- [18] M. Al Huda, K. Yamada, A. Hosokawa, and T. Ueda, “Investigation of temperature at tool-chip interface in turning using two-color pyrometer,” *Trans. ASME*, vol. 124, pp. 200–207, 2002.
- [19] N. R. Dhar, M. W. Islam, S. Islam, and M. A. H. Mithu, “The influence of minimum quantity of lubrication (MQL) on cutting temperature, chip and dimensional accuracy in turning AISI-1040 steel,” *J. Mater. Process. Technol.*, vol. 171, pp. 93–99, 2006.
- [20] K.-M. Li and S. Y. Liang, “Modeling of cutting temperature in near dry machining,” *J. Manuf. Sci. Eng.*, vol. 128, no. May 2006, pp. 416–424, 2006.
- [21] V. S. Sharma, M. Dogra, and N. M. Suri, “Cooling techniques for improved productivity in turning,” *Int. J. Mach. Tools Manuf.*, vol. 49, no. 6, pp. 435–453, May 2009.
- [22] C. S. Rakurty, P. I. Varela, and A. K. Balaji, “Effects of targeted minimum quantity fluid (MQF) application on surface integrity,” *Procedia CIRP*, vol. 8, pp. 462–468, 2013.
- [23] R. Komanduri and Z. B. Hou, “Thermal modeling of the metal cutting process - Part III : temperature rise distribution due to frictional heat source at the tool - chip interface,” *Int. J. Mech. Sci.*, vol. 43, no. 1, pp. 57–88, 2001.
- [24] G. Boothroyd and W. A. Knight, *Fundamentals of Metal Machining and Machine Tools*, 3rd ed. Boca Raton: CRC Press, 1989.
- [25] T. Ueda, A. Hosokawa, and K. Yamada, “Effect of oil mist on tool temperature in cutting,” *J. Manuf. Sci. Eng.*, vol. 128, no. 1, p. 130, 2006.
- [26] D. A. Stephenson, “Tool-work thermocouple temperature measurements—theory and implementation issues,” *J. Eng. Ind.*, vol. 115, no. 4, pp. 432–437, 1993.

- [27] W. F. Hastings and P. L. Oxley, "Predicting tool life from fundamental work material properties and cutting conditions," *CIRP Ann. Manuf. Technol.*, vol. 25, no. 1, p. 33, 1976.
- [28] T. Kurimoto, G. Barrow, and B. J. Davies, "The influence of aqueous fluids on the wear characteristics and life of carbide cutting tools," *CIRP*, vol. 31, no. 1, pp. 19–23, 1982.
- [29] X. J. Ren, Q. X. Yang, R. D. James, and L. Wang, "Cutting temperatures in hard turning chromium hardfacings with PCBN tooling," *J. Mater. Process. Technol.*, vol. 147, pp. 38–44, 2004.
- [30] H. Ay and W.-J. Yangt, "Heat transfer and life of metal cutting tools in turning," *Int. J. Heat Mass Transf.*, vol. 41523, no. 3, 1998.
- [31] A. D. Jayal, "An experimental investigation of the effects of cutting fluid application on machining performance," Ph.D. Dissertation, University of Utah, 2006.
- [32] P. J. Arrazola, T. Zel, D. Umbrello, M. Davies, and I. S. Jawahir, "Recent advances in modelling of metal machining processes," *CIRP Ann. - Manuf. Technol.*, vol. 62, pp. 695–718, 2013.
- [33] C. Shet and X. Deng, "Finite element analysis of the orthogonal metal cutting process," *J. Mater. Process. Technol.*, vol. 105, pp. 95–109, 1999.
- [34] X. Li, E. M. Kopalinsky, and P. L. B Oxley, "A numerical method for determining temperature - distributions in machining with coolant part 2: calculation method and results," *Proc. Inst. Mech. Eng. Part B J. Eng. Manuf.*, vol. 209, no. 1, pp. 45–52, 1995.
- [35] X. Li, "Study of the jet-flow rate of cooling in machining Part 2. Simulation study," *J. Mater. Process. Technol.*, vol. 62, pp. 157–165, 1995.
- [36] S. Y. Hong and Y. Ding, "Cooling approaches and cutting temperatures in cryogenic machining of Ti-6Al-4V," *Int. J. Mach. Tools Manuf.*, vol. 41, pp. 1417–1437, 2001.
- [37] B. T. Chao and K. J. Trigger, "The significance of thermal number in metal machining," *Trans. Am. Soc. Mech. Eng.*, vol. 75, pp. 109–120, 1953.
- [38] E. G. Loewen and M. C. Shaw, "On the analysis of cutting tool temperatures," *Trans. ASME*, vol. 76, pp. 217–231, 1954.
- [39] J. C. Jaeger, "Moving sources of heat and the temperature at sliding contacts," *Proc. R. Soc. NSW*, vol. 76, pp. 203–224, 1942.
- [40] H. S. Carslaw and J. C. Jaeger, *Conduction of Heat in Solids*, 2nd ed. New York:

Oxford University Press, 1959.

- [41] R. Komanduri and Z. B. Hou, “Thermal modeling of the metal cutting process - Part I: temperature rise distribution due to frictional heat source at the tool - chip interface,” *Int. J. Mech. Sci.*, vol. 42, no. 9, pp. 57–88, 2000.
- [42] R. Komanduri and Z. B. Hou, “Thermal modeling of the metal cutting process - Part II: temperature rise distribution due to frictional heat source at the tool - chip interface,” *Int. J. Mech. Sci.*, vol. 43, no. 1, pp. 57–88, 2001.
- [43] D. A. Stephenson, “Assessment of steady-state metal cutting temperature models based on simultaneous infrared and thermocouple data,” *J. Eng. Ind.*, vol. 113, no. 2, 1991.
- [44] P. K. Wright, S. P. McCormick, and T. R. Miller, “Effect of rake face design on cutting tool temperature distributions,” *J. Eng. Ind.*, vol. 102, no. 2, p. 123, May 1980.
- [45] P. K. Venuvinod and W. S. Lau, “Estimation of rake temperatures in free oblique cutting,” *Int. J. Mach. Tool. Des. Res.*, vol. 26, no. 1, pp. 1–14, 1986.
- [46] Y. Huang and S. Y. Liang, “Cutting temperature modeling based on non-uniform heat intensity and partition ratio,” *Mach. Sci. Technol.*, vol. 9, no. 3, pp. 301–323, 2005.
- [47] R. M’Saoubi and H. Chandrasekaran, “Experimental study and modelling of tool temperature distribution in orthogonal cutting of AISI 316L and AISI 3115 steels,” *Int. J. Adv. Manuf. Technol.*, vol. 56, no. 9–12, pp. 865–877, 2011.
- [48] Y. Karpat and T. Özel, “Predictive analytical and thermal modeling of orthogonal cutting process—Part II: effect of tool flank wear on tool forces, stresses, and temperature distributions,” *J. Manuf. Sci. Eng.*, vol. 128, no. 2, p. 445, 2006.
- [49] P. L. B. Oxley, “Development and application of a predictive machining theory,” *Mach. Sci. Technol.*, vol. 2, no. 2, pp. 165–189, 1998.
- [50] M. Groover, *Fundamentals of Modern Manufacturing*, 2nd ed. New York: John Wiley & Sons, 2002.
- [51] E. H. Lee and B. W. Shaffer, “The theory of plasticity applied to a problem of machining,” *J. Appl. Mech.*, vol. 18, pp. 405–413, 1951.
- [52] P. L. B. Oxley, *The Mechanics of Machining: An Analytical Approach to Assessing Machinability*, 1st ed. New York: Halsted Press, 1989.
- [53] G. S. Gad, E. J. A. Armarego, and A. J. . Smith, “Tool-chip contact length in orthogonal machining and its importance in tool temperature predictions,” *Int. J. Prod. Res.*, vol. 30, no. 3, pp. 485–501, 1992.

- [54] M. I. Sadik and B. Lindström, "The effect of restricted contract length on the tool performance," *J. Mater. Process. Technol.*, vol. 48, pp. 275–282, 1995.
- [55] X. Li, E. M. Kopalinsky, and P. L. B Oxley, "A numerical method for determining temperature distributions in machining with coolant part 1: modelling the process," *Proc. Inst. Mech. Eng. Part B J. Eng. Manuf.*, vol. 209, no. 1, pp. 33–43, 1995.
- [56] L. S. Tong and Y. S. Tang, *Boiling Heat Transfer and Two-Phase Flow*, 1st ed. Washington, D.C.: Taylor & Francis, 1997.
- [57] N. Sozbir, Y. W. Chang, and S. C. Yao, "Heat transfer of impacting water mist on high temperature metal surfaces," *Trans. Soc. Mech. Eng. J. HEAT Transf.*, vol. 125, no. 1, pp. 70–74, 2003.
- [58] J. D. Bernardin and I. Mudawar, "The leidenfrost point: experimental study and assessment of existing models," *Trans. ASME*, vol. 121, 1999.
- [59] C. E. Leshock and Y. C. Shin, "Investigation on cutting temperature in turning by a tool-work thermocouple technique," *J. Manuf. Sci. Eng.*, vol. 119, no. 4A, pp. 502–508, 1997.
- [60] "TPGN-322," 2007. [Online]. Available: https://www.greenleafglobalsupport.com/webapp/wcs/stores/servlet/Product_10001_10001_-1_21869. [Accessed: 12-Apr-2017].
- [61] Kennametal, "images._slash_cq_slash_endeca_slash_product_data_slash_web_normal_slash_44114.gif (302×187)." [Online]. Available: https://www.kennametal.com/images._slash_cq_slash_endeca_slash_product_data_slash_web_normal_slash_44114.gif. [Accessed: 07-Dec-2017].
- [62] H. S. Rama Iyengar, R. Salmon, and W. B. Rice, "Some effects of cutting fluids on chip formation in metal cutting," *J. Eng. Ind.*, vol. 87, no. 1, p. 36, 1965.
- [63] I. S. Jawahir and C. A. van Luttervelt, "Recent developments in chip control research and applications," *CIRP Ann.*, vol. 42, no. 2, pp. 659–693, Jan. 1993.
- [64] J. L. Santhanam, A.T.; Tierney, P.; Hunt, "Properties and selection: nonferrous alloys and special-purpose materials," in *ASM Handbook*, vol. 2, 1990, pp. 950–977.
- [65] A. K. Balaji, G. Sreeram, I. S. Jawahir, and E. Lenz, "The effects of cutting tool thermal conductivity on tool-chip contact length and cyclic chip formation in machining with grooved tools," *Ann. CIRP*, vol. 48, no. 1, pp. 33–38, 1999.
- [66] T. Ueda, M. Satoz, and K. Nakayama, "The temperature of a single crystal diamond tool in turning," *Ann. CIRP*, vol. 47, no. 1, pp. 41–44, 1998.

- [67] “Physical properties of carbon and low-alloy steels, properties and selection: irons, steels, and high-performance alloys,” *ASM Handb.*, vol. 1, pp. 195–199, 1990.
- [68] A. Santhanam, P. Tierney, and J. L. Hunt, “Cemented carbides, properties and selection: nonferrous alloys and special-purpose materials, vol. 2,” in *ASM Handbook*, ASM International, 1990, pp. 950–977.